THERMAL ENVIRONMENT MODELLING OF THE MONO-SLOPE SOLAR GREENHOUSE FOR COLD REGIONS

A Thesis Submitted to the College of Graduate and Postdoctoral Studies

In Partial Fulfillment of the Requirements

For the Degree of Master of Science

In the Department of Mechanical Engineering

University of Saskatchewan

Saskatoon, CANADA

By

SHUYAO DONG

PERMISSION TO USE

In presenting this thesis in partial fulfillment of the requirements for a Postgraduate degree from the University of Saskatchewan, I agree that the Libraries of this University may make it freely available for inspection. I further agree that permission for copying of this thesis in any manner, in whole or in part, for scholarly purposes may be granted by the professor or professors who supervised my thesis work or, in their absence, by the Head of the Department or the Dean of the College in which my thesis work was done. It is understood that any copying or publication or use of this thesis or parts thereof for financial gain shall not be allowed without my written permission. It is also understood that due recognition shall be given to me and to the University of Saskatchewan in any scholarly use which may be made of any material in my thesis.

Requests for permission to copy or to make other uses of materials in this thesis in whole or part should be addressed to:

Head of the Department of Mechanical Engineering

57 Campus Drive

University of Saskatchewan

Saskatoon, Saskatchewan

Canada, S7N 5A9

OR

Dean of the College of Graduate and Postdoctoral Studies

Room 116 Thorvaldson Building

110 Science Place

University of Saskatchewan

Saskatoon, Saskatchewan

Canada, S7N 5C9

ABSTRACT

The extremely cold outdoor temperatures in winter continue to be a barrier for the greenhouse growers. In Saskatoon, for example, it is less than -31.5°C for 1% of the year (ASHRAE, 2013). This limits the growth of the greenhouse industry in Saskatchewan which has around 250 billion square meters of farmland, and accounts for 38.5% Canada's farm area (Statistics Canada, 2016). Due to this fact, most traditional Canadian greenhouses in the Canadian Prairies shut down during the coldest months (from November to February) because of heavy heating bills. However, the local demand for food in the winter has been increasing in Saskatchewan due to a rise in population and consciousness of healthy food. If compare traditional local greenhouses with other greenhouse production techniques, Chinese mono-slope solar greenhouses do not primarily rely on supplemental heating. They rely on solar energy to maintain the indoor temperature. Fortunately, Saskatchewan has the most hours of sunshine annually in Canada which theoretically provides a favorable environment for the establishment and development of mono-slope solar greenhouses (Environment Canada, 2017). This also greatly reduces heating costs.

The objective of this study was to evaluate the thermal environment and predict the energy consumption of solar greenhouse production in Saskatchewan. This was done using an existing simulation model RGWSRHJ that was developed by Chengwei Ma in China (Ma, 2015). Several modifications were made to make the model SOGREEN that is suitable for the cold climate in Saskatchewan. These modifications included meteorological year data invoking, advanced front roof covering, summer solar screen, and so on. Later, the modified simulation model SOGREEN was validated using field data that were collected in a solar greenhouse in Elie, Manitoba. Solar greenhouse production was simulated under the weather conditions in Saskatoon, Saskatchewan. Finally, the energy consumption was analyzed using the simulated data to select the most suitable and economical energy resource for solar greenhouse production in cold regions.

From the validation results, there were 9.6% and 13.7% discrepancies in the model's predictions of indoor temperature and relative humidity, respectively. This has demonstrated that the modified model could simulate the thermal environment of a solar greenhouse with a

relatively high accuracy. While the simulation results confirmed that a large amount of energy was used for supplying heat from November to March, there was almost no supplemental heat needed between April and August. This illustrated that solar greenhouses can fully utilize the solar energy, dramatically reducing the annual energy consumption.

From an energy cost analysis, $26378.56, $2498.51 and $2610.00 was spent for supplemental heat with electricity, natural gas, and coal. Therefore, among these three energy resources, natural gas was the most affordable and most environmentally friendly option for greenhouse production. Compared with the natural gas expenses of Grandora Gardens, vegetable production in a solar greenhouse can save as much as 83.6% in energy costs. This demonstrates that solar greenhouse production in Saskatchewan is in fact economical for the Canadian Prairies.

ACKNOWLEDGEMENTS

TABLE OF CONTENTS

LIST OF FIGURES

LIST OF TABLES

LIST OF ABBREVIATIONS

CFD	Computational fluid dynamics
CO_2	Carbon Dioxide
EVA	Ethylene-vinyl Acetate
HVAC	Heating, ventilation, and air conditioning
MB	Manitoba
PC	Polycarbonate
PE	Polyethylene
PS	Polystyrene
PVC	Polyvinyl Chloride
RH	Relative Humidity
RSI	Thermal Resistance value in SI units
SK	Saskatchewan
T	Temperature
UV	Ultraviolet

LIST OF SYMBOLS

A Monthly total electrical rating, kW•h

ab Beam air mass exponents

A_c Cross-sectional area of solar greenhouse, m^2

ad Diffuse air mass exponents

A_F Front roof area, m^2

A_g Back roof area, m^2

A_s Indoor ground area, m^2

A_w North wall area, m^2

B Monthly total energy consumption, GJ

B_{hr} Included angle between horizontal plane and back roof, °

c_c Specific heat of steel construction materials, 470 J/(kg•K)

$C_{i,j}$ Specific heat of node (i,j), J/(kg•K)

c_p Average specific heat of plants, 3000 J/(kg•K)

C_p Air specific heat, J/(kg•K)

D_a Degree of aging

e Simulation accuracy, %

E_b Beam normal irradiance which is measured perpendicularly to rays of the sun, W/m^2

E_d Diffuse horizontal irradiance which is measured on horizontal surface, W/m^2

E_o Extraterrestrial radiant flux, W/m^2

E_r	Horizontal projection length of back roof, m
E_w	Horizontal projection length of slant north wall, m
f_k	Correction factor of heat transfer coefficient
G_d	Total condensation amount, $kg/(m^2 \bullet s)$
G_v	Water vapor amount escaped to the outdoor, $kg/(m^2 \bullet s)$
G_w	Total amount of evapotranspiration, including plants' transpiration, $kg/(m^2 \bullet s)$
H	Hour angle, °
H_b	Length of back roof, m
h_{cw}	Convective heat transfer coefficient between surface and indoor air, $W/(m^2 \bullet K)$
H_j	Height of j segment, m
H_r	Hight of roof ridge, m
H_s	Sinking depth of solar greenhouse, m
H_w	Height of north wall, m
i	Node number on the north wall
K	Overall heat transfer coefficient of the front roof, $W/(m^2 \bullet K)$
k_3	Luxuriant degree of plants
K_g	Correctional heat transfer coefficient of the front roof, $W/(m^2 \bullet K)$
K_{g0}	Theoretical value of front roof heat transfer coefficient, $W/(m^2 \bullet K)$
k_p	Coefficient of assumed shading area on the ground
L	Air exchange rate through ventilation and infiltration, m^3/s
L_{gh}	Total length of solar greenhouse, m

L_j	Width of j segment, m
L_s	Indoor span of solar greenhouse, m
m_c	Weight of steel construction materials per unit area, 8 kg/m^2
m_p	Plants' weight per unit area, kg/m^2
n	The day of year
N_c	Number of simulation cycle
N_{min}	Minimum simulation cycle, 6~12 cycles
n_v	Assumed ventilation frequency, times/h
p	Atmospheric pressure, Pa
p_w	Water vapor pressure of indoor air, Pa
p_{ws}	Saturated water vapor pressure of indoor air, Pa
q_a	Heat convected from indoor air, W
Q_e	Latent heat loss through indoor evaporation and transpiration, W
Q_g	Heat loss through front roof, W
Q_S	Heat transferred from ground to indoor environment, W
q_{sun}	Heat absorbed from direct solar radiation, W
Q_v	Heat loss from air exchange, W
Q_w	Heat transferred from wall and back roof to indoor environment, W
r	Evaporation latent heat of water, 2442 kJ/kg
R_o	Exterior surface heat transfer coefficient, W/(m^2•K)
S	Heat source, W/m^3

S_b	Solar irradiance on outdoor plane which was parallel to the back roof, W/m^2
S_{db}	Solar diffuse irradiance on outdoor plane which was parallel to the back roof, W/m^2
S_{dh}	Solar diffuse irradiance on outdoor horizontal plane, W/m^2
S_{dv}	Solar diffuse irradiance on outdoor plane which was parallel to the north wall, W/m^2
S_{hs}	Horizontal shading rate of front roof frame
$SS_{i,j}$	Heat source of node (i,j), W/m^3
S_v	Solar irradiance on outdoor vertical plane which was parallel to the north wall, W/m^2
S_{vs}	Vertical shading rate of front roof frame
t	Indoor air temperature, °C
t_i	Indoor temperature in next simulation step
t_{i0}	Initial indoor air temperature, °C
T_j	Ambient air temperature close to the j segment surface, °C
T_{j0}	Temperature of node [j][AAnwx[j]+1] , °C
T_l	Light transmission of front roof
t_s	Simulation step length, s
t_{ssj}	Surface temperature of ground, °C
t_w	Node temperature on north wall surface which is 1 m above the ground at the end moment, °C
t_{wn0}	Initial node temperature on north wall surface which is 1 m above ground, °C

t_{wsj}	Surface temperature of wall and back roof, °C
V_a	Air exchange rate, m³/s
V_{gh}	Indoor volume, m³
V_{set}	User-set ventilation rate, m³/(m²•s)
v_o	Outdoor wind speed, m/s
W_n	Width of the north wall, m
$(\Delta x)_i$	Width of node (i,j), m
$(\delta x)_i$	Center distance between node (i,j) and (i+1,j), m
Y_c	Monthly total coal cost, $
Y_e	Monthly total electrical cost, $
Y_G	Annual cost in energy consumption, $
Y_n	Monthly total natural gas cost, $
$(\Delta y)_j$	Height of node (i,j), m
$(\delta y)_j$	Center distance between j and (j+1) segment, m
a_i	Heat transfer coefficient of the interior surface, W/(m²•K)
a_j	Surface absorptivity of j segment on the wall
a_g	Surface absorptivity of the j segment on the ground
β	Solar altitude angle, °
δ	Solar declination, °
η_e	Energy saving rate, %
λ	Heat conductivity coefficient, W/(m•K)
$\lambda_{i,j}$	Heat conductivity coefficient of node (i,j), W/(m•K)

ρ	Air density, kg/m^3
$\rho_{i,j}$	Density of node (i,j), kg/m^3
τ	Time, s
φ	Azimuth angle, °

Chapter 1. INTRODUCTION

The extremely cold outdoor temperatures in winter (lower than -31.5°C for 1% of the year in Saskatoon) are a barrier for the greenhouse growers because of the huge supplemental heating requirement (ASHRAE, 2013). This limits the growth of the greenhouse industry in Saskatchewan which holds 250 billion square meters of farmland and accounts for around 38.5% of total Canadian farm area (Statistics Canada, 2016). Although HVAC technologies such as supplemental heating and dehumidification systems have been commonly applied in the traditional Canadian greenhouses (Fig. 1.1), the huge energy consumption and maintenance causes many challenges for greenhouse production. In northern latitudes, around 70% to 85% of the total operating costs of greenhouse production are associated with heating costs (Rorabaugh et al., 2002). Thus, most traditional Canadian greenhouses in the Canadian Prairies shut down during the coldest months due to heavy heating bills. The closure of local greenhouses during the winter leads to a lack of local produce, leaving imported vegetables and fruits to dominate the food market in the winter. However, the demand for local produce in Saskatchewan has been increasing due to an increase in the population as well as the increased consciousness of healthy, local food. As shown in Figures 1.2 and 1.3, different than traditional greenhouses, Chinese mono-slope solar greenhouses do not primarily rely on supplemental heating. They rely on solar energy to maintain indoor temperatures. Fortunately, Saskatchewan has the most hours of sunshine in Canada all year which theoretically provides favorable environmental conditions for the establishment and development of mono-slope solar greenhouses. This has the potential to reduce heating costs significantly.

Figure 1.1 Traditional greenhouse in Saskatoon, Saskatchewan

Figure 1.2 Mono-slope solar greenhouse in Elie, Manitoba
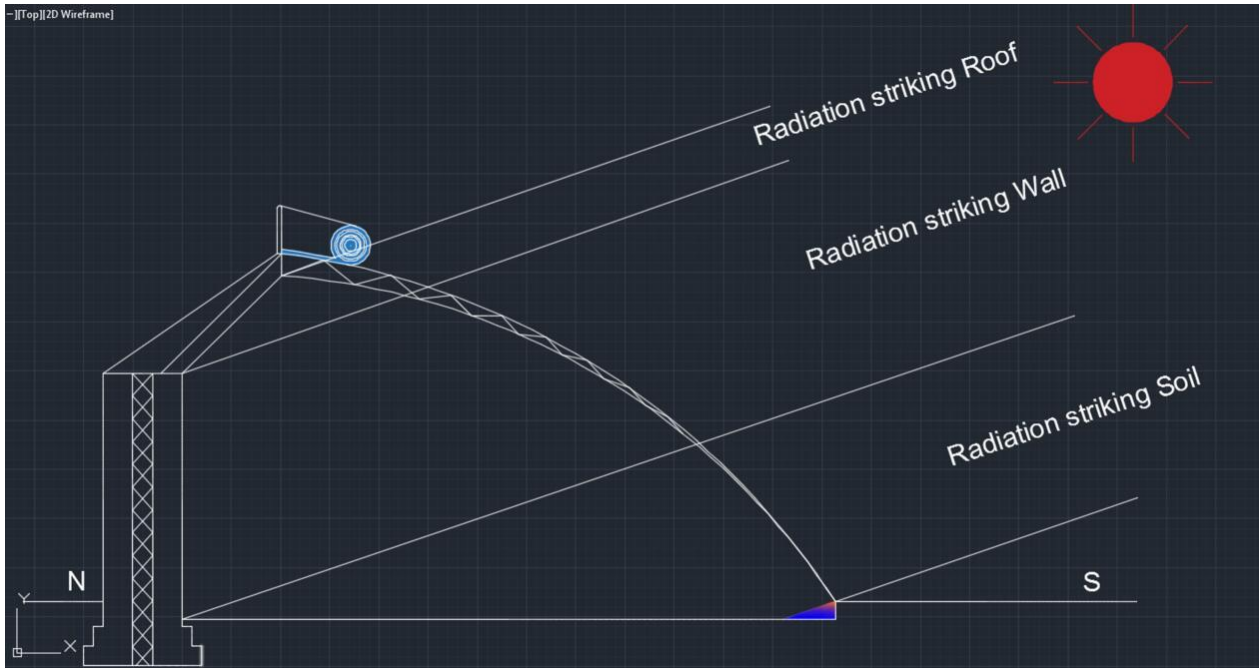
Figure 1.3 Cross sectional view of the mono-slope solar greenhouse

The thermal energy transfer process in the greenhouse is a fundamental theory in the development of the greenhouse simulation methods. Thermal energy transfers from a high temperature region to a low temperature region by conduction, radiation and convection. Thermal conduction is the diffusion of thermal energy through a continuous and stationary medium and it is the only method thermal energy can be moved through a solid. And thermal convection defines as thermal energy transfers within a fluid or between a fluid and a solid surface. While any objects at temperature above absolute zero emit thermal radiation. Temperature difference is the driving force in the heat transfer process (ASHRAE, 2013). According to the heat transfer theory, simulations of the thermal performance of solar greenhouses have been conducted by developing various simulation models using MATLAB, CFD, FORTRAN, and the VC++ method (Guo et al., 1994; Meng et al., 2009; Tong et al., 2007; Xu et al., 2013). However, some of these methods have many restrictions for a thermal environment simulation, and others are not accurate enough through validation. Therefore, they are not suitable for simulating a greenhouse indoor thermal environment in Saskatchewan. Ahamed et al. (2015) developed a mathematical model to simulate the heating requirement of conventional greenhouses. This model simulated the heat consumption of a single span gable

roof greenhouse (269.56 m^2) located in St. Louis, Saskatchewan. The total predicted heating energy requirement was 1052.3 GJ, which was close to the measured heat, 910 GJ, supplied to the greenhouse. However, this model cannot be used for mono-slope greenhouses. The field experiment conducted by Beshada et al. (2006) in Elie, Manitoba, showed that mono-slope solar greenhouse production method is a more energy-efficient design for greenhouses in cold regions than traditional gutter-connected greenhouses. Nonetheless, further studies were not conducted to evaluate the thermal environment conditions and energy consumption in solar greenhouses in cold regions.

The objective of the thesis research is to simulate the energy consumption of solar greenhouse production in Saskatchewan by modifying an existing simulation thermal model for solar greenhouses. This model RGWSRHJ was initially developed by Chengwei Ma in China (Ma, 2015), and its China-oriented simulation setting made it unusable in Canada. Hence, this study started by modifying the model to obtain the revised model SOGREEN. It was then validated and the model was used to simulate solar greenhouses in Saskatchewan. Many modifications made the model applicable to cold climates, such as Saskatchewan's climate. This included adding polystyrene pellet insulation, adding the double-layer inflated front-roof cover, resetting the wind speed and simulation month limitation as well as adding a work condition storage function. Furthermore, a research group member collected field data in a solar greenhouse in Elie, Manitoba to validate the accuracy of the modified simulation model SOGREEN. Subsequently, using this validated simulation model, simulation was conducted for the indoor thermal environment and energy consumption of a study solar greenhouse (100 m x 12 m) located in Saskatoon, Saskatchewan. With these results, greenhouse growers will know the difference in energy consumption between traditional gutter-connected greenhouses and mono-slope solar greenhouses. This will make local greenhouse vegetable production in the winter economical for the Canadian Prairies.

Chapter 2. LITERATURE REVIEW

2.1 Development history of mono-slope solar greenhouse

Back in the 1920s, the glass-covered solar greenhouses had been used in Liaoning province, China to produce vegetables (Li, 2005). The initial type of solar greenhouse was called 'one slope one stand type solar greenhouse'. Its north walls and roofs consisted of straw, grass mud and sorghum stalk, and its front roof was covered with glass. Then, in 1950s, the greenhouse researchers increased the lighting angle of the back roof and introduced some insulation measures and improved the heat storage capacity of the solar greenhouse (Wei et al., 2012). Simultaneously, small conventional greenhouses covered with polyethylene film had been developed in the northern China. In the 1970s, conventional greenhouses had been promoted in many Chinese provinces while the curved mono-slope solar greenhouse had been designed and constructed at the same time. The curved mono-slope solar greenhouses had a higher greenhouse ridge (2.2 m to 2.6 m) and a bigger span (6 m to 7 m), which increased the indoor space of the solar greenhouse. 'Ganwang type solar greenhouse' and 'Anshan Ⅰ type solar greenhouse' are the classic structure during this period. In the 1980s, the standardized solar greenhouses, in which front roof was built with galvanized steel pipes and single-layer plastic film, had been developed rapidly. The standardized solar greenhouses had a higher north wall in order to improve the heat storage capacity. 'Anshan II type solar greenhouse' was the most up-to- date greenhouse design in 1980s. The light transmittance rate of Anshan II type solar greenhouse rose by 7% to 10% compared with Anshan I type solar greenhouse, and the indoor temperature can be maintained between 25℃ and 30℃ in the winter (Wei et al., 2012). However, due to high cost of production and technical problems, the standardized solar greenhouses were limited in the use of research and experiments. Their advantages cannot be fully proven in the greenhouse industry. In the 1990s, the greenhouse covered area had been extended to more than 1.3 billion square meters with the development of planting technology and greenhouse management improvement. Since 1996, modern solar greenhouses had been built in the extended regions, ranging from 30° to 45° northern latitude. After 2000, the mono-slope solar greenhouses have dominated the new greenhouse production in northern China (Yan et al., 2013). 'Shouguang generation V type solar greenhouse' became the most

popular solar greenhouse structure because of the large span (10 m) and thickened soil trapezoidal north wall (wall base thickness is 3.5 m to 4.5 m), and the submerged ground level (0.3 m to 0.5 m). But the thickened north wall led to a low soil utilization rate and the submerged ground level had a negative influence on the lighting from the south roof (Wei et al., 2012). Afterwards, a new solar greenhouse type with a cool shed on the back was designed to make full use of the heat loss through the north wall and significantly improve the land utilization rate. The cool shed was used for vegetable or mushroom production. However, this greenhouse structure cannot be used in the cold regions because of the low temperature in the cool shed on the back. Another new type solar greenhouse called 'Gichun type solar greenhouse' was designed with double front roof cover structure which improved the heat preservation capacity but increased the capital cost at the same time (Wei et al., 2012).

In western countries, the attached greenhouses provide people with the conveniences of growing vegetables in their own garden more easily. By attaching a greenhouse to the south side of house, on one hand, the solar energy can be utilized for plants production on a sunny day. On the other hand, the attached greenhouse provides an additional layer of insulation to the house. This saves heating cost in the winter by using less fuel or burning less wood to supply excess heating to the house (Ziggy, 2012).

The hobby greenhouse is another commonly built greenhouse in Canada. It can be either a freestanding building or an attached building. The frames of greenhouse are normally made of aluminum and its triangular gable is the sloped roof of the greenhouse. Both gable and vertical sidewalls are cover with transparent board or glass. This type greenhouse has roof vents hinged on one side of the sloped roof. Most importantly, the capital cost of a small hobby greenhouse covered with plastic films can be as low as $600.While those large and sophisticated hobby greenhouses can cost $10,000 or more (Baird, 2011).

Compared to the attached greenhouse, the hobby greenhouse is a freestanding building and all sides are exposed to the weather. Thus, the hobby greenhouse needs superior framing and glazing to compete with harsh weather and reduce heat loss.

Hoop-house is also a popular type of freestanding greenhouse. Its archy frame is normally made of PVC pipes and covered with plastic film. The greenhouse growers can determine the structure length according to how much available space there is, so the soil utilization rate is

very high. However, the hoop-house is not a smart choice in windy regions because of its light weight (Baird, 2011).

2.2 Greenhouse Simulation Models

Studies have been conducted in China on Chinese solar greenhouses since 1994. Guo et al. (1994) developed a mathematical model TEMP to predict the thermal environment and optimize the building envelope of Chinese solar greenhouses. This model predicted the indoor air and surface temperature by considering the heat transfer of the greenhouse structures, moisture balance, solar transmittance of the front roof, and the heat storage of the north wall and ground. In this model, users needed to input the greenhouse location, structural features, thermal properties of the construction materials, outdoor wind speed, hourly outdoor temperature, working schedule of the thermal blanket and some other conditions, before simulations could be performed. Later, the model outputted the indoor air temperature and surface temperature during the simulation period. The results from three different greenhouse structures demonstrated that the model could satisfactorily simulate the indoor thermal environment for various structures. However, some important factors were not considered in this model such as transpiration from plants, evaporation from wet soil, the distance between the plants and the north wall, ventilation, and supplemental heat. The model also used the Fortran programming language and it was complicated to use.

Li et al. (1997) set up a theoretical model to describe the thermal environment of solar greenhouses, and the model was verified with experimental data. The simulation results show that solar radiation has a stronger influence on the indoor thermal environment compared to the influence of the outdoor weather conditions. Besides, the north wall plays a significant role in storing solar energy and maintaining the indoor temperature. This model had problems that were similar to the model of Guo et al. (1994).

Tong et al. (2007) built a simulation model using computational fluid dynamics (CFD) to predict the patterns in indoor temperature changes on a sunny day. They validated this model with measured data. To simulate the indoor temperature change on a sunny day, users need outdoor solar radiation, air temperature, wind speed, and soil temperature 1 m below the indoor

ground level. Results showed that the measured indoor temperature change followed the simulated trend, while there was a difference during daytime hours. However, this model could only be used for a particular greenhouse. It requires CFD skill, and it is very time-consuming to run too.

Meng et al. (2009) used MATLAB and VB to establish a thermal environmental simulation model. This model quantitatively described solar radiation, natural ventilation, heat convection and conduction, water phase transformation, and corresponding impacts on the thermal environment. Compared with the field data measured in Beijing in January 2008, the differences between the field data and simulated data for the indoor air temperature, north wall surface temperature, soil temperature and back roof surface temperature were all around 10%. Considering the local weather conditions, the model focused solely on predicting the thermal environment and it did not consider supplemental heat.

Soil has a negative impact on the growth of crops when it is at a relatively low temperature, which is particularly evident in the forefoot segment. To evaluate and strengthen the heat preservation of the solar greenhouse, Bai et al. (2010) established a mathematical model to analyze forefoot temperature field distribution in the Liaoshen--I solar greenhouse. Similarly, finite element analysis (ANSYS) was also used to simulate forefoot thermal conditions with and without the insulation ditch. Results showed that the indoor soil temperature, especially the temperature of the soil near the foundation increased when setting the cold-proof ditch along the foundation.

Ma et al. (2010) developed the greenhouse simulation model RGWSRHJ to predict and evaluate the thermal environment of a solar greenhouse. Users can see the daily thermal environment after inputting the greenhouse location, outdoor weather conditions, greenhouse structure, building materials and working schedules. With the simulation results, users can compare the thermal performance of different solar greenhouses and they can optimize the structure.

Xu et al. (2013) used a mathematical model to evaluate the indoor thermal environment of the Chinese solar greenhouse. The research focused on three aspects: 1) sunlight transmittance through the south roof with limited structural and equipment shading, interception; 2) heat penetration of solar radiation by the walls and ground; 3) insulation of the walls and back roof,

any of which makes a significant contribution to the thermal environment. The simulation results revealed the following results: 1) The thermal environment of the solar greenhouse improves by lowering the indoor ground level. 2) The temperature rises and heat released from the wall to indoor air turns to marginal values as the wall increases to a certain thickness. 3) The outer layer of the north wall should be built with insulation material and the inner layer should have appropriate thermal conductivity and specific heat.

The outdoor temperature is the key factor in the thermal environment simulation of a solar greenhouse. To accurately predict the outdoor winter temperature, Xu et al. (2013) measured winter temperatures from 14 stations in 5 Chinese provinces from 2009 to 2011. They developed a mathematical method to calculate hourly outdoor air temperature. This outdoor air temperature calculation method has been applied in the greenhouse simulation software RGWSRHJ developed by Dr. Ma (2015) due to its high precision (mean error was 0.3℃).

Ahamed et al. (2015) developed a simulation model using MATLAB to predict the energy requirement of a conventional greenhouse. The user needs to input the outdoor weather conditions, indoor environment set point, and greenhouse construction data before the simulation. Later, the simulation model calculates various greenhouse parameters and it estimates heat sources and sinks, and finally output energy demands. A single span gable roof greenhouse (29.3 m x 9.2 m) located in St. Louis, Saskatchewan was used to simulate the model. Simulation results showed that the predicted annual heat consumption was 1052.3 GJ, which was close to the actual 910 GJ of heating energy consumed from January to mid-December.

No research has been conducted outside of China on a solar greenhouse with the exception of Dr. Zhang's research group in Manitoba and Ahamed et al's work in Canada. The following literature demonstrates some simulation models for conventional greenhouses.

HORTISIM, an integrated model, developed by several research groups, contains seven sub-models (weather, greenhouse climate, soil, crop, greenhouse manager, soil manager and crop manager) and it contains a simulation process manager called Engine. This integrated model can simulate energy and water consumption, crop photosynthesis, fruit growth condition, etc. The energy balance validation results showed that the difference between the measured and

simulated instantaneous air temperature was most often less than 2°C in a Venlo-type glasshouse (Gijzen et al., 1998).

Navas et al. (1998) developed a dynamic model to predict the Mediterranean greenhouse climate. This model divides the greenhouse into 'process' and 'boundary' components. The former consists of the soil, crops, cladding and indoor air, while the latter comprises the sky, heating system, etc. The authors used this model to simulate a greenhouse with typical winter conditions in Madrid. The detected small-scale errors (~1°C or so) indicate a good prediction.

Benavente et al. (1998) studied the localized heating of greenhouse substrates, and a soil temperature model was built to predict the changes in substrate temperature and energy consumption with different electric wire configurations. The results showed an accurate prediction of energy consumption with a 7% average error.

The educational software, SIMULSERRE, was developed for students to establish greenhouse production strategies. In this model, users have to determine the location, construction set, heating and carbon dioxide enrichment systems, temperature set-point and many other aspects. Climate information, energy and CO_2 balances, crop growth and development are visualized through the output interface. Most importantly, different simulations regarding different planting strategies can be compared, evaluating the effectiveness of various strategies (Gary et al. 1998).

2.3 Supplemental Heating Systems

In most parts of the Canadian Prairies, the cold climate is a key reason for the padlock of local greenhouses. Another disadvantage is that natural solar radiation is not sufficient in Saskatchewan during the winter to heat the greenhouses. Therefore, introducing heat into the greenhouses is necessary even during the day (Vinje, 2013). There are various methods to supply low cost heat to the greenhouses and first method is the germination mat. This seedling heat mat increases the success of germination by gently warming the rooting area 5.6-11.1°C over the ambient temperature. The waterproof construction and standard-sized flat mats make it safe for indoor use (Planet Natural, 2017).

Second, composting organic wastes in the covered trench down the center of the greenhouse is a renewable energy source. This provides moderate root temperature for the plants in the greenhouse. On the other hand, the higher daytime temperature is beneficial for heating up the compost.

Third, placing several large black barrels with water in any practical location in the greenhouse is another sustainable heating method. The water in the black barrels can absorb heat during the daytime and it releases heat during cold nights (APEX Publishers, 2017).

Fourth, the electric space heater is the simplest of methods to heat the winter greenhouses. However, this heating method has the highest cost among all the heating methods (APEX Publishers, 2017).

Fifth, a soil electric heating cable can gently warm the growing media for better growth and faster germination. Its flexible cord can fit into any space, and the built-in thermostat is able to maintain the set temperature (APEX Publishers, 2017).

Sixth, wood and wood pellet stoves operate more effectively and economically than other fuels while the fossil fuel prices become more expensive. These are typically used in small greenhouses in China. In Canada, large commercial greenhouses have been using wood hydronic heating where waste wood products are available (APEX Publishers, 2017).

A seventh method is using hot water heating systems. Carrying heat from the boiler to the greenhouse through hot water is becoming more common for large-scale greenhouses. Compared to hot air space heating, hot water systems provide greater uniformity of temperature across the greenhouse. The hot water's temperature can be adequately low to heat pipes located around the vegetable plants in the greenhouse floor. For large greenhouses, the hot water heating system is more affordable, and it is a suitable heat distribution method. This is because 1) the central heating plant in a separate building saves more space for the plants and it provides flexibility to use alternative energy sources; 2) the partial load method performs more efficiently than the hot air distribution system; 3) load control and maintenance are cheaper and easier; 4) the possibility of plant damage caused by toxic flue gases is reduced because the combustion unit is located outside of the greenhouse (APEX Publishers, 2017).

An eighth method is the oil-fired unit heater. In the northeast of the U.S., oil-fired unit heaters are used more than in other regions. This style is valid for suspended installation. Oil-fired equipment generally needs more annual maintenance than other equipment.

A ninth method is the floor heating system. It is an effective method to save energy by using hot water pipes and solely heating the local growing area on the floor. The experiment results show that the crop root temperature maintained between 19°C and 25°C at night, and 28% of energy was saved by using the floor heating system (Qu et al., 2003).

Comparing initial unit costs with comparable heating capacities, hot water systems are the most economical followed by electric, gas and oil-fired units (National Greenhouse Manufacturers Association, 1998). In addition, the greenhouse growers could also place sealed water tanks and rock bed in the greenhouse, and paint black on the wall surface to store more solar heat in the daytime.

2.4 Cover Materials of South Roof

In Saskatchewan, the ambient temperature in the winter is extraordinarily low, which makes the heat loss through the south roof rise dramatically when the thermal blanket is rolled up during the daytime. In Saskatoon, for example, the outdoor temperature is lower than -31.5 °C for 1% of the year. Hence, covering materials with excellent thermal insulation properties bring a considerable reduction of heat loss during the daytime.

There are a wide variety of transparent materials that can be employed to cover greenhouses today. Covering materials include plastic film, plastic rigid sheets, solaro exterior reflective shade, glass, double-layer inflated film, and a polystyrene-pellet insulation system.

Plastic film is the most common covering material for solar greenhouses. This includes ethylene vinyl acetate copolymer (EVA), polyethylene (PE), and polyvinyl chloride (PVC). The film is a thick and flexible material with various thickness (commonly measured in mils). Greenhouse builders can cover the greenhouse with single or double layers according to insulation needs.

As shown in Figure 2.1, rigid plastic sheets are commonly used in the construction of traditional gutter-connected greenhouses. The air locks between the two panels act as an insulation layer. A regular polycarbonate (PC) panel offers excellent heat retention, high impact resistance, high UV resistant, and around 80% light transmission. Some may include an anti-condensate coating to prevent the interior surface from dripping.

Figure 2.1 PC sheet covers used in traditional greenhouses

A solaro exterior reflective shade is an open-structure screen for effective greenhouse cooling and it provides both shading and ventilation for plants.

Glass is one of the traditional cover materials. It provides a much longer service life (at least 30 years) for greenhouses, but it has a high cost. Compared with plastic film, clean glass always enables excellent light transmission, and the double-paned structure has a relatively high insulation value. However, the glass roof requires a sturdy and costly structure system, and it is expensive and difficult to replace if broken.

The double-layer inflated film is a relatively up-to-date cover structure in greenhouses. The blower pumps the indoor warm air into the double layer poly, and the generated 20 cm gas cell acts as an insulator. This reduces the heat transfer coefficient to 3.85 W/(m^2•K) (Garzoli and Blackwell, 1987). Although a double layer inflated film provides better insulation, its light

transmission is lower than single plastic film. However, the inflated film scatters the sunlight which makes the plant temperatures more stable.

Polystyrene-pellet insulation systems are rarely applied in greenhouses because of their poor mechanical reliability, incomplete sealing, and high initial costs. Pellets are pumped into the gaps between the double plastic films of greenhouses at sundown. They are removed at sunrise, which reduces the energy requirement at night by 80% (Short and Shah, 1981).

2.5 Research Gaps

From the above literature review, solar greenhouses are rarely used in Canada, and very limited research has been done on them. Very few thermal simulation models are available for solar greenhouses, and none can be readily used in Canada. Hence, an effective and user-friendly thermal environment simulation model should be developed for cold regions such as Canada. Research gaps are elaborated as follows.

First, most current solar greenhouse thermal environment simulation models are applied in Asian and European countries. Their local weather conditions such as low wind speed and moderate temperatures result in limitations for northern areas, especially Canada.

Second, there are no supplemental heating systems or winter heating built in most existing simulation models, and this is not a solution for greenhouse production in cold regions. In Saskatchewan for example, supplemental heating systems turn on even during cold, summer nights.

Third, compared to solar greenhouses in other regions, solar greenhouses in northern latitudes need to be armed with the advanced front roof covering materials to fight the extremely low outdoor temperatures and high winds. There have to be summer sun blockers to reduce the solar irradiance that enters at noon. However, current simulation models generally use single layer plastic film or glass to cover the front roof, and few models have functions for sun blocking.

Fourth, since it is a complicated process to simulate the thermal environment of greenhouse production, all simulation models are required to input many detailed parameters before

simulation, which makes the process too time-consuming. Thus, a new function is needed to save and invoke similar settings for further use.

Fifth, most existing simulation models focus on the thermal environment and crop status in greenhouse production while minimizing energy consumption is a priority for greenhouse production in northern areas.

Chapter 3. OBJECTIVES

According to the research gaps, the goal of this study was to evaluate the thermal environment and predict the annual energy consumption of solar greenhouse production in cold regions such as Saskatchewan. In the meantime, the evaluation and prediction process should also provide guidance on solar greenhouse crop selection for growers.

The first objective was to modify an existing thermal environment simulation model. Considering the weather conditions in the Canadian Prairies, the model was needed to predict the thermal environment of the mono-slope solar greenhouse with both a supplemental heating system and a ventilation system. The model RGWSRHJ developed by Dr. Ma was a comprehensive and user-friendly simulation model for use in China. This made it the best choice for this research.

The second objective was to validate the modified simulation model with field data. A classic mono-slope solar greenhouse located in Elie, Manitoba, was selected for field measurements to validate the model results and thereby quantify the accuracy of the modified simulation model.

The third objective was to simulate the thermal environment of a study solar greenhouse assumed in Saskatoon and predict its annual energy requirement. This was done by designing a large-scale mono-slope solar greenhouse in Saskatoon and setting its working conditions including the set point temperature, thermal blanket schedule and ventilation schedule. The simulation model can predict the hourly indoor thermal environment parameters and energy consumption. Thus, local greenhouse growers will see the energy consumption of greenhouse production during the winter and determine whether winter local greenhouse vegetable production is economical for Saskatoon and other locations in the Canadian Prairies.

The final objective was to analyze the energy requirement and cost for supplemental heat. Based on the simulated energy consumption of the solar greenhouse, the annual energy costs of various energy resources can be calculated, and an optimal energy resource can be selected for greenhouse production in the Canadian Prairies.

Chapter 4. MATERIALS AND METHODS

Based on the objectives stated above, this research intended to modify the model RGWSRHJ, and validate it to simulate energy consumption of a solar greenhouse in Saskatoon. The materials and methods for each section are explained below.

4.1 RGWSRHJ Model Theory
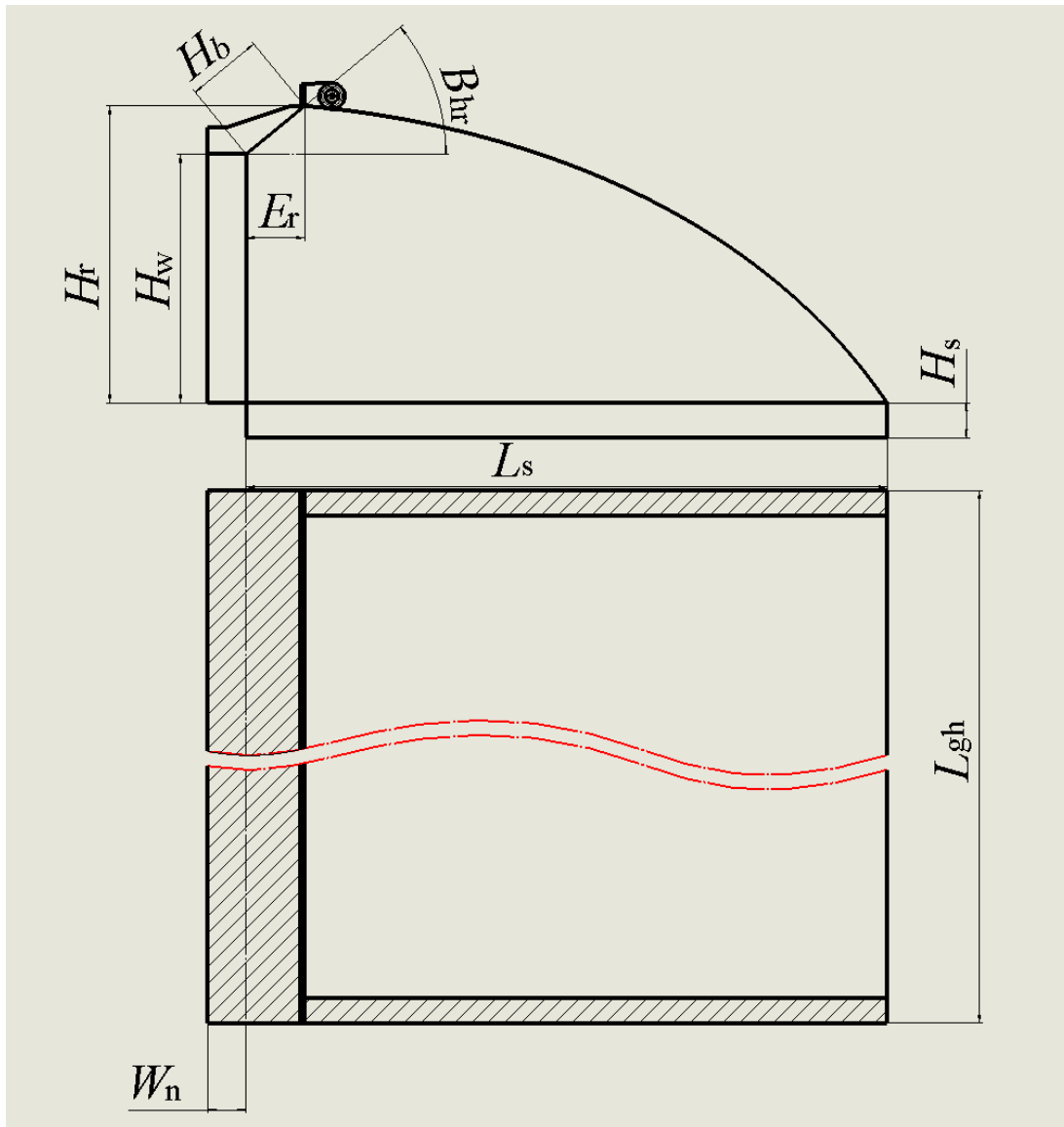
Figure 4.1 Greenhouse cross-sectional view and top view

4.1.1 Core algorithm

Heat transfer from the wall, back roof, and ground area employs the two-dimensional unsteady state heat transfer method. The following is the differential form of its control equation:

$$\rho C_p \frac{\partial t}{\partial \tau} = \frac{\partial}{\partial x}\left[\lambda \frac{\partial t}{\partial x}\right] + \frac{\partial}{\partial y}\left[\lambda \frac{\partial t}{\partial y}\right] + S \tag{4.1}$$

where ρ is the air density, kg/m³; C_p is the air specific heat, J/(kg•K); t is the indoor temperature, °C; τ is the time, s; x and y are coordinates in the heat transfer plane, m; λ is the heat conductivity coefficient, W/(m•K); and S is the heat source, W/m³.

Discretizing the control equation with the appropriate transformation, the differential equation can be transformed into the following differencing linear equation set:

$$\begin{cases} P_{0,j}t_{0,j} - A_{0,j}t_{1,j} = K_{0,j}t_{0,j,0} + SS_{0,j} \\ -A_{i-1,j}t_{i-1,j} + P_{i,j}t_{i,j} - A_{i,j}t_{i+1,j} = K_{i,j}t_{i,j,0} + SS_{i,j} \\ -A_{n,j}t_{n,j} + P_{n+1,j}t_{n+1,j} = K_{n+1,j}t_{n+1,j,0} + SS_{n+1,j} \end{cases} \tag{4.2}$$

where $A_{i,j} = \frac{\lambda_{i,j}(\Delta y)_j}{(\delta x)_i}$; $A_{i-1,j} = \frac{\lambda_{i,j}(\Delta y)_j}{(\delta x)_{i-1}}$;

$B_{i,j} = \frac{\lambda_{i,j}(\Delta x)_i}{(\delta y)_j}$; $B_{i,j-1} = \frac{\lambda_{i,j}(\Delta x)_i}{(\delta y)_{j-1}}$; $K_{i,j} = \frac{\rho_{i,j}C_{i,j}(\Delta x)_i(\Delta y)_j}{\Delta \tau}$;

$P_{i,j} = B_{i,j-1} + A_{i-1,j} + K_{i,j} + A_{i,j} + B_{i,j}$;

$SS_{i,j} = S_{i,j}(\Delta x)_i(\Delta y)_j + B_{i,j}t_{i,j+1} + B_{i,j-1}t_{i,j-1}$;

$\Delta \tau$ is the simulation step length, s; $(\Delta y)_j$ is the height of the node (i,j), m; $(\Delta x)_i$ is the width of the node (i,j), m; $(\delta y)_j$ is the center distance between the j and $(j+1)$ segment, m; $(\delta x)_i$ is the center distance between the node (i,j) and (i+1,j), m; $\lambda_{i,j}$ is the heat conductivity coefficient of the node (i,j), W/(m•°C); $\rho_{i,j}$ is the density of the node (i,j), kg/m³; $C_{i,j}$ is the specific heat of the node (i,j), J/(kg•°C); and $SS_{i,j}$ is the heat source of the node (i,j), W/m³.

The above differencing linear equation set can be written in the following matrix form:

$$\begin{bmatrix} P_{0,j} & -A_{0,j} & 0 & 0 & 0 & 0 \\ -A_{0,j} & P_{1,j} & -A_{1,j} & 0 & 0 & 0 \\ 0 & -A_{1,j} & P_{2,j} & -A_{2,j} & 0 & 0 \\ \cdots & \cdots & \cdots & \cdots & \cdots & \cdots \\ 0 & 0 & 0 & -A_{n-1,j} & P_{n,j} & -A_{n,j} \\ 0 & 0 & 0 & 0 & -A_{n,j} & P_{n+1,j} \end{bmatrix} \begin{bmatrix} t_{0,j} \\ t_{1,j} \\ t_{2,j} \\ \cdots \\ t_{n,j} \\ t_{n+1,j} \end{bmatrix} = \begin{bmatrix} K_{0,j}t_{0,j,0} + SS_{0,j} \\ K_{1,j}t_{1,j,0} + SS_{1,j} \\ K_{2,j}t_{2,j,0} + SS_{2,j} \\ \cdots \\ K_{n,j}t_{n,j,0} + SS_{n,j} \\ K_{n+1,j}t_{n+1,j,0} + SS_{n+1,j} \end{bmatrix}$$

(4.3)

After setting the construction materials of the north wall, it would be divided into finite element grids by the model automatically. In the meshing process, the density of grids was higher in the surface area than those in the middle of the construction materials. Take part of the north wall for example, the model started to mesh from both interior and exterior surface to the middle of the wall. On the vertical direction, the height of each grid was 0.01 m. And on the horizontal direction, the distance between first node (set on the surface) and second node was dx[0]= 0.001 m. Then, the node distance increased as meshing process went further, which was dx[i]= $0.001 + 0.00005i^2$ m (where i is the node number counted from 0 on the surface to the middle of the wall). As shown in Fig 4.2, if the wall consisted with more than two materials, the node must be arranged on the interface of different materials. However, the properties of the interface node kept the same with the northern material. When the total meshed width equaled to half width of the north wall, the meshing process ended, and the model saved each node position, thermal properties and grid width.
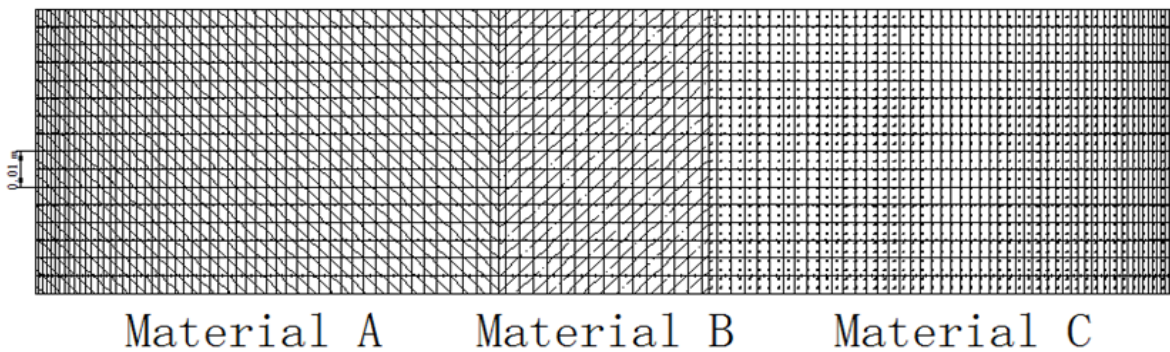
Figure 4.2 Meshing grid example of the north wall

This tridiagonal matrix can be efficiently solved with the Thomas algorithm. The solution shows the temperature field of the wall, back roof and ground area and the model calculates the heat transferred from the wall, back roof and ground to the indoor environment.

4.1.2 Simulation flow chart

This simulation model was developed with VC++, and Figure 4.3 demonstrates the flow chart of the simulation model. The simulation process starts from a basic simulation condition input, including the location and weather condition setting, greenhouse structure setting, and greenhouse work schedule. Then, the model starts calculating the indoor thermal field of the next simulation step and records the thermal parameters of each step. When the simulation process comes to the final moment, the model compares the temperature of the specified point to the corresponding initial temperature and it replaces the initial temperature with the temperature of the final moment. After several simulation cycles, the fluctuation in indoor thermal parameters comes in a certain range, and the simulation model can output the simulation results to the user.
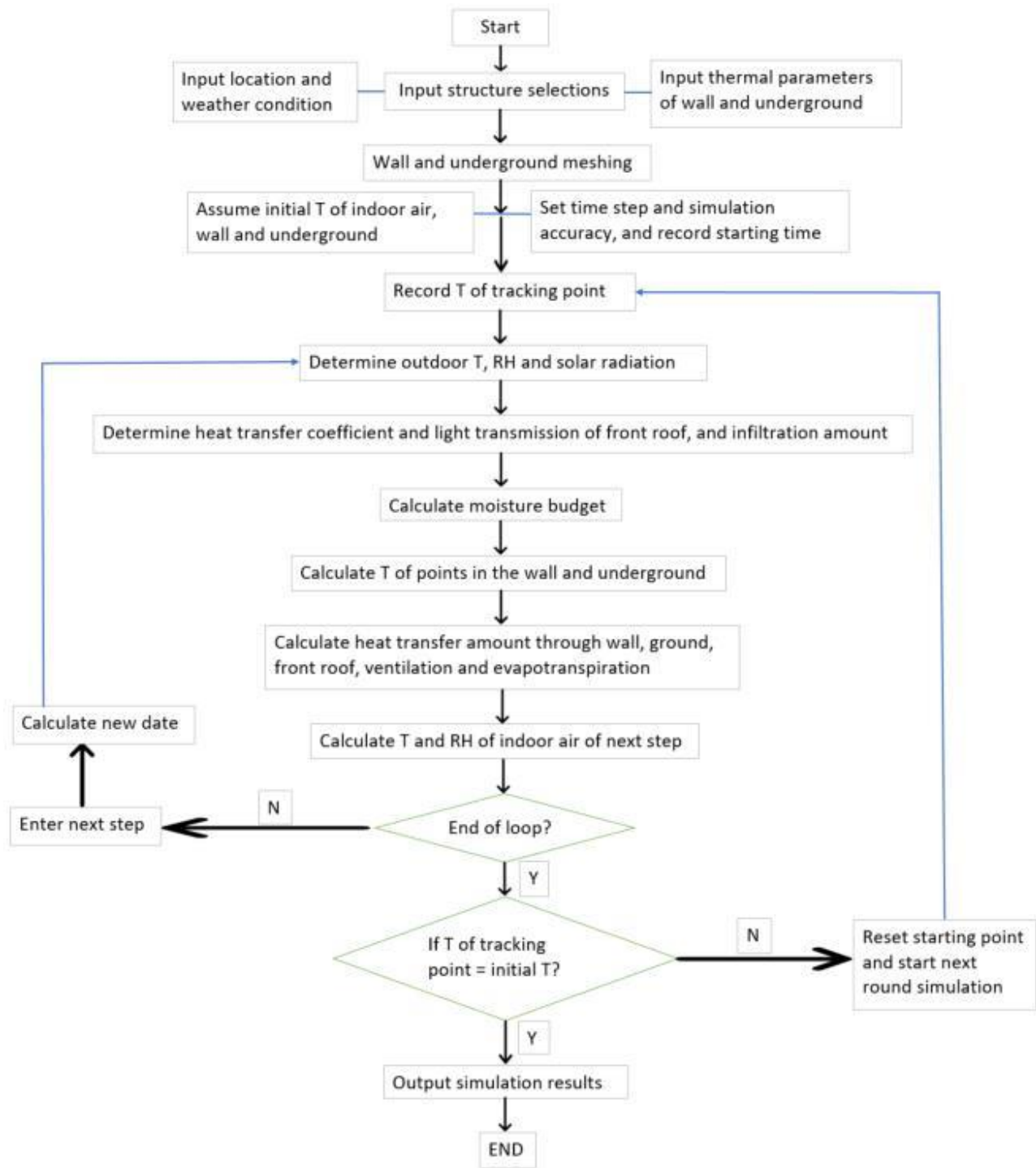
Figure 4.3 The flow chart of thermal environment simulation model in solar greenhouse

4.1.3 Greenhouse dimensions

According to the flow chart above, the structural setting and initial conditions should be inputted by the user. As shown in Fig. 4.1, the greenhouse dimensions can be determined by the following equations:

1) North wall area:

$$A_\text{w} = L_{gh} \sqrt{H_\text{w}^2 + E_\text{w}^2} \tag{4.4}$$

where L_{gh} is the total length of the solar greenhouse, m; H_w is the height of the north wall, m; and E_w is the horizontal projection length of the slant north wall, m.

2) Back/North roof area:

$$A_\text{r} = L_\text{gh} \, H_\text{b} \tag{4.5}$$

where H_b is the height of the back roof, m.

3) Cross-sectional area of the solar greenhouse:

$$A_\text{c} = 0.5 H_\text{b}\cos(B_\text{hr}) H_\text{b}\sin(B_\text{hr}) + 0.5 E_\text{w} H_\text{w} + E_\text{r} H_\text{w} + L_\text{s} H_\text{s} + 0.6 \, (L_\text{s} - E_\text{r}) H_\text{r} \tag{4.6}$$

where B_hr is the included angle between the horizontal plane and the back roof, °; E_r is the horizontal projection length of the back roof, m; L_s is the indoor span of the solar greenhouse, m; H_s is the sinking depth of the solar greenhouse, m; and H_r is the height of the roof ridge, m.

4) Front/South roof area:

$$A_\text{f} = L_\text{gh}[0.6 \sqrt{H_r^2 + (L_s - E_r)^2} + 0.4(H_\text{r} + L_\text{s} - E_\text{r})] \tag{4.7}$$

5) Indoor ground area:

$$A_\text{s} = L_\text{gh} L_\text{s} \tag{4.8}$$

6) Indoor volume:

$$V_\text{gh} = L_\text{gh} A_\text{c} \tag{4.9}$$

4.1.4 Thermal parameter setting

The initial thermal condition is an important factor in the thermal simulation process. A part of the simulation models uses measured data as the initial setting, but this is impractical for RGWSRHJD during the prediction process and because of the unavailability of solar greenhouses. In this model, the default setting of the initial values is based on Chinese solar greenhouse conditions. The initial node temperature of the wall surface and ground surface was 12°C, the indoor air temperature was 15°C and the indoor relative humidity was 80%. Then, the simulation step length (5 s to 30 s) is selected according to the corresponding simulation speed and simulation accuracy (an error control variable of 0.003 to 0.01 can be selected), and the starting moment is recorded. After all of the setting processes are complete, the model simulates the indoor environment according to the input and typical meteorological year data.

4.1.4.1 Front roof cover materials

The material and the degree of ageing both affect the light transmission of the front roof cover. According to Ma and Li (2000) and Zhou (1999), each cover material in the model has a certain light transmission value. The user selects the degree of aging before the simulation, and slight, minor, moderate and major aging have coefficients of 1, 0.95, 0.90 and 0.85, respectively. The light transmission of the cover material will be set to 0 when the thermal blanket covers the front roof at night.

Thus, the total light transmission of the cover material is calculated by the following equation:

$$D_a T_l \left(1 - \sqrt{(S_{hs}^2 + S_{vs}^2)}\right) \tag{4.10}$$

where D_a is the degree of ageing; T_l is the original light transmission of the cover material; S_{hs} is the horizontal shading rate of the front roof frame; and S_{vs} is the vertical shading rate of the front roof frame.

In addition to the light transmission, the heat transfer coefficient of the front roof is a determining factor in the thermal environment change as well. The front roof cover material can be selected before the simulation, and its corresponding heat transfer coefficient (K_{g0}) is a

theoretical value that is measured in the lab conditions (Ma, 2015; Li et al., 2000). According to Ma's field experiments, a correction factor of $f_k = 1.65 + 0.04 \times T_{\min}$ and an exterior surface heat transfer coefficient R_o were introduced in the program (Ma, 2015). Furthermore, based on the thermal design code for civil building (China Academy of Building Research, 2017),

$$K_g = f_k K_{g0} \tag{4.11}$$

$$R_o = 15.32 + 3.84 v_0 \tag{4.12}$$

$$t_p = \left(\frac{1}{K_g}\right) - \left(\frac{1}{23}\right) + \left(\frac{1}{R_o}\right) \tag{4.13}$$

$$K = \frac{1}{t_p} \tag{4.14}$$

where K_{g0} is the theoretical value of the front roof heat transfer coefficient, W/(m^2•K); v_0 is the outdoor wind speed, m/s; $(1/K_g) - (1/23)$ is the sum of the heat transfer resistance of the interior surface and the thermal conduction resistance of the covering material; R_o is the exterior surface heat transfer coefficient under a certain outdoor wind speed, W/(m^2•K); t_p is a temporary parameter, (m^2•K) /W; and K is the overall heat transfer coefficient of the front roof, W/(m^2•K)

4.1.4.2 Air exchange rate calculation

The air exchange including infiltration and ventilation also play a role in the indoor thermal environment. Before the simulation, the user can select the airtightness of the solar greenhouse. According to Dr. Ma's summarization of the previous field experiment, the air exchange rate (V_a, m^3/s) of a solar greenhouse without ventilation can be determined as (Ma, 2015):

$$V_a = \frac{2.25 A_f n_v (0.8 + 0.1 v_o)}{3600} \ (\text{m}^3/\text{s}) \tag{4.15}$$

where A_f is the front roof area, m^2; v_o is the outdoor wind speed, m/s; and n_v is the assumed air exchange rate, times/h. If the thermal blanket covers the front roof at night, n_v is equal to 0.8/h, 0.6/h, 0.45/h, 0.35/h, and 0.25/h when selecting terrible, bad, ordinary, good, and excellent airtightness of the greenhouse, respectively. During the daytime, when the thermal blanket is

rolled up, n_v is equal to 1/h, 0.7/h, 0.5/h, 0.4/h, and 0.3/h with its corresponding airtightness levels (Ma, 2015).

However, during the user-set ventilation period, the ventilation rate determines the air exchange rate and

$$V_a = V_{set}A_s \tag{4.16}$$

where V_{set} is the ventilation rate per unit area that is set by the user, m³/(m²•s); and A_s is the indoor ground area, m².

4.1.4.3 Heat released to indoor air

The model then calculates the heat transferred to the indoor air from the wall, back roof, and ground based on the indoor temperature and,

$$Q_w = \sum a_i(\Delta y)_j L_{gh}(t_{wsj} - t_i) \tag{4.17}$$

$$Q_s = \sum a_i(\Delta y)_j L_{gh}(t_{ssj} - t_i) \tag{4.18}$$

where Q_w is the heat transferred from the wall and back roof to the indoor air, W; Q_s is the heat transferred from the ground to the indoor air, W; a_i is the heat transfer coefficient (includes convection and radiation heat transfer) of the interior surface, W/(m²•K); $(\Delta y)_j$ is the height of the node (i,j), m; L_{gh} is the total length of the solar greenhouse, m; t_{wsj} is the surface temperature of the wall and the back roof, °C; and t_{ssj} is the surface temperature of the ground, °C.

4.1.4.4 Heat absorbed by wall and ground

At the same time, the model will also calculate the solar heat absorbed by each component of the greenhouse. In a real greenhouse production, indoor surfaces may be shaded by nearby structures and plants growing in the solar greenhouse. So, the program considers the following conditions:

1) Heat absorbed by the north wall with direct solar radiation:

$$q_{sun} = a_j T_l S_v H_j \tag{4.19}$$

where a_j is the surface absorptivity of the j segment on the wall; T_l is the light transmission of the front roof; S_v is the solar irradiance on the outside vertical plane that was parallel to the north wall, W/m²; and H_j is the height of the j segment, m.

2) Heat absorbed by the back roof with direct solar radiation:

$$q_{sun} = a_j T_l S_b H_j \tag{4.20}$$

where S_b is the solar irradiance on the outside plane that was parallel to the back roof, W/m².

3) Heat absorbed by the shaded area on the north wall:

$$q_{sun} = a_j T_l S_{dv} H_j \tag{4.21}$$

where S_{dv} is the solar diffuse irradiance on the outdoor plane that was parallel to the north wall, W/m².

4) Heat absorbed by the shaded area on back roof:

$$q_{sun} = a_j T_l S_{db} H_j \tag{4.22}$$

where S_{db} is the solar diffuse irradiance on the outdoor plane that was parallel to the back roof, W/m².

5) Heat absorbed by the ground with direct solar radiation:

$$q_{sun} = a_g T_l S_h L_j \tag{4.23}$$

where a_g is the surface absorptivity of the j segment on the ground; S_h is the solar irradiance on the outdoor horizontal plane, W/m²; and L_j is the width of the j segment, m.

6) Heat absorbed by the shaded area on the ground:

$$q_{sun} = a_g T_l S_{dh} L_j \tag{4.24}$$

where S_{dh} is the solar diffuse irradiance on the outdoor horizontal plane, W/m².

In this section, the coefficient k_p ($k_p = -3k_3^2 + 5k_3 - 1.1$) was calculated by assuming the shaded area with leaves, and k_3 (ranging from 0.8 to 1.2) is the luxuriant degree of plants

selected by the user before the simulation (Ma, 2015). The solar irradiance used to calculate the heat absorbed by the indoor ground was discounted by lowering the light transmission of the front roof ($T_{cl} = k_p T_l$).

The wall, back roof, and ground do not only absorb heat from solar irradiance, but they also have convective heat transfer.

1) Convection heat transfer between the north wall or back roof and indoor air:

$$q_a = h_{cw}(T_j - T_{j0})H_j \tag{4.25}$$

where h_{cw} is the convective heat transfer coefficient between the surface and indoor air, W/(m²•°C); T_j is the ambient air temperature close to the j segment surface, °C; and T_{j0} is the temperature of the node [j][AAnwx[j]+1] , °C.

2) Convective heat transfer between the ground and indoor air:

$$q_a = h_{cg}(T_g - T_{g0})L_j \tag{4.26}$$

where h_{cg} is the convective heat transfer coefficient between the ground and indoor air, W/(m²•°C); T_g is the ambient air temperature close to the j segment surface, °C; T_{g0} is the temperature of the node [j][0], °C; and L_j is the width of the j segment, m.

4.1.4.5 Heat loss through each component

Compared to the heat gain in the solar greenhouse, heat loss is another determining factor in the thermal environment of solar greenhouses. Heat loss may occur through conduction and convection heat transfer, ventilation, infiltration as well as evapotranspiration.

1) Heat loss through the front roof can be calculated as:

$$Q_g = KA_f(t_i - t_o) \tag{4.27}$$

where K is the overall heat transfer coefficient of the front roof, W/(m²•K).

2) Heat loss from air exchange by ventilation and infiltration:

$$Q_v = L\rho C_p(t_i - t_o) \tag{4.28}$$

where L is the air exchange rate through ventilation and infiltration calculated by the setting value, m^3/s.

3) Heat loss from evapotranspiration:

$$Q_e = rA_s(G_w - G_d) \tag{4.29}$$

where G_w is the total amount of evapotranspiration, including plants' transpiration, kg/(m^2•s); G_d is the total condensation amount, kg/(m^2•s); r is the evaporation latent heat of water, 2442 kJ/kg; A_s is the indoor ground area, m$_2$; and Q_e is the heat loss from evapotranspiration, W.

4.1.4.6 Indoor thermal parameters in next step

After calculating the above thermal transfer process in each step, the model turns to calculate the indoor air thermal condition. The change in air temperature t_i was determined by the indoor air, plants, and building materials. So, the total heat balance, whether there is heat gain or loss during the next simulation step, is affected by the air, plants, and building materials,

$$t_i = t_i + \frac{Q_t t_s}{m_p c_p A_s + m_c c_c A_s + \rho c_a V_{gh}} \tag{4.30}$$

where t_s is the simulation step size, s; m_p is the plants' mass per unit area, ranging from 1.5 to 15, kg/m^2; c_p is the average specific heat of plants, 3000 J/(kg•K); m_c is the mass of the steel construction materials per unit area, 8 kg/m^2; c_c is the specific heat of steel construction materials, 470 J/(kg•K); ρ is the air density, 1.2 kg/m^3; c_a is the specific heat of indoor air, 1030 J/(kg•K); and V_{gh} is the indoor volume, m^3 (Ma, 2015).

Relative humidity ϕ can be calculated with the following equation:

$$\phi = \frac{p_w}{p_{ws}} \tag{4.31}$$

where p_w is the water vapor pressure of indoor air, Pa; and p_{ws} is the saturated water vapor pressure of indoor air, Pa, and if $p_s > p_{ws}$, the return relative humidity equals 1.

4.1.4.7 Pre-simulation complete judgement

Next, the model runs continuously, and the node temperature, indoor air temperature and relative humidity at the final moment return to the initial parameter setting. After several simulation cycles, the periodical change in temperature distribution gradually becomes stable, eliminating the effect of the program's initial thermal environment settings. When the following three conditions are simultaneously met, the model can begin to simulate using the satisfied initial thermal parameter setting:

$$\begin{cases} N_c \geq N_{min} \\ |t_{w0} - t_w| \leq e \\ |t_{i0} - t_i| \leq e \end{cases} \tag{4.32}$$

where N_c is the number of simulation cycles; N_{min} is the minimum simulation cycle, 6~12 cycles; t_{w0} is the temperature of the monitoring point on the north wall surface at the beginning moment, °C; t_w is the temperature of the monitoring point on the north wall surface at the final moment, °C; t_{i0} is the initial indoor air temperature, °C; and e is the error control variable which is set by the user before the simulation, 0.003 is the most accurate setting, 0.006 the accurate setting and 0.01 a moderate setting (Ma, 2015).

4.1.4.8 Output simulation results

Finally, after the simulation process is complete, the model output shows the thermal environment condition of the solar greenhouse, including the indoor air temperature, RH, and other thermal parameters for the entire simulation period. It also shows the hourly and daily energy consumption, heat transfer amounts from each component, greenhouse work schedules, wall temperature in different depths, ground temperature in different depths, and so on.

4.2 Model Operation

The thermal simulation model operates in a user-friendly way. Users need to input weather data and the construction parameters of a solar greenhouse. Then, they need to select simulation parameters before the simulation. Figure 4.4 shows the initial interface of the

simulation model. It contains weather condition settings, greenhouse construction design, construction materials selection, indoor environment control, etc. All figures in the section are shown using the modified model SOGREEN.
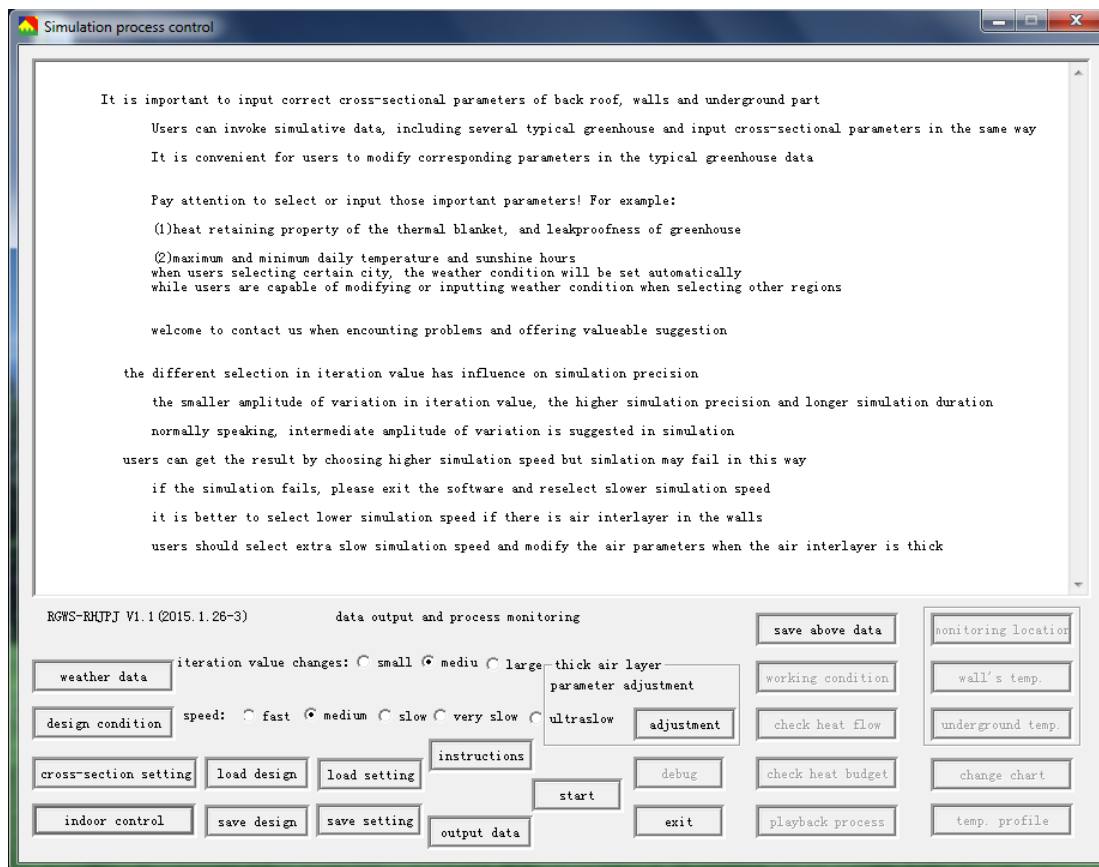
Figure 4.4 Initial interface of simulation model

The first step is to invoke outdoor weather conditions. In this section, there are three types of outdoor weather conditions, including user-defined weather conditions, measured weather conditions, and built-in weather conditions. The first type is weather conditions that are collected in a specific format by the user. The second type is measured data collected from field experiments. The final type is calculated with weather conditions from several Chinese cities. Figure 4.5 illustrates the weather condition setting interface. In the following simulation portion, typical meteorological year data were collected as user-defined weather conditions. The simulation period, location (latitude and longitude), and elevations are also needed to input this interface.
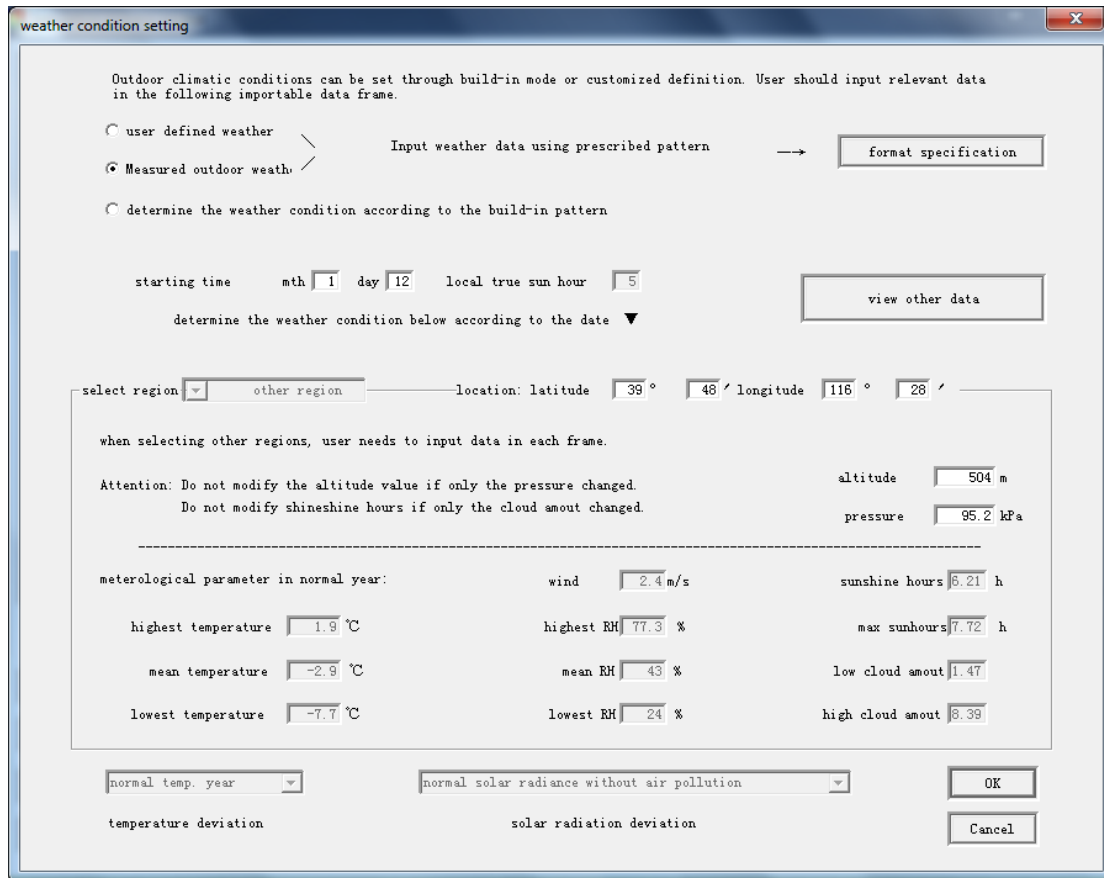
Figure 4.5 Weather condition interface

The next step is to set the solar greenhouse design conditions, including the greenhouse structural information, plant information, and the building material condition. The greenhouse length can be designed from 2 m to 300 m, depending on the requirements of the greenhouses and their sizes. The front roof cover material selection consists of plastic films, glass, PC board, a PS pellet insulation system and a double-layer inflated film. All can be used in cold regions. Considering that the degree of aging may affect the rate of light transmission of cover materials, the model allows users to select the degree of aging based on their own judgment. The thermal blanket is also an important part in the heat preservation of the greenhouse and so, a wide range of thermal properties of the thermal blanket is provided in the model from RSI-3.0 to RSI-0.5. Furthermore, greenhouses cannot be built completely airtight, and this may lead to air leakage. Users can select the airtightness of the greenhouse according to their judgment, and this selection determines the air exchange rate. The ground floor and wetness level can affect the evaporation rate and the indoor thermal environment. So, users also need to select the indoor floor type from the soil, mulch, and concrete floor, as well as its wetness level.

31

Then, based on the plant condition, users need to select the plant density among very sparse, sparse, ordinary, dense, and very dense to determine the plant mass per unit area, which will be used in the transpiration calculation. Finally, the plant height and distance to the north wall play a role in calculating the shaded area on the north wall. Figure 4.6 shows the interface for inputting of the above parameters.
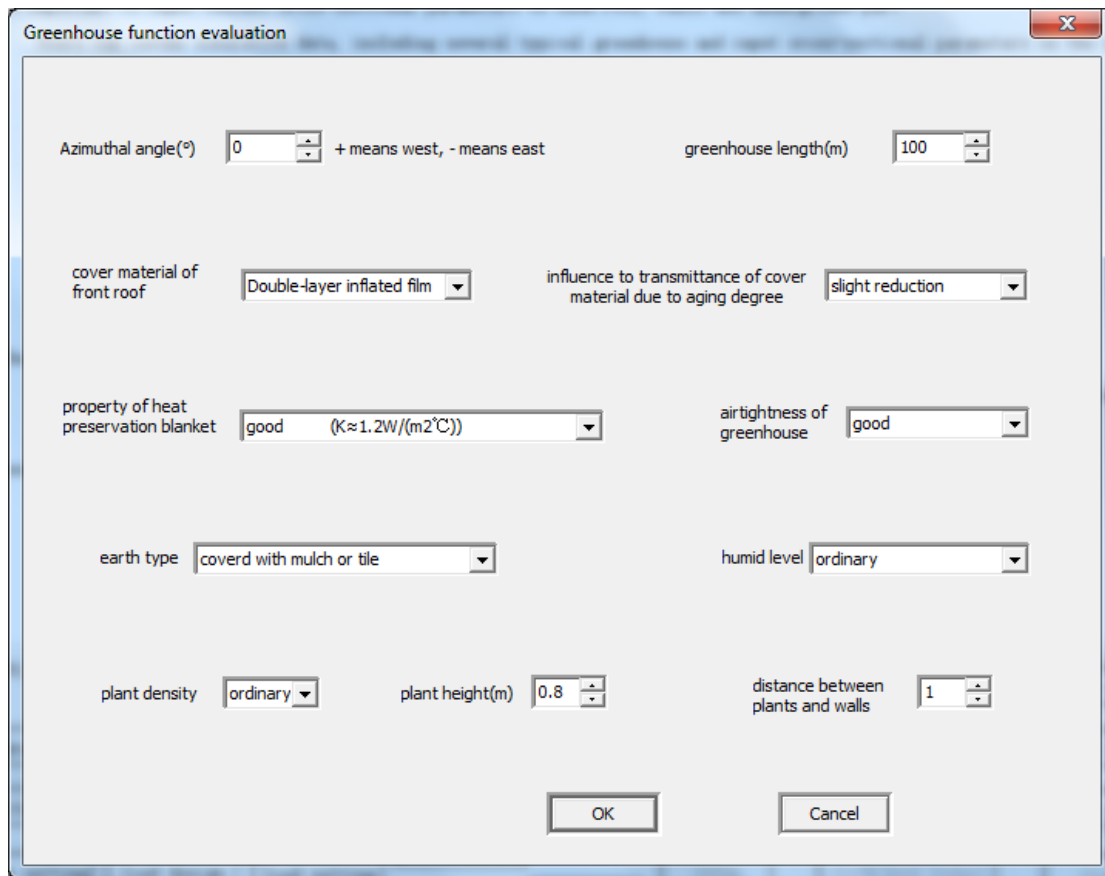
Figure 4.6 Greenhouse design condition interface

The next step is to design a solar greenhouse structure and set thermal parameters for the building materials. In this section, the dimensions and building materials are set for the back roof, north wall and floor. For example, for the north wall as shown in Fig. 4.7 and Fig. 4.8, users input the segment lengths in the north wall and the thermal parameters of the building material. This includes density, thermal conductivity, and specific heat.
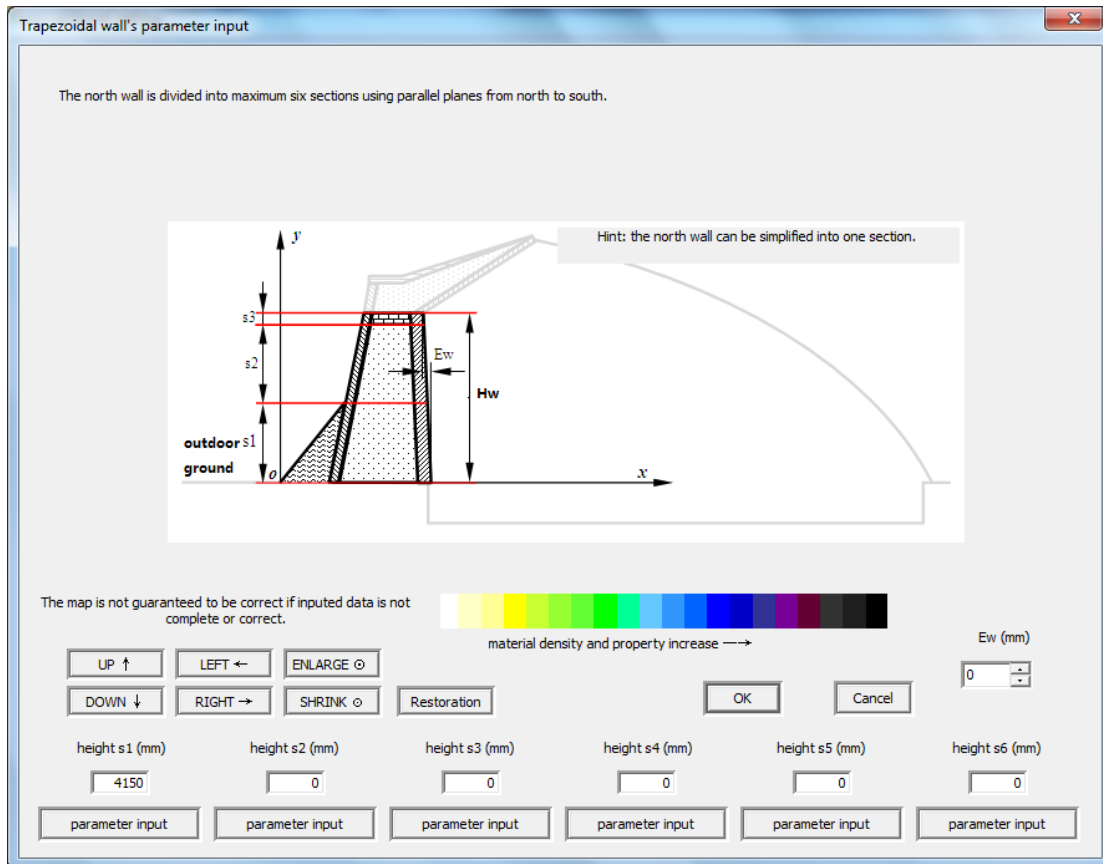
Figure 4.7 Segment length input of north wall
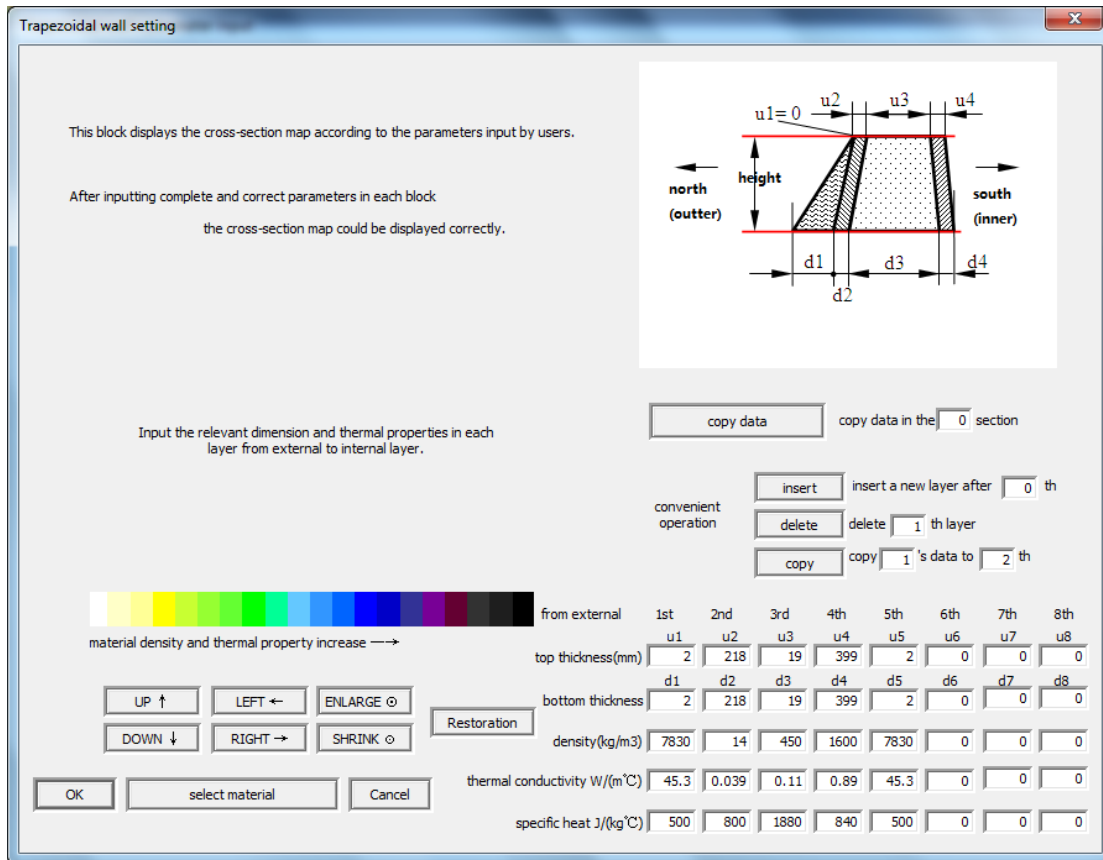
Figure 4.8 Thermal parameter setting of building materials

The model has a built-in material library that facilitates users to find commonly used materials. The material library contains the thermal parameters of each construction material and users can select and invoke material to a particular layer. Figure 4.9 shows the material library.
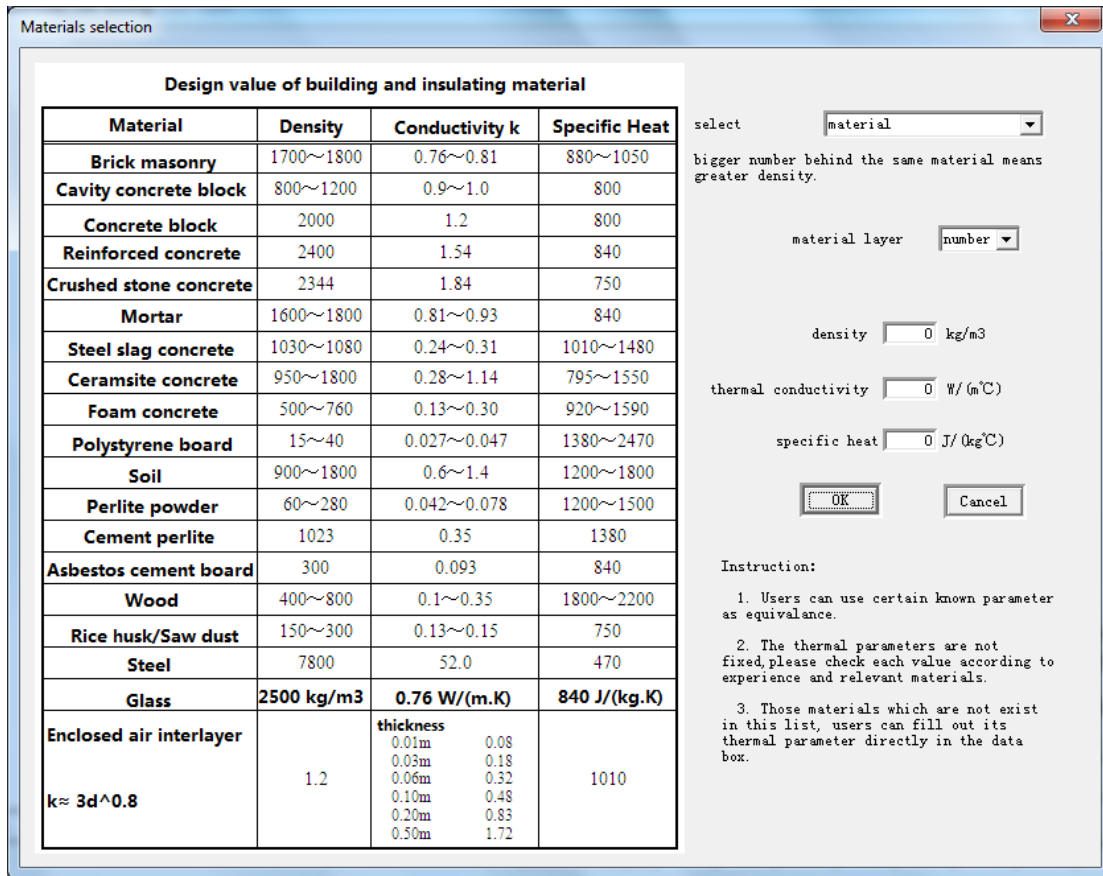
Figure 4.9 Building material library

When all of the detail values are inputted, the model will automatically show the greenhouse dimensional parameters such as the ridge height, the width of the back roof, wall height, thickness and span. Figure 4.10 illustrates the interface of the structural setting.
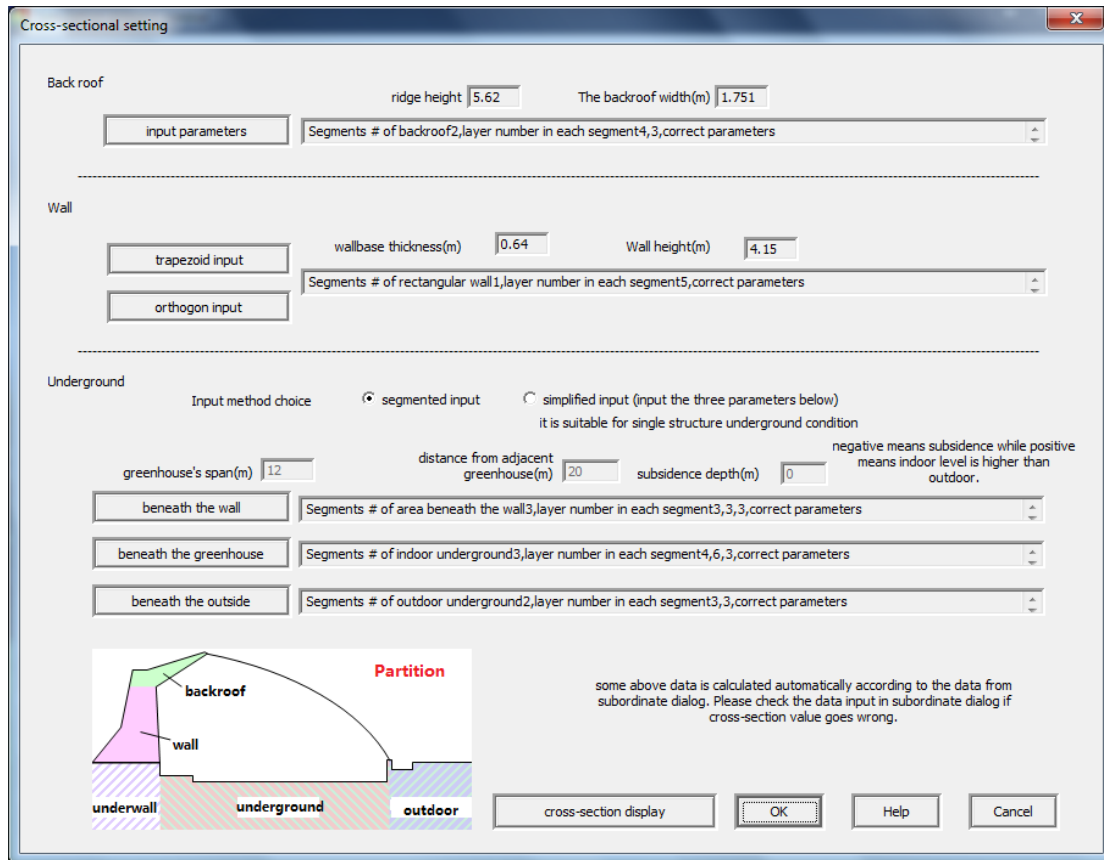
Figure 4.10 Interface of structural setting

The next step is the greenhouse work schedule setting. It contains a thermal blanket cover, an uncover schedule, a supplemental heating schedule, a set point, a ventilation rate and schedule. In the first part, the model can automatically cover and uncover the thermal blanket based on whether the outdoor horizontal solar radiation is higher than 80 W/m^2 or not. The thermal blanket uncovers in the morning when the outdoor solar radiation rises to 80 W/m^2 and it covers at sunset when the solar radiation drops below 80 W/m^2. Users can also assign its work schedule for each simulation day. No supplemental heating schedule, indoor temperature set-point, and heating power are included in the model. In Section 4.4 of Model Validation, the third pattern (heating power) was used because the hourly heating power of the electrical heater was known. Section 4.5, Simulation in Saskatoon, used a temperature set-point schedule. The last part, the Ventilation schedule, sets the ventilation rate and schedule. In the cold months, the solar greenhouse normally only relies on infiltration when the temperature is low and it employs a high ventilation rate by opening all vents during the daytime when temperatures are too high. Figure 4.11 shows the interface of the greenhouse work schedule.

Indoor environmental control setting

Blanket

☐ inner thermal blanket ☐ inner shield cover

cover method choice ○ automatically judge ↗solar radiance > [0] W/m2 uncover ● assign cover time assign daily cover time
↘solar radiance < [0] W/m2 cover

	day1	day2	day3	day4	day5	day6	day7	day8	day9
uncover moment (h, m)	8 30	8 30	8 30	8 30	8 30	8 30	0 0	0 0	0 0
cover moment (h, m)	18 0	18 0	18 0	18 0	18 0	18 0	0 0	0 0	0 0

Attention: In the automatically judge, cover shedule will change with different geographical and meteorological condition

heating condition

heating control: ○ No heating ● set indoor temperature ○ set heating quantity

(24 hour time-system)

1st time frame: [0] h [0] m to [24] h [0] m temp. setting [18]℃ heating watt per unit area [70] W/m2 total watt [___] W
2nd time frame: [0] h [0] m to [0] h [0] m temp. setting [0]℃ heating watt per unit area [0] W/m2 total watt [___] W
3rd time frame: [0] h [0] m to [0] h [0] m temp. setting [0]℃ heating watt per unit area [0] W/m2 total watt [___] W
4th time frame: [0] h [0] m to [0] h [0] m temp. setting [0]℃ heating watt per unit area [0] W/m2 total watt [___] W
5th time frame: [0] h [0] m to [0] h [0] m temp. setting [0]℃ heating watt per unit area [0] W/m2 total watt [___] W
6th time frame: [0] h [0] m to [0] h [0] m temp. setting [0]℃ heating watt per unit area [0] W/m2 total watt [___] W

Ventilation set

(24 hour time-system)

1st time frame: [10] h [0] m to [11] h [0] m ventilation rate [3] m3/(m2h) total rate [3600] m3/h
2nd time frame: [13] h [30] m to [15] h [30] m ventilation rate [10] m3/(m2h) total rate [12000] m3/h
3rd time frame: [0] h [0] m to [0] h [0] m ventilation rate [0] m3/(m2h) total rate [0] m3/h
4th time frame: [0] h [0] m to [0] h [0] m ventilation rate [0] m3/(m2h) total rate [0] m3/h
5th time frame: [0] h [0] m to [0] h [0] m ventilation rate [0] m3/(m2h) total rate [0] m3/h
6th time frame: [0] h [0] m to [0] h [0] m ventilation rate [0] m3/(m2h) total rate [0] m3/h

[time division] [OK] [Cancel]

Default setting is zero ventilation condition. Ventilation rate generally set from 5 to 100m3/(m2h) according to the field temperature.

Figure 4.11 Interface of greenhouse work schedule

After all of the settings are done, the user can start the simulation process, which generally takes 15 min to 90 min depending on the selected simulation speed (shown in Fig. 4.4). Then, the model outputs the following results to demonstrate the indoor thermal environment.

51.txt - Notepad
File Edit Format View Help

1 cycle: temp. of tracepoint 20.99907 ℃ 17.99961 ℃ simulating progress = 0 %
2 cycle: temp. of tracepoint 21.56469 ℃ 17.99981 ℃ simulating progress = 2 %
3 cycle: temp. of tracepoint 21.74729 ℃ 17.99959 ℃ simulating progress = 8 %
4 cycle: temp. of tracepoint 21.84447 ℃ 17.99956 ℃ simulating progress = 14 %
5 cycle: temp. of tracepoint 21.90714 ℃ 17.99961 ℃ simulating progress = 21 %
6 cycle: temp. of tracepoint 21.95138 ℃ 17.99974 ℃ simulating progress = 28 %
7 cycle: temp. of tracepoint 21.98423 ℃ 17.99987 ℃ simulating progress = 37 %
8 cycle: temp. of tracepoint 22.00829 ℃ 17.99988 ℃ simulating progress = 49 %
9 cycle: temp. of tracepoint 22.02573 ℃ 17.99983 ℃ simulating progress = 65 %
10 cycle: temp. of tracepoint 22.03833 ℃ 18.00000 ℃ simulating progress = 89 %
11 cycle: temp. of tracepoint 22.04693 ℃ 17.99947 ℃ simulating progress = 100 %

Simulation and calculation start

======= The following part shows hourly parametric change during the simulation period =======

date	time	blanket 1=uncover 2=cover	outd temp ℃	ind temp ℃	indoor wall temp ℃	indoor ground temp ℃	outdoor horizontal irradiance W/m2	outdoor vertical irradiance W/m2	wall indoor releaseheat W/m2	undgrnd indoor releaseheat W/m2	unitarea supheating heatflux W/m2	greenhouse heating power kW	indoor relative humidity %
3m25d	5.00h	2	-9.20	18.00	21.63	22.51	0.0	0.0	31.31	38.18	24.0	28.8	89.1
3m25d	6.00h	2	-9.40	18.00	21.39	22.23	0.0	0.0	29.24	35.72	21.1	25.3	92.4
3m25d	7.00h	2	-10.10	18.00	21.19	21.98	-0.0	-0.0	27.47	33.55	31.1	37.4	90.9
3m25d	8.00h	2	-8.80	18.00	21.01	21.76	67.0	5.3	25.94	31.72	29.9	35.9	91.1
3m25d	9.00h	1	-7.60	18.00	21.40	24.80	174.0	45.5	29.37	58.33	28.1	33.7	88.5
3m25d	10.00h	1	-5.30	20.75	23.70	29.81	341.0	145.8	25.40	77.94	0.0	0.0	84.1
3m25d	11.00h	1	-3.30	26.18	27.45	34.80	408.0	214.4	10.48	73.49	0.0	0.0	88.0
3m25d	12.00h	1	-1.10	28.01	31.15	39.50	500.0	289.3	26.46	98.04	0.0	0.0	83.4
3m25d	13.00h	1	-1.00	26.32	33.64	42.19	531.0	317.2	62.56	135.69	0.0	0.0	70.5
3m25d	14.00h	1	-1.70	25.54	34.45	43.22	541.0	316.4	76.29	151.34	0.0	0.0	66.4
3m25d	15.00h	1	-1.20	24.95	34.15	42.69	475.0	256.1	78.92	151.90	0.0	0.0	66.5

Figure 4.12 Simulation result output interface

Figure 4.13 (51.txt - Notepad):

date	time	blanket 1=uncover 2=cover	outd temp ℃	ind temp ℃	indoor wall temp ℃	indoor ground temp ℃	outdoor horizontal irradiance W/m2	outdoor vertical irradiance W/m2	wall indoor releaseheat W/m2	undgrnd indoor releaseheat W/m2	unitarea supheating heatflux W/m2	greenhouse heating power kW	indoor relative humidity %
3m26d	2.00h	2	-9.10	18.00	21.41	22.24	0.0	0.0	29.40	35.83	29.1	35.0	90.1
3m26d	3.00h	2	-9.40	18.00	21.19	21.97	0.0	0.0	27.42	33.46	37.6	45.1	88.8
3m26d	4.00h	2	-9.70	18.00	20.99	21.74	0.0	0.0	25.75	31.45	39.1	46.9	89.3

Total heating power = 360.2

date	time	blanket 1=uncover 2=cover	outd temp ℃	ind temp ℃	indoor wall temp ℃	indoor ground temp ℃	outdoor horizontal irradiance W/m2	outdoor vertical irradiance W/m2	wall indoor releaseheat W/m2	undgrnd indoor releaseheat W/m2	unitarea supheating heatflux W/m2	greenhouse heating power kW	indoor relative humidity %
3m26d	5.00h	2	-9.40	18.00	20.83	21.54	0.0	0.0	24.30	29.72	40.5	48.6	89.4
3m26d	6.00h	2	-9.60	18.00	20.68	21.37	0.0	0.0	23.04	28.21	42.9	51.5	89.3
3m26d	7.00h	2	-9.90	18.00	20.55	21.22	-0.0	-0.0	21.92	26.86	45.3	54.4	89.1
3m26d	8.00h	2	-9.00	18.00	20.44	21.08	117.0	9.2	20.91	25.73	46.4	55.7	89.0
3m26d	9.00h	1	-7.80	18.00	21.26	26.41	277.0	72.7	28.15	72.40	14.0	16.8	84.5
3m26d	10.00h	1	-5.70	21.28	24.10	31.83	431.0	184.5	24.17	90.62	0.0	0.0	80.7
3m26d	11.00h	1	-4.00	26.93	28.88	38.50	557.0	293.0	16.36	98.66	0.0	0.0	83.8
3m26d	12.00h	1	-3.10	30.57	33.68	44.38	644.0	373.0	26.10	117.73	0.0	0.0	83.7
3m26d	13.00h	1	-2.10	29.61	37.49	48.72	683.0	408.4	67.20	163.37	0.0	0.0	72.9
3m26d	14.00h	1	-1.50	25.20	35.22	43.66	450.0	263.4	86.00	157.80	0.0	0.0	68.4
3m26d	15.00h	1	-1.50	25.51	35.20	44.33	486.1	262.3	83.10	161.07	0.0	0.0	67.3
3m26d	16.00h	1	-1.40	22.65	30.63	35.67	142.0	64.1	68.52	110.95	0.0	0.0	86.0
3m26d	17.00h	1	-2.30	24.06	29.76	36.54	271.0	81.8	48.80	106.98	0.0	0.0	85.7
3m26d	18.00h	1	-2.60	23.27	28.03	34.90	186.0	14.2	40.78	99.94	0.0	0.0	89.7
3m26d	19.00h	1	-4.20	18.54	25.64	29.50	39.0	3.5	61.32	93.79	0.0	0.0	91.4
3m26d	20.00h	2	-4.40	19.87	24.55	26.83	0.0	0.0	40.34	59.26	0.0	0.0	89.9
3m26d	21.00h	2	-4.30	19.11	23.69	25.43	0.0	0.0	39.45	53.83	0.0	0.0	90.3
3m26d	22.00h	2	-4.60	18.38	22.89	24.32	0.0	0.0	38.87	50.54	0.0	0.0	90.7
3m26d	23.00h	2	-4.90	18.00	22.22	23.46	0.0	0.0	36.43	46.44	13.9	16.7	88.3
3m26d	24.00h	2	-5.20	18.00	21.79	22.93	0.0	0.0	32.72	41.79	18.1	21.7	88.9
3m27d	1.00h	2	-5.70	18.00	21.47	22.52	0.0	0.0	29.89	38.25	29.2	35.1	87.3
3m27d	2.00h	2	-5.80	18.00	21.20	22.19	0.0	0.0	27.62	35.41	27.5	33.0	89.1
3m27d	3.00h	2	-5.60	18.00	20.99	21.92	0.0	0.0	25.73	33.05	34.9	41.9	87.7
3m27d	4.00h	2	-5.30	18.00	20.80	21.69	0.0	0.0	24.14	31.06	36.0	43.2	87.9

Total heating power = 418.7

date	time	blanket 1=uncover 2=cover	outd temp ℃	ind temp ℃	indoor wall temp ℃	indoor ground temp ℃	outdoor horizontal irradiance W/m2	outdoor vertical irradiance W/m2	wall indoor releaseheat W/m2	undgrnd indoor releaseheat W/m2	unitarea supheating heatflux W/m2	greenhouse heating power kW	indoor relative humidity %
3m27d	5.00h	2	-5.00	18.00	20.64	21.50	0.0	0.0	22.76	29.35	38.6	46.3	87.6
3m27d	6.00h	2	-5.20	18.00	20.51	21.32	0.0	0.0	21.56	27.85	41.4	49.7	87.3
3m27d	7.00h	2	-5.30	18.00	20.38	21.17	-0.0	-0.0	20.50	26.53	37.9	45.5	89.0

Figure 4.13 Daily simulation results

Figure 4.14 (52.txt - Notepad):

1day   uncover moment in the morning is   8h 0min and cover moment is   19h 0min

ventilation is arrange from 11h 0min to 12h 0min,and total ventilation rate is 3600m3/h

ventilation is arrange from 12h 30min to 15h 30min,and total ventilation rate is12000m3/h

date	time	cloud	blanket 1=u 2=c	shadow on the wall m	frontroof transmittance	front roof HTC W/m2℃	outdoor windspeed m/s	ventilation or infiltration m3/s	heat flux pua W/m2	total heating power kW	indoor RH %
3m25d	5.00h	1.00	2	8.537	0.000	1.671	1.90	0.289	24.0	28.8	89.14
3m25d	6.00h	1.00	2	19.724	0.000	1.652	1.10	0.266	21.1	25.3	92.38
3m25d	7.00h	1.00	2	20.000	0.000	1.699	3.60	0.339	31.1	37.4	90.93
3m25d	8.00h	1.00	2	20.000	0.000	1.692	3.10	0.324	29.9	35.9	91.10
3m25d	9.00h	1.00	1	0.000	0.618	4.435	1.90	0.331	28.1	33.7	88.51
3m25d	10.00h	1.00	1	0.000	0.618	4.435	1.90	0.331	0.0	0.0	84.10
3m25d	11.00h	1.00	1	0.000	0.618	4.056	-0.00	0.267	0.0	0.0	87.95
3m25d	12.00h	1.00	1	0.000	0.618	4.694	4.20	0.408	0.0	0.0	83.38
3m25d	13.00h	1.00	1	0.000	0.618	4.694	4.20	3.333	0.0	0.0	70.46
3m25d	14.00h	1.00	1	0.000	0.618	4.694	4.20	3.333	0.0	0.0	66.36
3m25d	15.00h	1.00	1	0.000	0.618	4.735	4.70	3.333	0.0	0.0	66.49
3m25d	16.00h	1.00	1	0.000	0.618	4.694	4.20	0.408	0.0	0.0	85.79
3m25d	17.00h	1.00	1	0.000	0.618	4.778	5.30	0.444	0.0	0.0	94.53
3m25d	18.00h	1.00	1	20.000	0.618	4.864	6.70	0.491	0.0	0.0	92.89
3m25d	19.00h	1.00	1	20.000	0.618	4.864	6.70	0.491	0.0	0.0	93.15
3m25d	20.00h	1.00	2	20.000	0.000	1.717	5.30	0.389	0.0	0.0	91.06
3m25d	21.00h	1.00	2	10.350	0.000	1.731	7.20	0.444	0.0	0.0	91.48
3m25d	22.00h	1.00	2	0.800	0.000	1.738	8.30	0.476	0.0	0.0	90.35
3m25d	23.00h	1.00	2	0.800	0.000	1.720	5.60	0.397	13.9	16.6	89.76
3m25d	24.00h	1.00	2	0.800	0.000	1.720	5.60	0.397	20.7	24.9	89.81
3m26d	1.00h	1.00	2	0.800	0.000	1.720	5.60	0.397	25.6	30.7	89.81
3m26d	2.00h	1.00	2	0.800	0.000	1.717	5.30	0.389	29.1	35.0	90.14
3m26d	3.00h	1.00	2	0.800	0.000	1.735	7.80	0.462	37.6	45.1	88.81
3m26d	4.00h	1.00	2	0.800	0.000	1.728	6.70	0.430	39.1	46.9	89.25

Figure 4.14 Daily simulation results with hourly greenhouse work condition

4.3 Model Modifications

The previous version RGWSRHJ was developed by Dr. Ma in China. It intends to evaluate the design scheme of a solar greenhouse, predict its thermal environment, and provide greenhouse operation guides to greenhouse growers for weather conditions like China. So, it

is inevitable that some limits may exist due to weather differences between Canada and China. For instance, although the Canadian Prairies are the sunniest region in Canada, the extremely cold weather in the winter and the high wind speed drive the energy consumption up. So, various supplemental heating technologies are used in the greenhouses. Thus, the first and most important part of this research is to modify this simulation model and make it suitable for the conditions in Canada, especially in Saskatchewan.

4.3.1 Translation and location

Dr. Ma initially developed the simulation model in a Chinese environment. So, the first step was to translate the model into an English environment to make it usable in Canada. After several attempts with various translation methods, the best way was found to be to translate each string in the string table because of the following reasons. First, building a string table can avoid a repeated translation process for the same string. This significantly saves time and the work load. Second, the code is less likely to fail by connecting the inherent ID of each string to the translated string. Finally, it is easier to translate the simulation model into other languages by making changes directly in the string table. Figure 4.15 shows the interface of the string table.
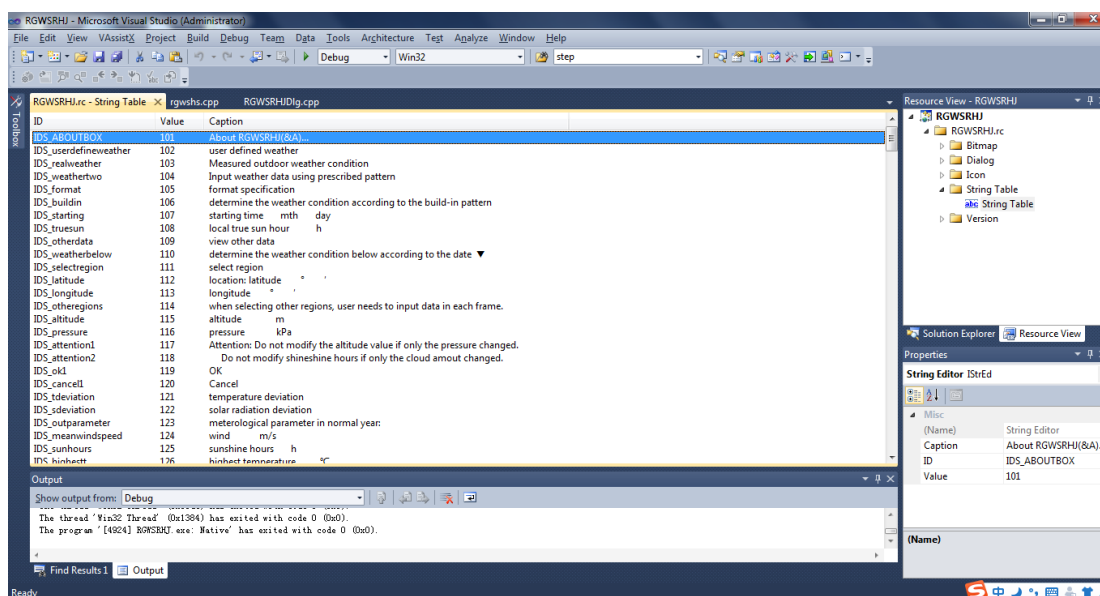
Figure 4.15 Interface of the string table

The simulation model limits the simulation location in 15°~60° N, 0°~179° E. However, the Canadian Prairies are not located in this range. So, the simulation location was extended to 0°~90° N, -179°~179° E. This makes the simulation model applicable in Canada.

4.3.2 Typical meteorological year data of Saskatoon

In the original model, the weather condition function calculates each weather parameter for simulation use, and this function was built based on the measurements at many weather stations in China. Thus, the calculated weather conditions cannot be applied in Canada. To solve this problem, Saskatoon's typical meteorological year data were downloaded from Environment Canada (Environment Canada, 2017) and it was organized in the required format for the simulation model. The typical meteorological year data are generally used in building simulations for calculating the expected heating and cooling loads for a building. For a particular location, typical meteorological year data are selected from a data bank to present the weather conditions. It contains location information, the hourly dry bulb temperature, dew point, relative humidity, pressure, wind speed, cloud cover and other information (Samuel, 2016). Among the information selected in the typical meteorological year data, the hourly outdoor temperature, RH, solar radiation, and wind speed were organized in the specific format used in the simulation model.

4.3.3 Solar-related calculation

The original simulation model RGWSRHJ used a simplified calculation method to determine solar radiation. To allow SOGREEN to give an accurate solar energy value, the solar irradiance calculations were updated. The beam and diffuse optical depths τ_b and τ_d were inputted, and the extraterrestrial radiant flux E_o of each month were updated according to 2013 ASHRAE Handbook (ASHRAE, 2013). Solar declination is expressed as

$$\Delta = 23.45\sin\left(360°\frac{n+284}{365}\right) \qquad (4.33)$$

where n is the day of the year, $n = 1$ means January 1 and $n = 32$ means February 1.

40

The solar altitude angle β is calculated as

$$\sin\beta = \cos L \cos\delta \cos H + \sin L \sin\delta \qquad (4.34)$$

where L is the local latitude, °N; and H is the hour angle.

The azimuth angle ϕ is calculated with the following equations:

$$\begin{cases} \sin\varphi = \dfrac{\sin H \cos\delta}{\cos\beta} \\ \cos\varphi = \dfrac{\cos H \cos\delta \sin L - \sin\delta \cos L}{\cos\beta} \end{cases} \qquad (4.35)$$

Finally, the air mass exponent variables ab and ad are used to calculate solar radiation on a clear day.

$$ab = 1.454 - 0.406\,\tau_b - 0.268\,\tau_d + 0.021\,\tau_b\tau_d \qquad (4.36)$$

$$ad = 0.507 + 0.205\,\tau_b - 0.080\,\tau_d - 0.190\,\tau_b\tau_d \qquad (4.37)$$

$$E_b = E_o \exp[-\tau_b m^{ab}] \qquad (4.38)$$

$$E_d = E_o \exp[-\tau_d m^{ad}] \qquad (4.39)$$

where ab and ad are beam and diffuse air mass exponents; E_b is the beam normal irradiance which is measured perpendicularly to the rays of the sun, W/m^2; E_d is the diffuse horizontal irradiance which is measured on a horizontal surface; and m is air mass, W/m^2.

The following Figure 4.16 shows the updated equations in the code.
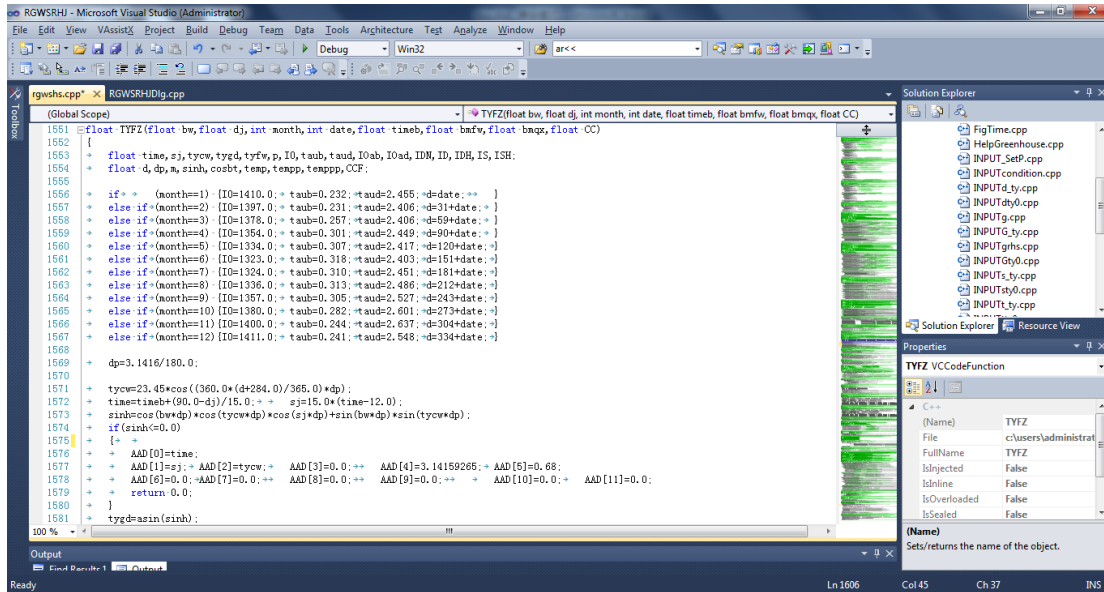
Figure 4.16(a) Codes for the solar related calculation
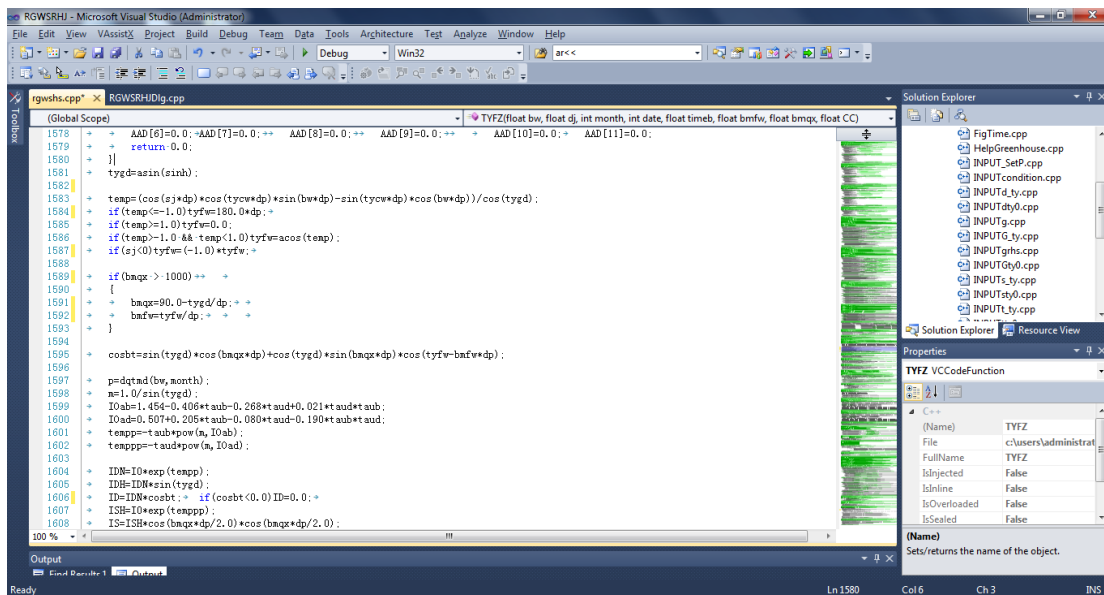
Figure 4.16(b) Codes for the solar related calculation

4.3.4 Wind speed

Based on Saskatoon's typical meteorological year data (Environment Canada, 2017), the maximum wind speed throughout the year was 16.9 m/s and the monthly average and maximum wind speed is shown in Fig. 4.17. The average wind speed was greater than 5 m/s

42

in April, May, and September, which means that the mild months were windier than the cold and warm months. While previous versions of the simulation model limited the wind speed to 10 m/s in the weather condition setting, this does not represent the windy weather conditions in the Canadian Prairies. Thus, the wind speed restriction was changed from 10 m/s to 17 m/s in order to get the typical meteorological year data.
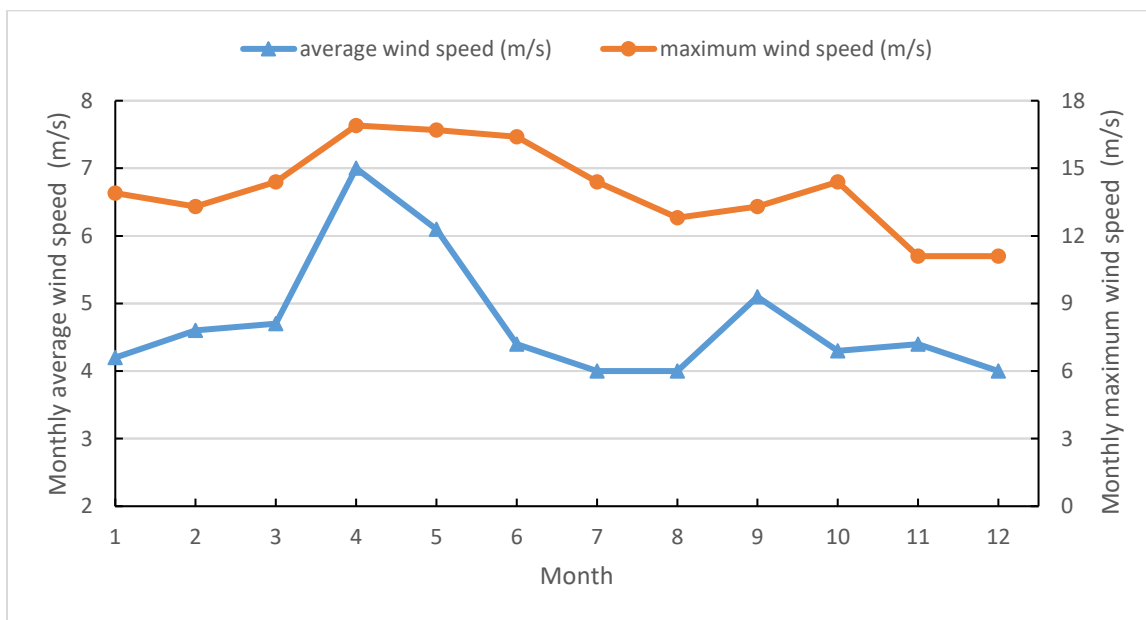
Figure 4.17 Monthly average and maximum wind speed in Saskatoon

4.3.5 Exterior high insulation front roof cover

Short and Shah (1981) reported on the portable polystyrene (PS)-pellet insulation system for greenhouses. Polystyrene pellets were pumped into the interlayer which had an average thickness of 13 cm between the double layer plastic films of the front roof at sunset. They were removed at sunrise. Thus, according to the field measurement, the U value of the front roof during the daytime was 4.0 W/(m^2•K) and 0.3 W/(m^2•K) at night. This reduced the night supplemental heating requirement by 80-90%. To allow the simulation of this insulation technology, the SOGREEN added a new selection, the PS pellet, in the front roof cover material box. It inputted its corresponding thermal parameter in the code.

In addition to the PS-pellet insulation system, the double-layer inflated cover is another common front roof cover that is used in Canadian greenhouses. It has a good insulation value

and it is simple to operate. The whole system consists of a double layer plastic film, holding clamp, air blower, check valve, inflation hose, and control system (Li, 2000). Garzoli and Blackwell (1987) calculated the theoretical heat transfer coefficient of the double-layer inflated cover as 3.85 W/(m^2•K). According to Li (2000), the overall heat transfer coefficient of a 6 cm thick double-layer inflated cover was 4.45 W/(m^2•K), and the heat transfer coefficient did not fluctuate much when the air layer thickness was changed. However, the light transmission rate was also reduced by around 10% (Zhou, 1999). Figure 4.18 shows a part of the codes regarding the above two covering materials.

Figure 4.18 Codes for advanced front roof covering materials

4.3.6 Summer solar screen

The Canadian Prairies are the sunniest region in Canada, but every coin has two sides. If the intensity of the solar radiation goes high, tomatoes for example can have cracking, sunscald, and uneven coloration at maturity. Thus, we need to add solar screens like other traditional greenhouses do in the summer. The solar screen is typically made of knitted polyethylene fabric and it is an effective method to reduce solar radiation at noon. The performance of a solar screens varies from 30% to 90% for blocking the sun, according to the different material proportions. In this study, the most commonly used 50% sun blocker was applied to apply in

the solar greenhouse. The summer solar screen function was added in the greenhouse work condition interface. Then, from 12:00 to 17:00, the solar screens were pulled over the solar greenhouse to reduce the solar irradiance that entered the greenhouse. Figure 4.19 shows a part of the codes.
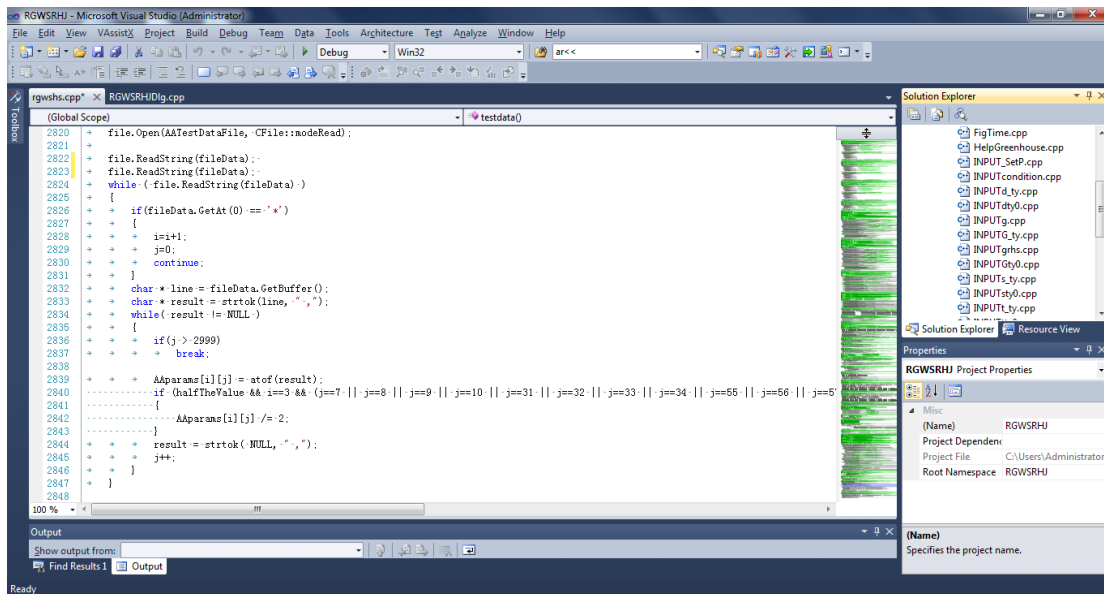
Figure 4.19 Codes for the solar screen function

4.3.7 Daily heat consumption output

In the Canadian Prairies, supplemental heat requirement is not only high, but it is also longer than most regions in the world. So, predicting the heating demand becomes very important, especially in the cold seasons. To demonstrate the daily consumed energy in the simulated greenhouse, the SOGREEN model added a function to output daily energy consumption after each day of simulation. However, because the previous code outputs greenhouse thermal parameters day by day until the end of the simulation period, the energy consumption will not be outputted for the last day. To solve this problem, codes were added, and this is shown in Fig. 4.20. The model can output energy consumption of the last simulation day by allowing the simulation process to go further than the total simulation steps.
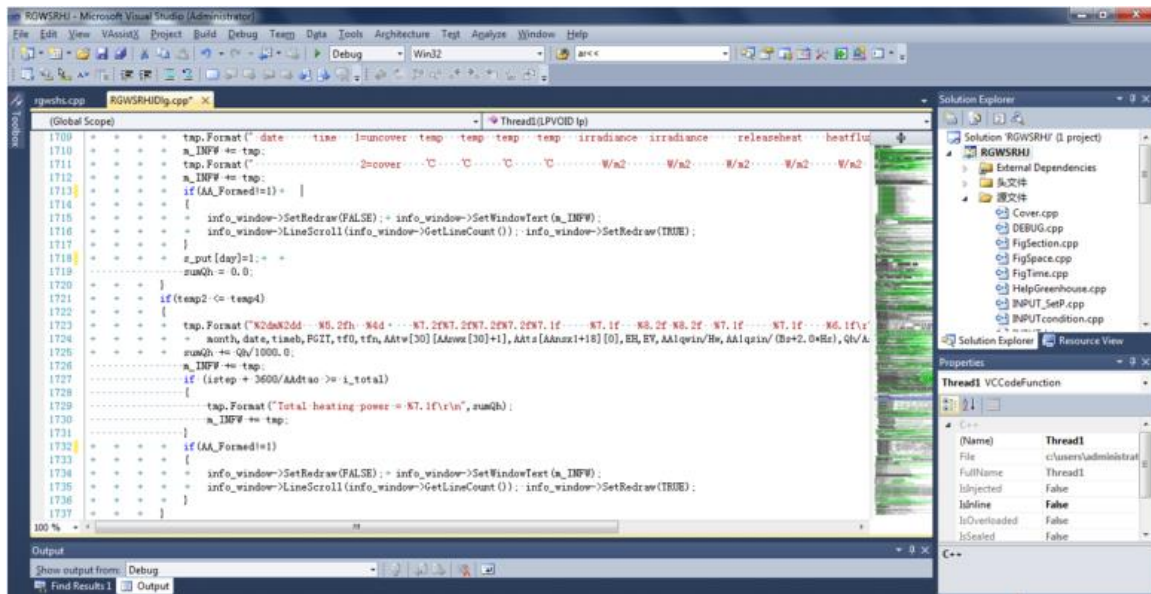
Figure 4.20 Codes for outputting energy consumption of the last day

4.3.8 Interior thermal screen

Due to the extremely cold weather in the Canadian Prairies, traditional thermal blankets, which cover the exterior surface of the front roof cover, may fail to work because of mechanical failure or frozen blankets. Most importantly, the failure of thermal blankets in the winter in the Canadian Prairies will bring a devastating economic loss for the greenhouse growers. To avoid this, an interior thermal screen needs to be prepared. The SOGREEN model added the interior thermal screen selection function. The interior thermal screen can be equipped with the same mechanical device as summer solar screens, which greatly simplify this component of installation. The interior thermal screen is made of a combination of polyester and aluminum. The aluminum layer can restrict the radiation of heat and greater energy conservation can be achieved by adding more aluminum (Ozturk and Ik, 2003). The performance of interior thermal screens is normally evaluated by their fractional energy savings. This is the difference in the thermal conductivity coefficient of the front roof when equipped with and without interior thermal screens divided by the thermal conductivity coefficient of the front roof without applying interior thermal screens. Ling et al. (2002) reported that when equipped with an interior thermal screen, the average thermal conductivity coefficient of the front roof is 2.9 W/(m•K). Figure 4.21 shows a part of the corresponding

codes and the method for adding the interior thermal screen function. When thermal blankets fail to work, the interior thermal screen can invoke the work schedule of the thermal blanket as its own schedule. When the inner thermal blanket is used, the thermal conductivity coefficient of the front roof will turn to 2.9 W/(m•K). This method significantly improved the reliability of the interior thermal screen and it saved space for the greenhouse work condition interface because users do not need to input schedules for the interior thermal screen.
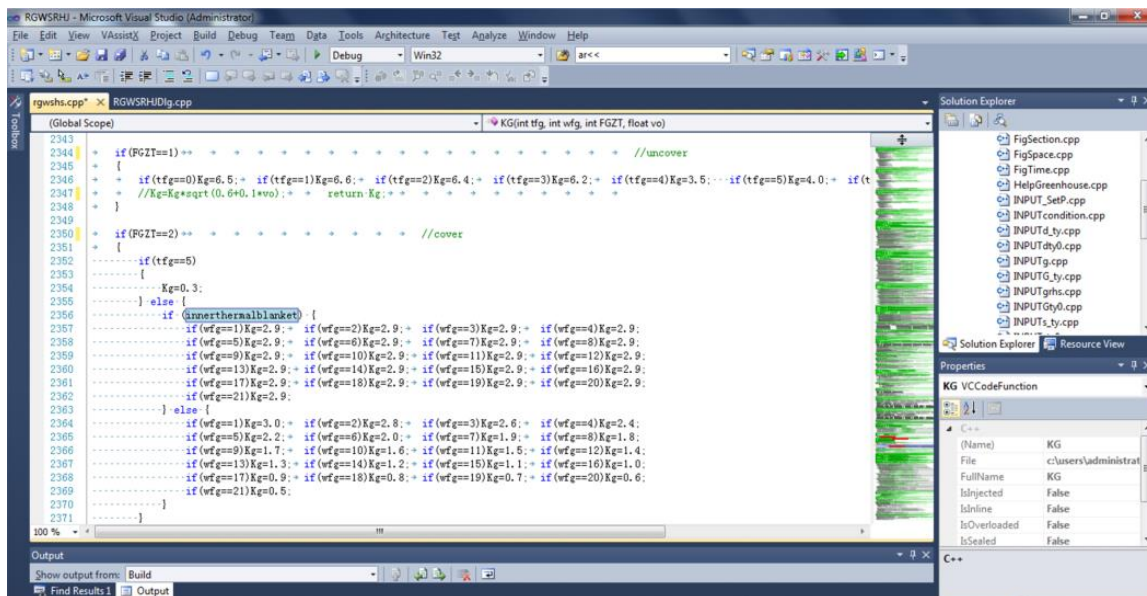
Figure 4.21 Codes for interior thermal screen

4.3.9 Work setting Save/Load function

As shown in Fig. 4.9, the user has to input laborious setting parameters in the thermal blanket work schedule, supplemental heating schedules and ventilation rate each time. This is time consuming. To simplify the operating process for users, a save/load function was built in the simulation model to save and invoke work schedules. Figures 4.22 and 4.23 show the codes for this function. The control variable AAI[35] sets a supplemental heating method. 0 represents no supplemental heat is needed, 1 means the user can input a set point temperature for a specific period, and 2 denotes that users can input supplemental heating power for a specific period. Variable AAI[44] assigns a thermal blanket work schedule. 0 means the model can set a schedule according to the default outdoor solar irradiance while 1 according to the

customized outdoor solar irradiance, and 2 means the user can set the cover and uncover time of the thermal blanket in the corresponding input box. Variable AAI[45] judges if the user has inputted the ventilation rate and schedule. 0 means not yet while 1 represents it has been inputted.
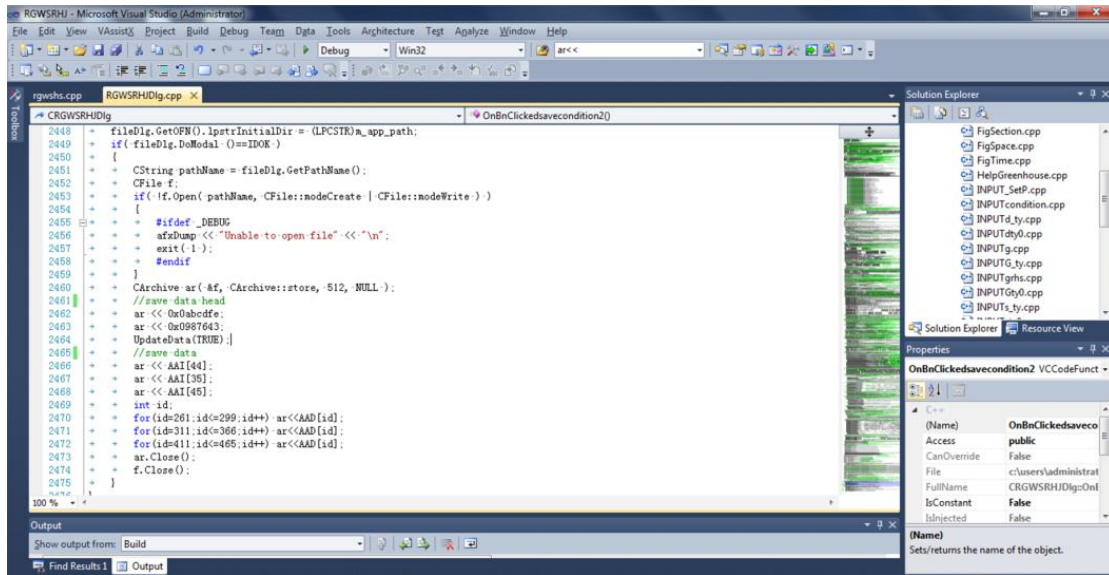
Figure 4.22 Codes of saving greenhouse work condition
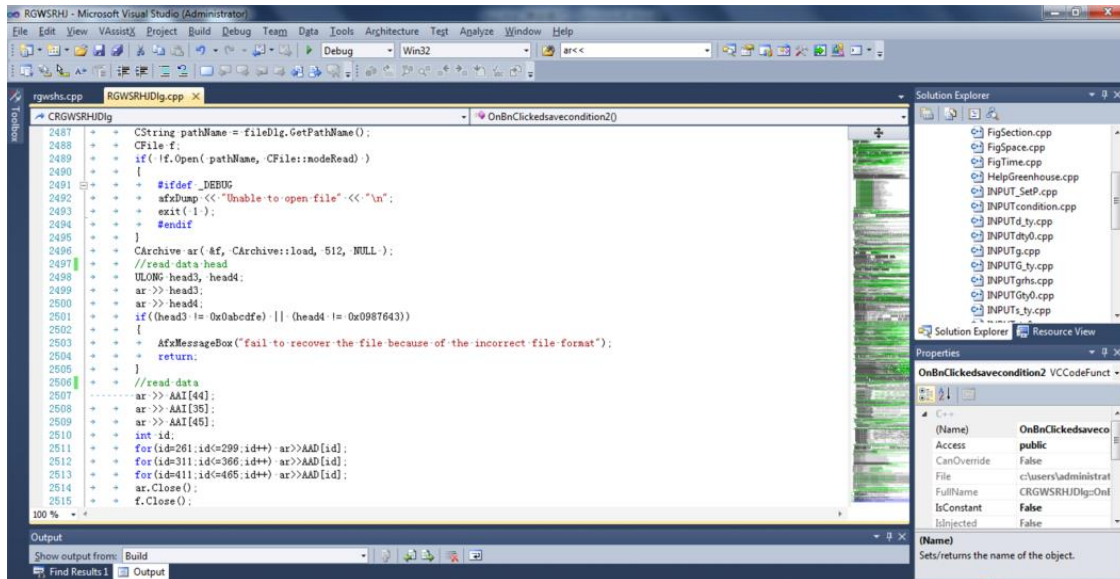
Figure 4.23 Codes of invoking greenhouse work condition

4.4 Model Validation

Before simulating a greenhouse environment in Saskatchewan using the modified model SOGREEN, it is necessary to validate its accuracy with field data. A commercial solar greenhouse was operating in Elie, Manitoba (49°55′ N, 97°28′ W), and research group measured field data from March 26th to 29th, 2017 (Ahamed, 2017). These data were used in the study for model validation.

4.4.1 Description of experimental greenhouse

The commercial solar greenhouse operating in Elie followed the classic structure of the mono-slope solar greenhouse. This made it suitable for the thermal environment validation. According to the measurement data, this greenhouse was 28 m in length and 6.7 m in width. Its north wall height was 2.2 m, the ridge height was 3.3 m, and the angle between the north roof and horizontal plane was 34°. The south roof had a steel frame and it was covered with a 6-mil single-layer polyethylene film, while the cotton thermal blanket (RSI-1.2) covered the south roof from the outside at night. Figure 4.24(a) shows the construction materials of the walls, including a 2-mm corrugated galvanized sheet steel, 152-mm fiberglass insulation, 13-mm plywood, 152-mm sand and 2-mm corrugated galvanized sheet steel from external to internal. Portions of the interior surface of the north wall were painted black for more absorption of solar energy. Fiberglass (RSI-3.5) played a role in thermal insulation and sand had a higher ability for heat storage. Figure 4.24(b) shows the construction materials of the north roof, including the 2-mm corrugated galvanized sheet steel, 152-mm fiberglass insulation, 13-mm plywood, and 2-mm plastic film.
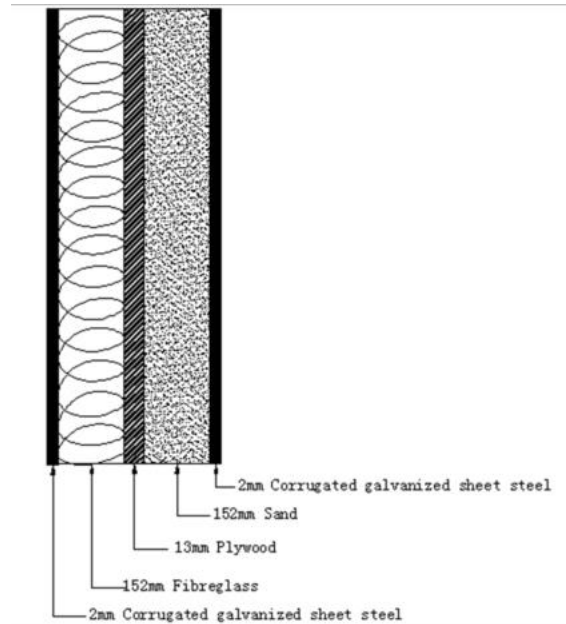
Figure 4.24 (a) Construction material of the north wall
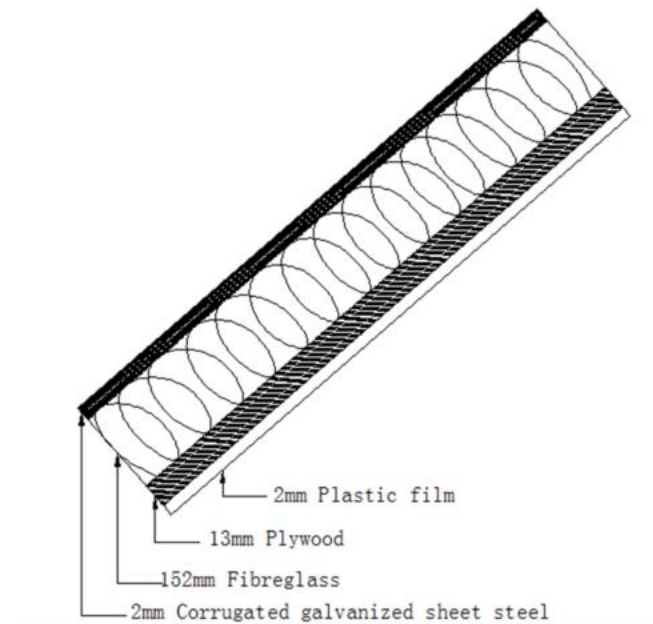
Figure 4.24 (b) Construction material of the north roof

During the measurements, young tomato plants with a 14-cm height were raised in the wet soil with flood irrigation. The ground had soil with no cover. The distance between the tomato plants was about 31 cm, and the distance between the north wall and the plants was 96 cm. The outdoor temperature in March was still low. However, an electrical heater controlled by a thermostat with 3.6 kW space heat supplied warm air from 18:00 to 9:00 when the

temperature had to be in a required range for the tomato plants. The cotton thermal blanket, another component to reduce the heat loss at night, covered the south roof at sunset (17:30). It was uncovered at sunrise (7:00). To reduce the indoor air temperature at noon for a suitable range for the tomato plants, greenhouse growers manually opened the ridge roof when needed. The greenhouse door was frequently used causing additional infiltration, compared to that during the night.

4.4.2 Validation process using the model

During the three-day field measurement period, the outdoor air temperature was getting warmer, the RH fluctuated around 80%, and the solar irradiance almost doubled compared to that in January. For the first measuring day, the outdoor temperature remained below 0°C before sunrise. It then gradually increased to 3.06°C at 16:00 pm, and dropped to 1°C at the end of the day. The outdoor RH changed in an opposite trend. The RH continued to go down from a maximum 84.2% at 6:00 am to 66.8% at 13:00 pm. It then slowly moved up to around 78% during the night. This was because of the rising temperature after sunrise and due to some ventilation around noon. The wind speed was mild on the first day with an average wind speed of 4.03 m/s, reaching its highest value of 6.67 m/s at 12:00 pm and lowest value of 1.94 m/s at 22:00 pm. The solar irradiance started in the greenhouse from 7:00 am with a value of 127.6 W/m^2. It climbed to 425.4 W/m^2 at 11:00 am and then descended to 15.6 W/m^2 at 18:00 pm. However, the outdoor temperature on the second day soared to 10.8°C at 14:00 pm and it gradually dropped to around 7°C at midnight. The RH was also higher than that of the first day. It was above 75% during the daytime and it climbed to 98.1% at 21:00 pm. In addition to the outdoor temperature and RH, the wind speed also was stronger at an average of 5.7 m/s. The solar irradiance was measured as 55.4 W/m^2 at 7:00 am. It reached 420 W/m^2 at 10:00 am and then fell to 27.4 W/m^2 at 17:00 pm. The same trend was seen on the third day of measuring. Outdoor temperatures ascended to 11.4°C at 14:00 pm and then dropped to 3.9°C at the end of the day. The RH declined to 71.1% at 13:00 pm and it rose to 94.4% at 22:00 pm. The wind was even stronger than the second day with an average of 6.9 m/s. It reached a maximum of 10.8 m/s at 13:00 pm. Solar irradiance was 82.5 W/m^2 at 7:00 am when the thermal blanket

was rolled up and it was 69.1 W/m^2 at 17:00 pm when the blanket was covered, reaching the peak of 441.4 W/m^2 at noon. Figure 4.25 shows the weather change during this period.
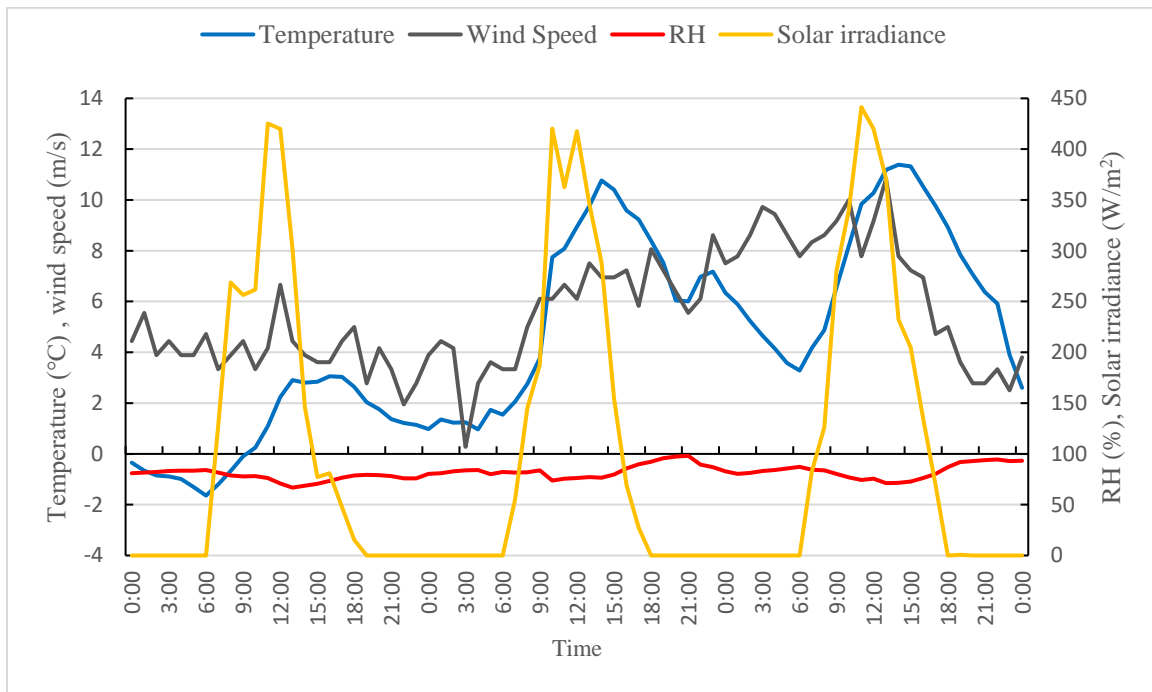
Figure 4.25 Weather conditions during the measurement period

In addition to the above measured local weather conditions, the local geographic information (49°55′ N, 97°28′ W) and local elevation (239 m) of Elie, Manitoba, was entered. For the greenhouse design conditions, a single-layer PE film, RSI-1.2 thermal blanket, ordinary airtightness, humid soil ground, 0.14 m plants height, and 0.96 m between plants and north wall were selected for the operation interface. Table 4.1 and Table 4.2 show the thermal parameters of the wall and north roof materials. These were selected according to the ASHRAE Handbook 2013 (ASHRAE, 2013) and built-in material.

Table 4.1 Thermal properties of wall construction materials from external to internal

Layer of materials	L1	L2	L3	L4	L5
Material	steel	fiberglass	plywood	soil	steel
Top thickness (mm)	2	152	13	152	2
Bottom thickness (mm)	2	152	13	152	2
Density (kg/m^3)	7830	14	460	1600	7830
Conductivity (W/(m•K))	45.3	0.039	0.093	0.89	45.3
Specific heat (J/(kg•K))	500	800	1880	840	500

Table 4.2 Thermal properties of north roof construction materials from external to internal

Layer of materials	L1	L2	L3	L4
Material	steel	fiberglass	plywood	Plastic film
Top thickness (mm)	2	152	13	2
Bottom thickness (mm)	2	152	13	2
Density (kg/m^3)	7830	14	460	900
Conductivity (W/(m•K))	45.3	0.039	0.093	5.5
Specific heat (J/(kg•K))	500	800	1880	1900

After all construction settings were completed, the cross-sectional setting boxes showed the corresponding material values, including 6.7 m of greenhouse span, 0.321 m of wall thickness, 1.63 m of back roof width, and 3.3 m of ridge height.

Then, the greenhouse work condition was set. First, the thermal blanket covered the front roof from 17:30 at sunset to 7:00 at sunrise. Second, according to the measurement data, the heating power of the space electrical heater remained at around 3.6 kW at night. It then dropped at around half power before 8:30 in the morning and it shut down after 9:00. Thus, 19.2 W/m^2 (3.6 kW) of supplemental heating from 18:00 to 8:30; and then 10 W/m^2 (1.876 kW) from 8:30 to 9:00. Third, due to the fact that greenhouse growers manually opened the roof for natural ventilation, assumptions in the ventilation rate were made based on the indoor temperature fluctuation and CO_2 needs. Table 4.3 shows the ventilation setting.

Table 4.3 Ventilation rate schedule

Ventilation schedule	Ventilation rate per m^2	Ventilation rate
8:00-11:00	3 m^3/(m^2•h)	0.156 m^3/s
11:00-13:00	10 m^3/(m^2•h)	0.521 m^3/s
13:00-14:30	11 m^3/(m^2•h)	0.573 m^3/s
14:30-17:00	3 m^3/(m^2•h)	0.156 m^3/s

Finally, the user can save the above settings and the greenhouse work condition settings to start the simulation process in the model later.

4.5 Model Simulation

In this study, the model modification and validation process built a stepping stone for the greenhouse simulation in Saskatchewan. Using the results of the predicted thermal environment and energy consumption, users and greenhouse growers can be aware of the economic benefit of greenhouse production in a mono-slope solar greenhouse. Thus, the last part of this study is to simulate greenhouse heating needs for a solar greenhouse located in Saskatoon.

4.5.1 Description of study greenhouse in SK

Using construction materials similar to the solar greenhouse built in Elie, MB, the solar greenhouse remains an indoor thermal environment within the plants' required temperature range. So, the north wall was built with a corrugated galvanized sheet steel, fiberglass, plywood, soil and a corrugated galvanized sheet steel from external to internal. The greenhouse is 100 m x 12 m, and 5.62 m high in ridge. Considering larger growing spaces, thicker insulation and heat storage materials were inputted into the model to protect the required indoor temperature. Table 4.4 shows the thermal parameters of each construction material.

Table 4.4 Thermal properties of north wall building materials from external to internal

Layer of materials	L1	L2	L3	L4	L5
Material	steel	fiberglass	plywood	soil	steel
Top thickness (mm)	2	218	19	399	2
Bottom thickness (mm)	2	218	19	399	2
Density (kg/m^3)	7830	14	450	1600	7830
Conductivity (W/(m•K))	45.3	0.039	0.11	0.89	45.3
Specific heat (J/(kg•K))	500	800	1880	840	500

Table 4.5 Thermal properties of north roof building materials from external to internal

Layer of materials	L1	L2	L3	L4
Material	steel	fiberglass	plywood	Plastic film
Top thickness (mm)	2	218	19	2
Bottom thickness (mm)	2	218	19	2
Density (kg/m^3)	7830	14	450	900
Conductivity (W/(m•K))	45.3	0.039	0.11	5.5
Specific heat (J/(kg•K))	500	800	1880	1900

It is shown in Table 4.5 that the back roof was built with steel, fiberglass, plywood and plastic film which was similar to the solar greenhouse in Elie. The angle between the back roof and horizontal plane was 40°. The height of the north wall and ridge was 4.15 m and 5.62 m respectively. An underground heat barrier was set beneath the north wall and south end. It was constructed with a fiberglass board and plywood to reduce the heat loss through the underground area. Figure 4.26 shows the cross-sectional plan of the study solar greenhouse in Saskatoon. Unlike the solar greenhouse in Elie, the front roof of the study solar greenhouse was covered with a double-layer inflated film which has a better thermal performance compared with single-layer plastic film. This is a common practice in Canada. The indoor ground was covered with landscaping fabric which makes a better working place for greenhouse growers.
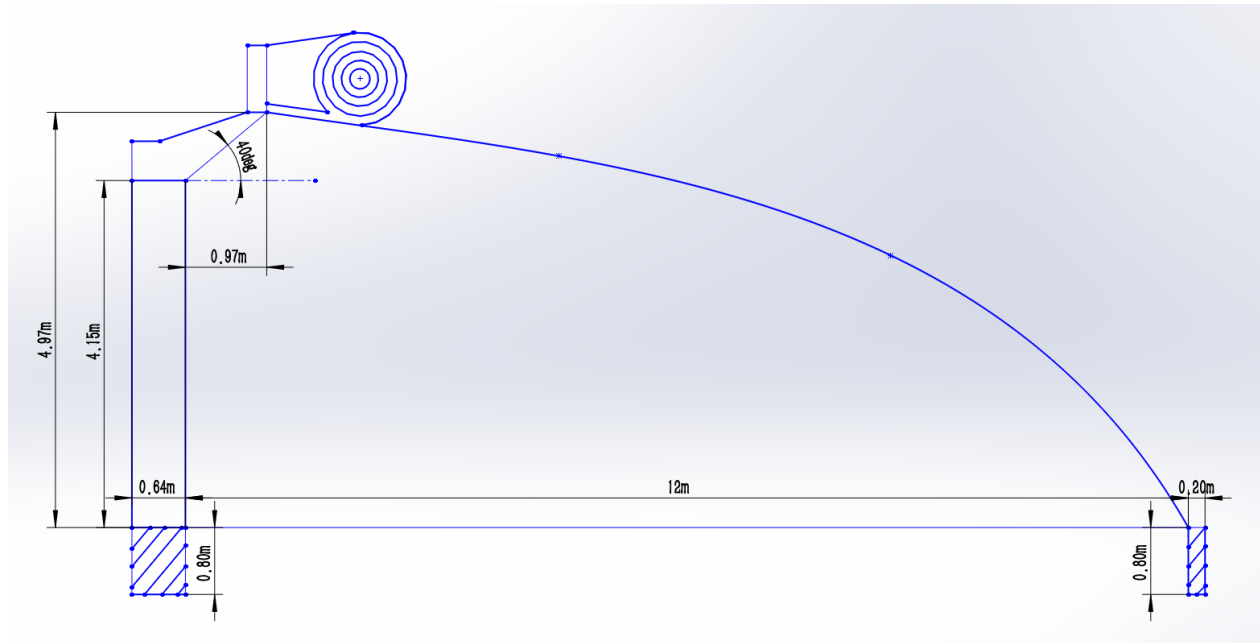
Figure 4.26 Cross-sectional plan of the study solar greenhouse in Saskatoon

4.5.2 Assumptions in simulation

Some assumptions were made for the greenhouse in Saskatoon. First, the distance between the study greenhouse and an adjacent building was 20 m. This was used to calculate the shading area on the north wall. Second, tomato plants (0.8 m) were grown in the solar greenhouse. Third, the distance between the north wall and tomato plants was 1 m, and this was used to calculate the shading area on the north wall caused by the plants. Fourth, the airtightness of the study solar greenhouse was good, so the infiltration rate was low in the simulation. Fifth, the greenhouse was automatically controlled by fans and inlets, and low ventilation rates were applied during the winter for CO_2 enrichment in the morning.

4.5.3 Work schedule setting

To simulate a thermal environment in a solar greenhouse, different greenhouse work schedule settings were used according to the weather conditions in each month. The thermal blanket covered the front roof before sunset and it was uncovered after sunrise while supplemental

heating systems were turned on when the indoor temperature fell below the set point of 18℃. During the cold months, a low ventilation rate was set in the morning for CO_2 enrichment purposes and moderate ventilation rates were also arranged at noon in the mild months while high ventilation rates with a long ventilation duration were applied in the warmer months. A sun shade screen was applied to block half of the total solar irradiance between June and August when it was needed. Table 4.6 shows the work schedule of the solar greenhouse production simulation.

Table 4.6 Greenhouse work schedule

	January	February	March	April	May	June
Thermal Blanket	16:30-10:00	17:00-9:30	8:30-18:00	7:00-19:00	6:30-19:30	6:00-21:00
Temperature Set Point (°C)	18	18	18	18	18	18
Ventilation Rate (m³/s)	12:00-13:00: 0.67	11:00-12:00: 1; 13:30:15:00: 1.67	10:00-11:00: 1; 13:00-14:00: 2.67	8:30-9:00: 1; 10:30-12:30: 5.67; 12:30-18:00: 5	7:30-10:00: 3.33; 10:00-12:30: 8.33; 12:30-18:30: 6.67	6:30-10:00: 3.33; 10:00-12:00: 8.33; 12:00-17:00: 3.33; 17:00-21:00: 8.33

	July	August	September	October	November	December
Thermal Blanket	5:30-24:00	6:30-23:00	7:40-18:00	8:30-17:00	10:00-16:00	10:30-16:00
Temperature Set Point (°C)	18	18	18	18	18	18
Ventilation Rate (m³/s)	6:30-9:00: 3.33; 9:00-22:00: 8.33	7:30-9:00: 3.33; 9:00-11:30: 8.33; 11:30-18:00: 10; 18:00-20:00: 5	9:30-12:00: 1; 12:00-17:00: 5	10:00-11:00: 1; 12:00-15:00: 4	11:30-12:00: 1	12:00-12:30: 1

Chapter 5. RESULTS AND DISCUSSIONS

5.1 Validation Results

Using the field data collected in Elie, Manitoba, and the predicted data, comparisons of the indoor temperature, RH, wall temperature and soil temperature were made to evaluate the accuracy of the simulation model SOGREEN.

5.1.1 Field data

During the field measurement period in Elie, Manitoba, the hourly indoor air temperature, RH, wall interior surface temperature, ground temperature, and electrical heater ampere were collected. The indoor temperature and RH were measured at 122 cm above ground level and Fig. 5.1 shows that the indoor air temperature and RH changed in this period. The indoor temperature started to increase from around 16°C at sunrise to its peak value at noon. It later dropped sharply due to the increased ventilation rate by the ridge vent. The electrical heater was turned on at 18:00. to keep the indoor temperature above the set point. While the indoor RH remained above 75% during the night, it plummeted after sunrise because of the rise in temperature. Nevertheless, the indoor RH climbed back up when the ventilation roof was opened because cooler air entered the solar greenhouse.
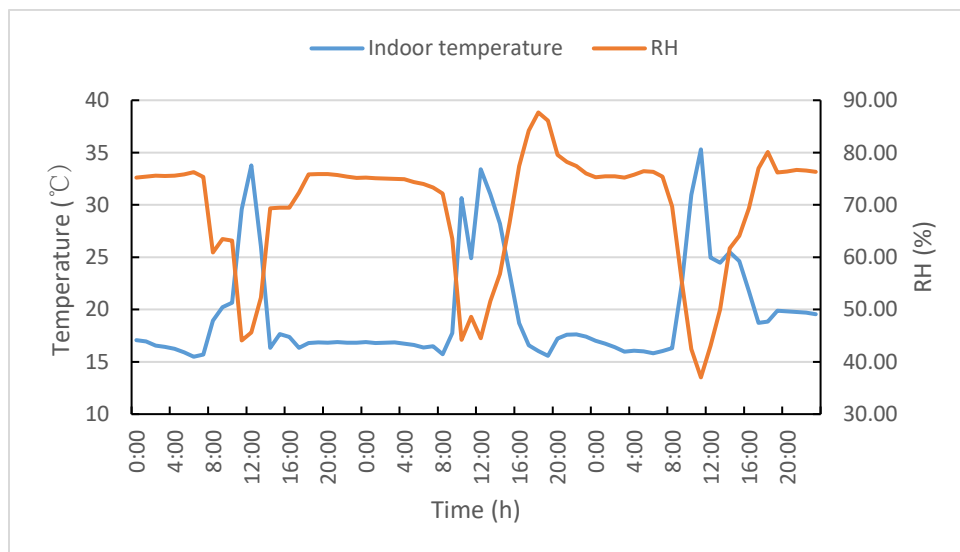
Figure 5.1 Indoor temperature and RH of field measurement

Further, two soil temperature sensors were buried at a depth of 5 cm under the ground surface. Their distance to the north wall was 214 cm, and two wall temperature sensors were installed 76 cm above the bottom of the north wall surface. Figure 5.2 shows the change in the wall and ground temperature. Indoor wall temperatures fluctuated with the same trend as the indoor air temperature. As expected, the rising speed of the wall temperature lagged behind that of the indoor temperatures before noon due to the slow convection heat transfer process. Its diving speed was also slower from noon to sunset because the north wall kept releasing heat to the indoor environment. The soil temperature fluctuated more moderately than the wall temperature. There was a big difference between the temperature in the wall and soil at night. At night, the soil temperature was always higher than the wall temperature because the soil was very wet. Water, with a higher specific heat, can resist changes in temperature better.
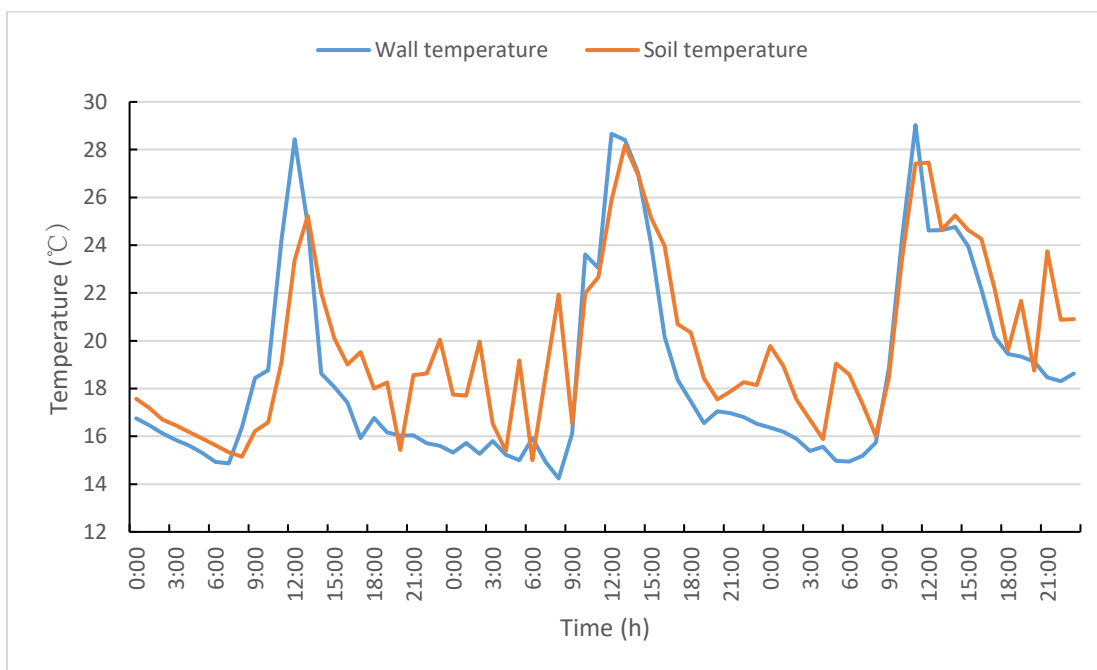
Figure 5.2 Change in wall and ground temperatures

Most importantly, greenhouse growers are concerned with energy consumption. The current of the electrical heater was measured and converted to power with its 220 V rated voltage. Figure 5.3 shows the power change during the field measurement. The heating schedule started at 18:00 and it was turned off at 9:00.

Figure 5.3 Heating power pattern in field measurement

5.1.2 Predicted data

Figure 5.4 shows that the model predicted and measured indoor thermal environment are quite similar. In the predicted setting, the supplemental heating power followed the same value as the measured electrical heater power. This means that it became a control variable in the simulation process. Thus, indoor thermal environment parameters such as air temperature and RH were the best parameters for the evaluation of accuracy. The indoor temperature increased from morning to noon, while there was a decline in the indoor RH. When opening the ventilation roof at noon, the temperature dropped by around 18°C and the RH climbed by approximate 35% until sunset. During the night, the thermal blanket covered the front roof for heat preservation, so the indoor temperature fluctuated moderately from 15°C to 20°C. The indoor RH also fluctuated slightly from 80% to 90%.

5.1.3 Comparison between field data and predicted data

In the validation process, the indoor air temperature and RH were the most important parameters since energy consumption acted as a controlled variable. As shown in Fig. 5.4, the

predicted temperature change pattern closely followed the measured one, especially from sunset to sunrise on the following day. Most of the significant differences appeared at noon, which may be caused by the sudden increase in the ventilation rate. For instance, during the measurement period on the first morning, predicted temperatures presented a sharp climb from 8:00 am while the measured temperature rose much slower because the door and roof were frequently opened by the researcher. This led to more than a 20% discrepancy between 8:00 and 10:00 am. On the third measurement day, the indoor temperature at 11:00 am was 35.3℃, while it dropped dramatically to below 25℃ in the following two hours due to opening the ridge roof. However, the simulated result showed a gradual decline instead of a sharp one. Nevertheless, the average temperature difference was still within 10% (9.6%).

Although the overall predicted trend of the indoor RH fluctuated in a similar pattern to the measured one, the difference during the whole period was 13.7%, which was higher than that of the indoor temperature. Two factors likely caused this discrepancy. First, the young tomato plants were only 14 cm in height. Transpiration from the plants was weak and evaporation from the wet soil dominated the moisture production. In the model prediction, a high indoor ground humidity level was assumed based on the field conditions so that stronger evaporation may be applied to the model. This caused a high increase in the indoor RH. Second, the ventilation rate was getting higher as the outdoor wind speed kept increasing during the measurement period. The model used an air exchange rate that might be lower than its real value, resulting a higher RH in the greenhouse. Although the average outdoor RH was 82%, the outdoor humidity ratio was much lower due to the low outdoor air temperature.
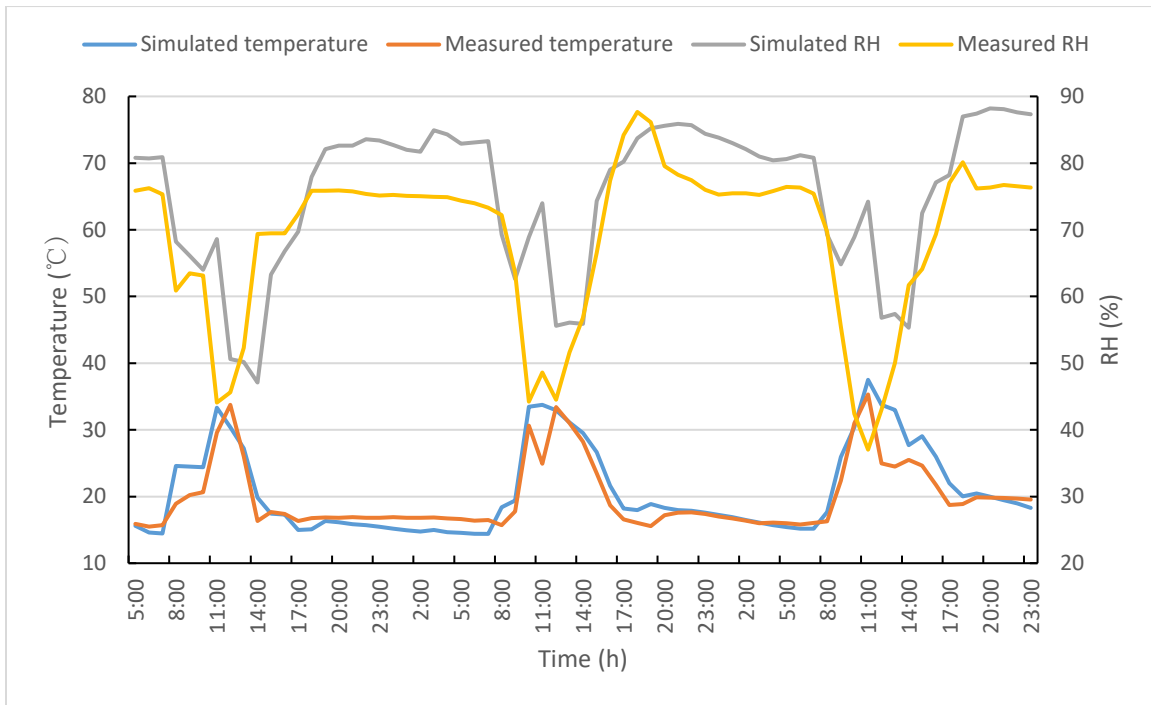
Figure 5.4 Comparisons between measured data and predicted indoor temperature and RH

In addition to the indoor temperature and RH, the inner surface temperatures of the north wall and soil temperature were also compared for validation. Figures 5.5 and 5.6 illustrate the temperature change pattern of the wall and soil and the difference between the predicted and measured value.

First, the interior building material of the north wall was a 2-mm corrugated galvanized sheet of steel which has a high thermal conductivity. The corrugated shape made the heat transfer area of the sheet steel much larger than that of the flat sheet, while the shape of the construction material could be only defined as flat. In Fig. 5.5, the wall temperature that was measured and predicted from 9:00 am to 12:00 pm was close, during which the north wall stored heat from both direct solar radiation and indoor air with a higher temperature. However, the difference between the measured and predicted values began to increase at noon because of the larger heat transfer area and the faster heat released to the indoor air. Thus, during the field measurement, the temperature of the north wall surface dropped to just above 15°C at sunset when the electrical heater was turned on. In the model, its temperature declined slower to around 23°C at sunset and then, it continued to drop until the next morning. Due to the

63

influence of the heat transfer area, the average discrepancy in the wall surface temperature was as high as 19.4%.
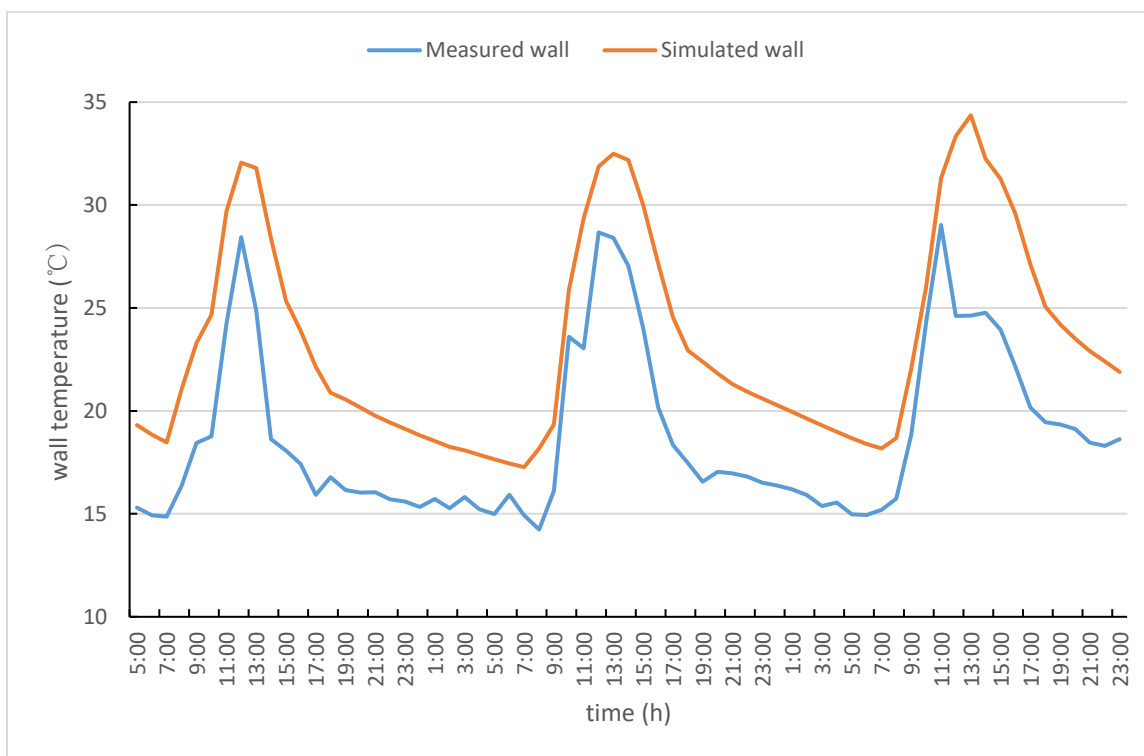
Figure 5.5 Discrepancy in wall temperatures between measured and predicted results

According to the field measurement conditions, the tomato plants were planted in wet soil, and several water buckets were placed on the ground for irrigation. Thus, in the simulation process, wet was selected for the design condition interface to represent the indoor ground wetness level. As expected, before noon, when high ventilation rates were applied, the temperature of the ground surface rose rapidly because of the increasing air temperature and direct solar radiation. Similar to the indoor temperature change pattern, the frequent opening of the door for instrument testing during the first morning caused more air leakage. This made the soil surface temperature lower than the predicted value. After 12:00 pm on the first day, the difference in the soil temperature was gradually getting smaller. Another big difference appeared on the third afternoon when the measured indoor temperature and wall temperatures were also lower than the predicted values. The reason for this might be that the wall and soil did not absorb and release as much heat as predicted.
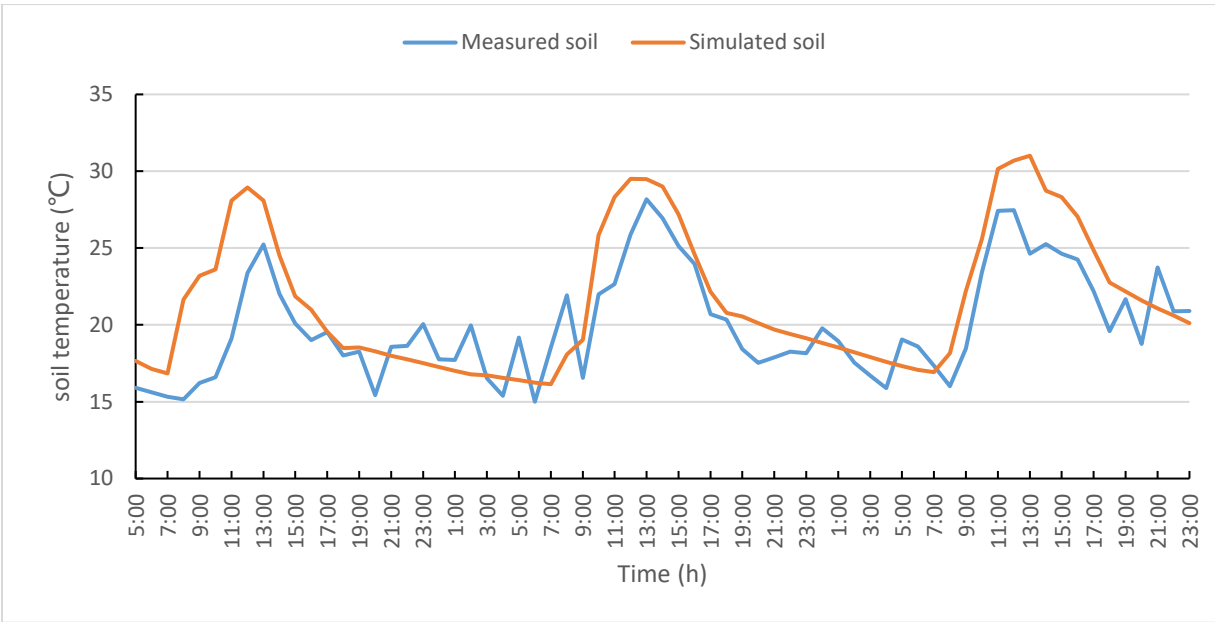
Figure 5.6 Comparison of measured and predicted soil temperatures

In the greenhouse validation process, the indoor temperature is the most important parameter to verify the accuracy of the simulation results because of the fixed heating consumption. According to the validation results, the mean absolute percentage error between measured and predicted indoor temperature was only 9.6% (within 10%). This demonstrated that the accuracy of the modified simulation model SOGREEN is acceptable and it could be used in the further simulation process.

5.2 Simulation Results

Using the validated simulation model SOGREEN, an annual greenhouse simulation was done in Saskatoon, Saskatchewan, to evaluate the thermal environment of the solar greenhouse and predict its heating requirements. Simulations in cold, mild and warm months were also conducted in order to provide specific greenhouse working schedules during different seasons. The energy saving rate of the solar greenhouse was calculated by comparing the energy cost between the study greenhouse and the local traditional greenhouse.

5.2.1 Annual simulation on energy consumption

Through simulation of a study solar greenhouse under the weather and geographic conditions in Saskatoon, the thermal environment and energy consumption were obtained. Figure 5.7 shows the monthly average thermal parameters and energy consumption. As a dominant outdoor thermal parameter, the outdoor temperature remained below 0°C from November to March, when most greenhouses shut down in the Canadian Prairies. However, there are still a few overwinter production greenhouses in operation. The mean outdoor temperature in January was -15.6°C with a minimum value of -38.1°C. It slowly rose to -7.8°C in March with a minimum value of – 31°C. It jumped to above 0°C (3.8°C) from April and it continued to go up to 18.8°C in July. It is worth noting that outdoor temperatures were above 0°C throughout June. Then, the mean outdoor temperature started gradually dropping to 4.9°C in October and to -13.8°C in December. On the other hand, the indoor temperature maintained the required temperature zone for the tomatoes, which was above 18°C. It increased steadily to 25.2°C in July and descended back to 18°C in December. As for the outdoor RH, it fluctuated between 70% and 80% from November to March and it went down to below 70% in April, August, September and October. It dropped below 60% during the rest of year because of warmer temperatures. In terms of the outdoor humidity ratio, it rose from 0.63 g/kg in January to 7.79 g/kg in August. It then descended to 0.78 g/kg in December. The most important factor, energy consumption, fluctuated dramatically with the changes in the weather conditions each month. In January and December, the daily energy consumption could be as high as 7312.2 MJ and 7546.4 MJ because of the extremely low outdoor temperature. In February, March and November, when the outdoor temperature was still below 0°C, the daily energy consumption dropped to 6214.1 MJ, 4092.9 MJ, and 4262.9 MJ respectively. However, only a small amount of energy was consumed in April, September, and October because of the increasing outdoor temperature (average of 3.8°C, 10.5°C, 4.9°C respectively). Supplemental heat was not needed from May to August, and this reflected the heat storage capacity of the solar greenhouse.
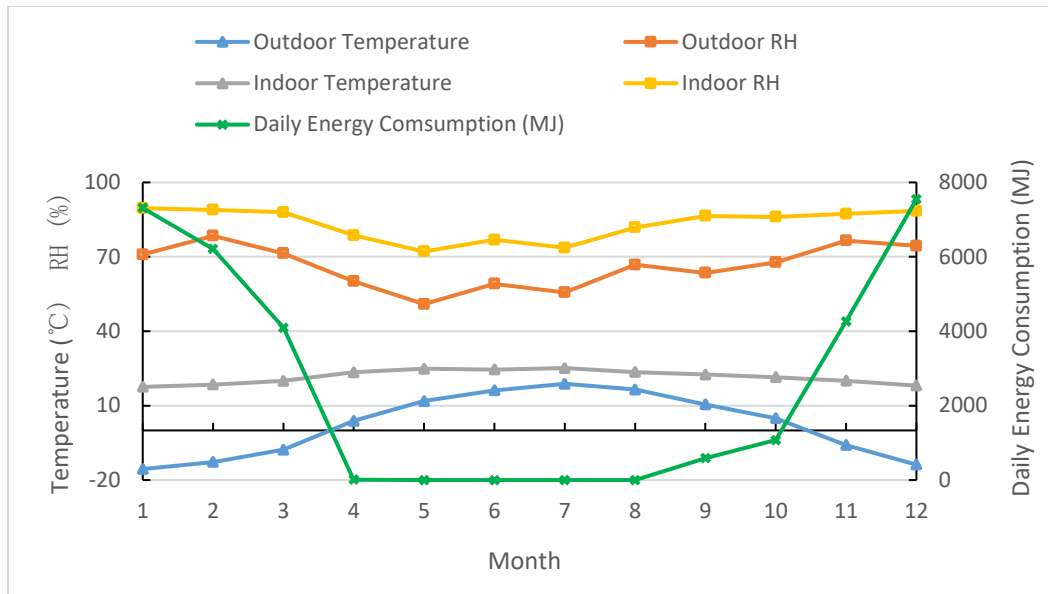
Figure 5.7 Average monthly thermal environment and energy consumption of the study solar greenhouse in Saskatoon

5.2.2 Full simulation in various seasons

The above annual analysis of the thermal environment and energy consumption illustrates the corresponding changes in each month. However, both the indoor and outdoor thermal conditions greatly changed throughout the different seasons. For example, in the coldest months, the outdoor air was extremely cold and dry and supplemental heating systems were required all day long. In the summertime, no additional heat was applied in the solar greenhouse. Thus, December, March, and July were selected to represent cold, mild and warm months respectively.

First, December was selected to represent a cold season. It had a comparable outdoor temperature and humidity ratio with January and the same amount of supplemental energy was consumed to maintain the indoor temperature for greenhouse production. As shown in Figure 5.8, the outdoor temperature was never above 0°C throughout the month. It fluctuated around -20°C before December 18th and it rose to around -10°C afterwards. However, the indoor temperature did not fluctuate too much, and it maintained at 18°C due to the supplemental heating system. The outdoor RH also fluctuated greatly for the first ten days and then, it

changed moderately. The indoor RH went up suddenly on December 4th and it dropped back to below 90% on the next day. It stayed below 90% for the rest of month. In addition to the temperature and RH, the daily total solar irradiance and daily total energy consumption were also analyzed. There was a negative correlation between the total solar irradiance and energy consumption. The energy consumption rose to more than 13,000 MJ on December 5th when the daily total solar irradiance was only 135 W/m^2. It plunged to below 6,500 MJ on December 9th and 10th when the solar irradiance soared to 1,145 W/m^2. The following days also had the same trend. The increasing daily total solar irradiance led to less energy consumption, and vice versa. To sum up, the duration of sunshine duration was short and the solar irradiance was low in December. So, the north wall had limited solar heat storage during the daytime and it released heat slowly for the rest of the day. The energy consumption was high, especially for those days with low outdoor temperature and solar irradiance.
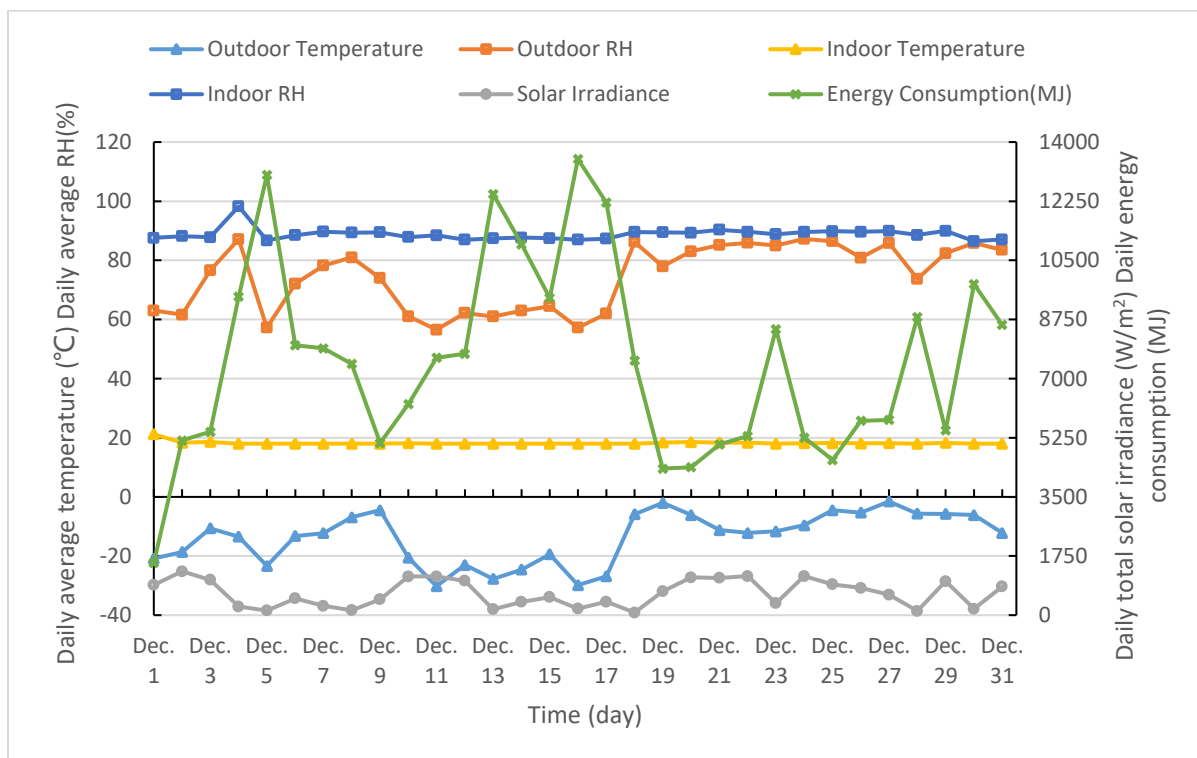
Figure 5.8 Daily changes in the thermal environment and energy consumption in December

In March, selected as a mild month, the energy consumed was much lower than that of December. Besides, most traditional greenhouses in the Canadian Prairies have started to work

in March. So, it is a good time to make a comparison of energy consumption between solar and traditional greenhouses. Figure 5.9 shows the simulated thermal environment and energy consumption of the greenhouse in March. The outdoor temperature fluctuated slightly between -15°C and -21°C from March 1st to March 8th. It then rose gradually to -2°C on March 11th and it fluctuated between -10°C and 2°C. Compared to December, the indoor temperatures in March maintained levels at the set point and then fluctuated around 20°C which meant that less supplemental heat was needed. Since the outdoor temperature rose, the outdoor RH would go down compared to that of December. In the first eight days, the outdoor RH fluctuated around 60%. It then increased gradually to 84% on March 15th and fluctuated between 65% and 85% during the following days with a peak of 90% on March 29th. The indoor RH did not fluctuate that much, and it maintained above 85% in the month. On the other hand, the average daily total solar irradiance almost quadrupled that of December due to the longer duration of sunshine daily and doubled hourly solar irradiance at noon. The energy consumption was no longer greatly affected by the solar irradiance because the outdoor temperature was getting warmer and the north wall had more time to store solar heat in the daytime. As shown in the figure, the outdoor temperature was quite low in the first eight days, and the energy consumption still had a negative correlation with the total solar irradiance. For instance, less energy was consumed on March 2nd when the solar irradiance rose sharply. Increasing energy was consumed on March 5th when the lowest total solar irradiance occurred in March. However, the daily energy consumption was below 2000 MJ from March 10th to 13th and from 22nd to 26th when the outdoor temperature maintained around 0°C. For the rest of the days of the month, energy consumption rose moderately when the solar irradiance dropped sharply. March 14th, 17th, and 27th are an example of this.
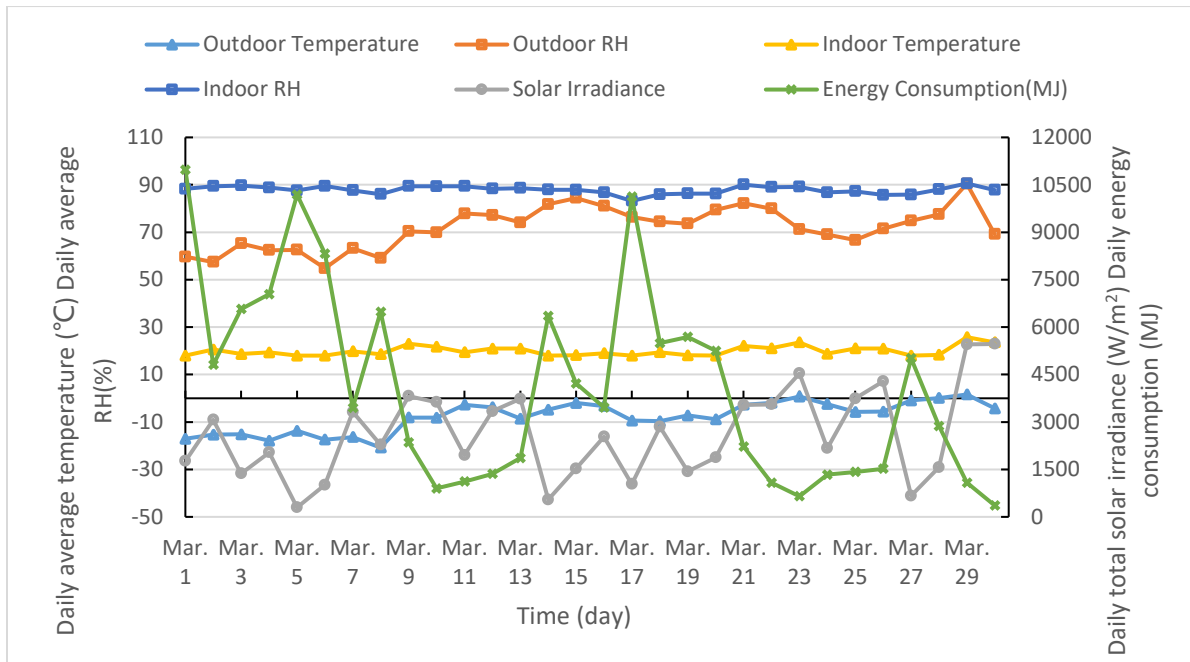
Figure 5.9 Daily changes in the thermal environment and energy consumption in March

Finally, July was selected to represent the warmest season and it had a higher temperature and lower RH. Due to the long duration of sunshine duration and high solar irradiance at noon, the traditional and solar greenhouse had to apply sun blockers to reduce the solar heat entering the greenhouse. As shown in Fig. 5.10, the outdoor temperature reached its peak value in this month. The monthly average temperature fluctuated around 20°C with a maximum value of 25.4°C. The indoor temperature followed a similar trend to the outdoor temperature. For instance, the indoor temperature dropped slightly from July 10th to July 19th because of the decreasing outdoor temperature. It then peaked on the 22nd because of a sharp rise in outdoor temperature and it then fluctuated between 20°C and 25°C. The outdoor RH changed greatly. It climbed to 63% RH on July 4th, and then fell to 42% on July 8th. It rose again to around 70% in mid-July and it finally dropped and fluctuated around 50% in the last 10 days. Compared to the indoor RH change in December and March, the indoor RH fluctuated more in July because of the high ventilation rate and much longer duration of ventilation. It started at 77% RH on July 1st and it descended to below 70% in the following days. Then, it rose in mid-July and fluctuated with a peak value of 81%. As expected, the daily total solar irradiance was doubled to that of March, and so, a sun blocker was needed to protect the tomato plants. On most days

in July, the total daily solar irradiance was above 6000 W/m^2. However, July 3rd, 17th, and 28th showed a sharp decline, and the total solar irradiance dropped to 1978 W/m^2, 4557 W/m^2, and 2722 W/m^2 respectively. As for the energy consumption, no day used supplemental heat except for July 25th. On this day, the supplemental heating system turned on at 8:00 am with a power of 12.6 kW because the thermal blanket was rolled up before 6:00 am. The morning outdoor temperature was below 10 °C which caused high loss of heat through the front roof.
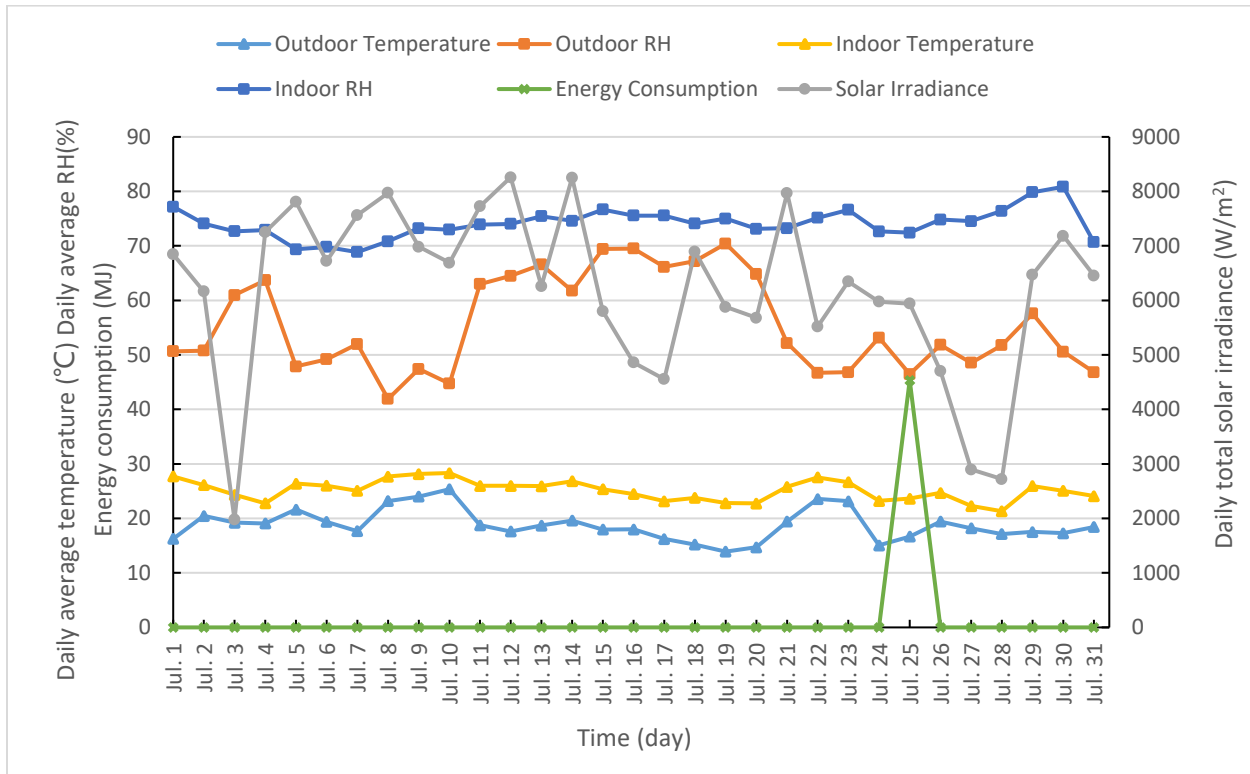
Figure 5.10 Daily changes in the thermal environment and energy consumption in July

5.2.3 Sensitivity analysis

The study solar greenhouse was simulated mainly for predicting the supplemental heating requirement, so the sensitivity of the model input parameters on the supplemental heating demand was analyzed for the selected coldest period (from Jan 25th to Jan 30th) of the year in Saskatoon, Saskatchewan.

First, the thermal properties of the front roof cover materials play an important role in the heat loss process due to their low thermal resistance. All the built-in selections, including PS pellet

insulation system (U= 4.0 W/(m^2•K) in the daytime and U= 0.3 W/(m^2•K) in the night), double-layer inflated film (U= 4.45 W/(m^2•K)), glass (U= 6.2 W/(m^2•K)), PC board (U= 3.5 W/(m^2•K)), PVC film (U= 6.4 W/(m^2•K)), EVA film (U= 6.5 W/(m^2•K)), PE film (U= 6.6 W/(m^2•K)), were analyzed. As shown in the Fig. 5.11, the supplemental heating requirement was almost doubled for changing the cover material from PS pellet insulation system to single-layer PE film. The distinct differences in the supplemental heating demand rely on the thermal transmittance (U value) and a lower thermal transmittance leads to a lower supplemental heating demand. The results demonstrated that compare to the single-layer PE film, 48.7%, 37.1% and 20.9% heating energy can be saved using PS pellet insulation system, PC board and double-layer inflated film respectively. However, glass, PVC film and EVA film only saved less than 5% energy because of their high thermal transmittance.
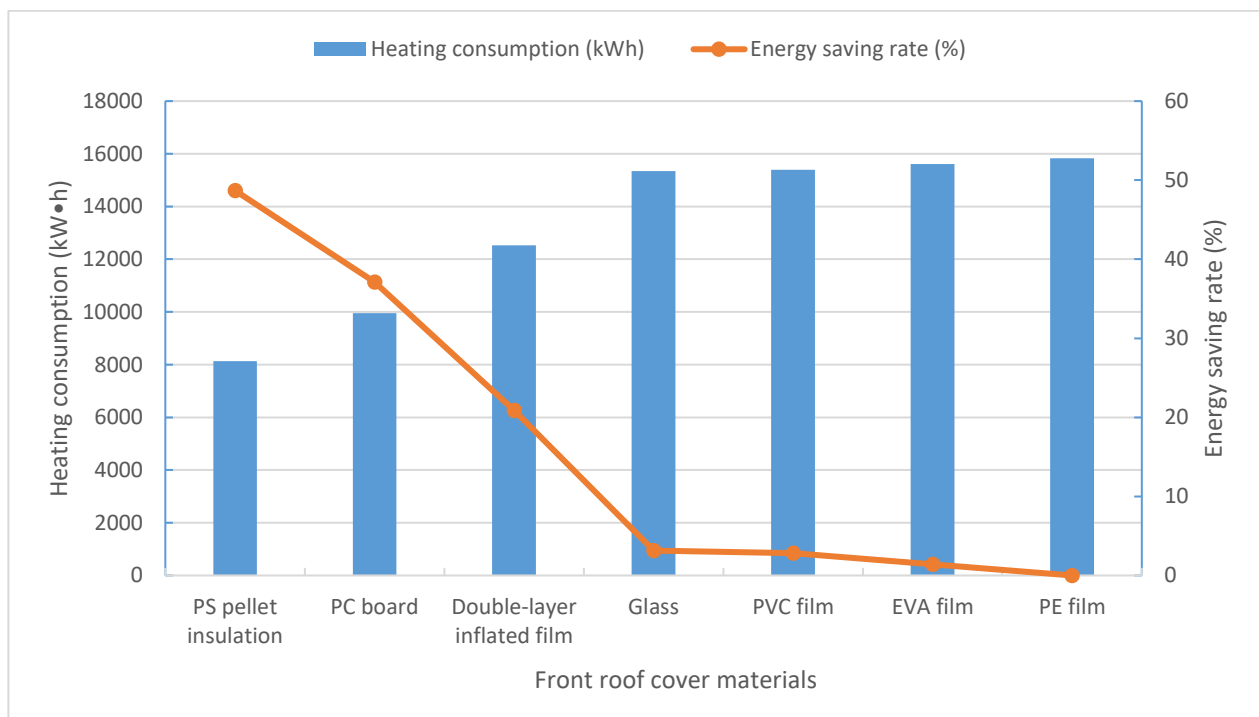
Figure 5.11 The sensitivity of the front roof cover materials (energy saving is compared to PE film)

Second, the indoor ground condition has an influence on the heat loss through ground area. Thus, concrete, landscaping fabric and soil ground greenhouses were simulated. As shown in

Fig. 5.12, concrete was the ground selection with least supplemental heating demand while the soil was the one with the most heating demand. Although the concrete ground has a higher thermal conductivity, it can store more heat in the daytime due to its higher specific heat. Another reason is that the soil ground contains more moisture which may absorb latent heat in the evapotranspiration process. The landscaping fabric ground can reduce latent heat consumption as well in the greenhouse. So, compare to the soil ground, the concrete and landscaping fabric ground can save 0.18% and 0.09% of the heating energy.
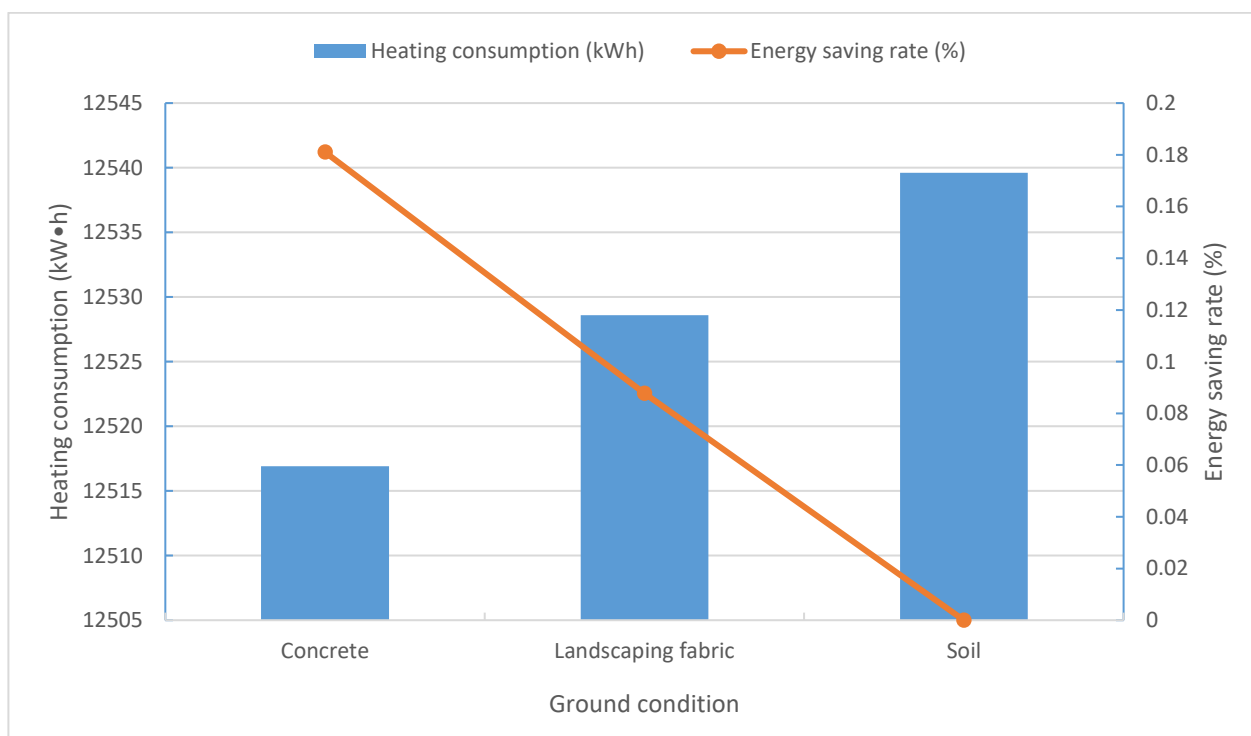
Figure 5.12 The sensitivity of the ground materials (energy saving compared to soil)

Third, the inner part of the north wall functions as a heat storage layer. The heat storage capacity of the construction materials determines the supplemental heating demand, especially the night heating requirement. The best option for the heat storage layer is the material with high specific heat and thermal conductivity because more thermal energy can be penetrated deep into the material. In this study, materials with different specific heat values were selected as contrasting materials, including polystyrene board, wood, cement perlite and sand. As shown in Fig. 5.13, constructing the heat storage layer with polystyrene board (specific heat =

2400 J/(kg•K)) required the least supplemental heat throughout the simulation period, and it was followed by wood (specific heat = 2000 J/(kg•K)), cement perlite (specific heat = 1380 J/(kg•K)) and sand (specific heat = 840 J/(kg•K)). This is why some greenhouses use sealed water (specific heat = 4200 J/(kg•K)) tanks as additional heat storage (ASHRAE, 2013). However, the difference in the supplemental heating demand was less than 1% compared to sand ground. Because although the polystyrene board has the highest specific heat, its thermal conductivity is only 0.035 W/(m•K). So, the thermal energy cannot penetrate deep into the polystyrene board. Instead, most of the thermal energy gathers close to the south surface, which leads to a high temperature gradient across the board. On the opposite, sand has the highest thermal conductivity among these four selections, so thermal energy can penetrate deep into the sand easier in the daytime although it has the lowest heat storage capacity.
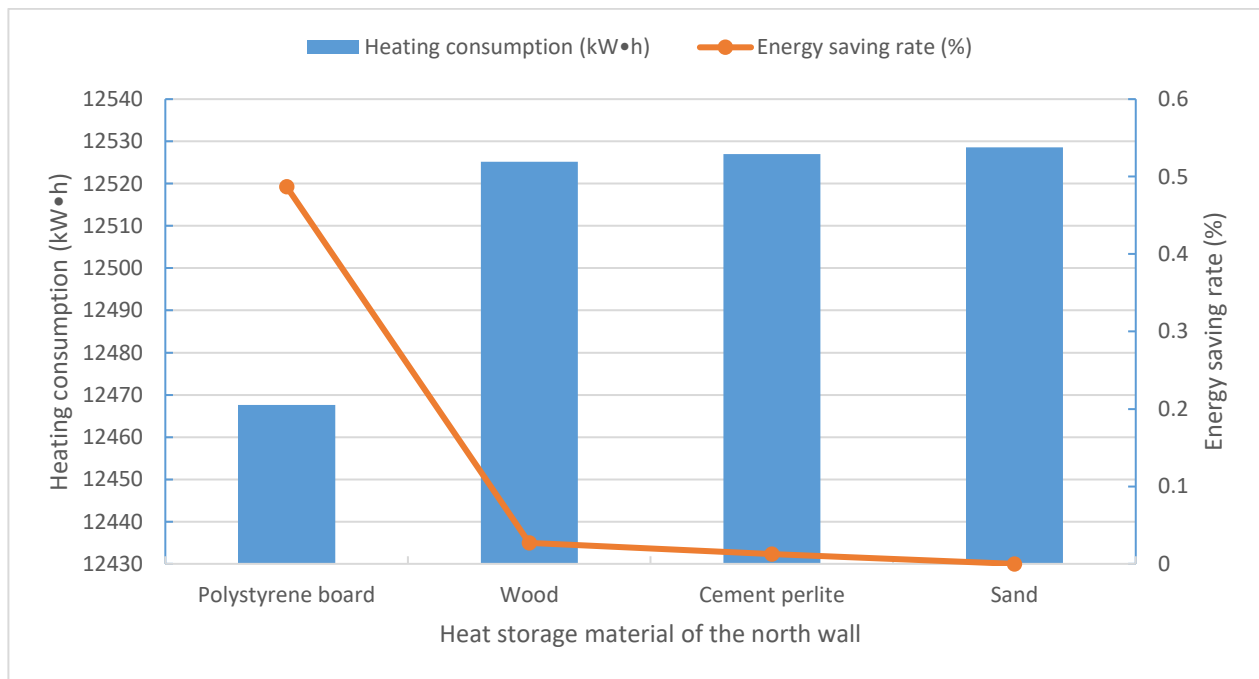
Figure 5.13 The sensitivity of the heat storage materials of the north wall (energy saving is compared to sand)

Finally, the thermal blanket is another important component in reducing the supplemental heating demand. Low supplemental heating requirement can be achieved by covering the thermal blankets with low thermal transmittance in the night. As shown in the Fig. 5.14,

various thermal blankets with U value ranging from 0.6 W/(m^2•K) to 3 W/(m^2•K) were analyzed. Compare the total supplemental heating demand of poor-quality thermal blanket (3 W/(m^2•K)), 44.8% heating energy can be saved when use premium thermal blanket (0.6 W/(m^2•K)). This demonstrated that the thermal blankets selection is a significant factor on heating demand.
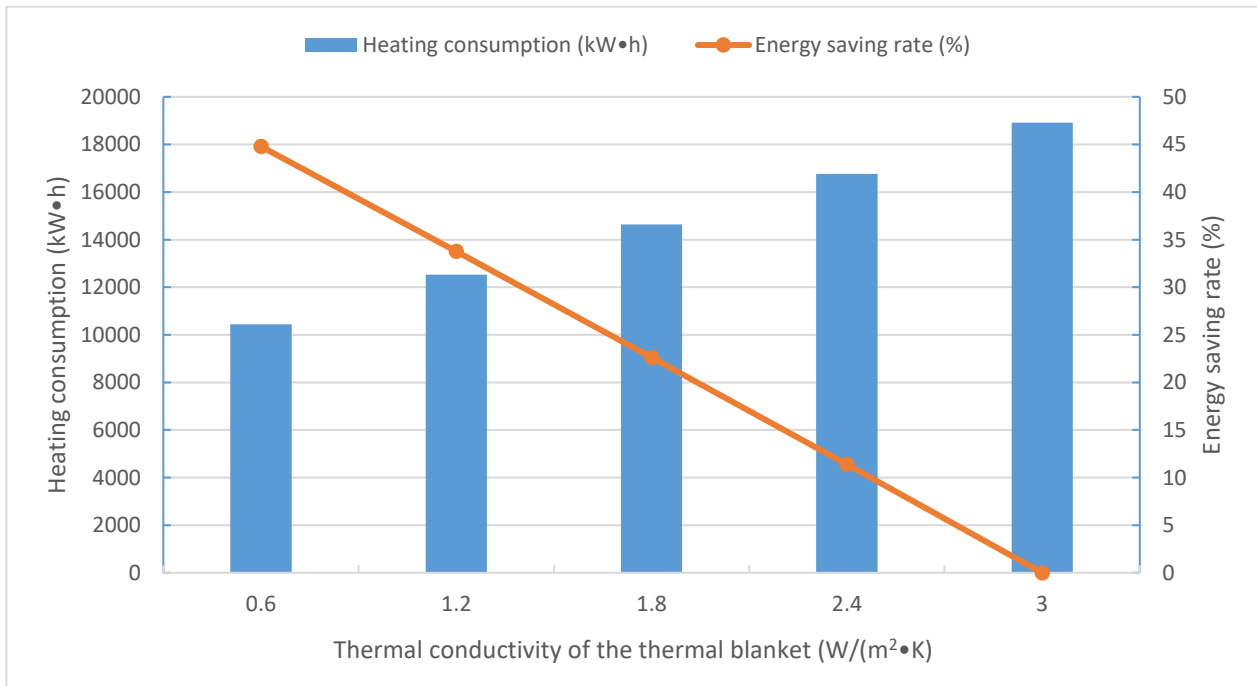
Figure 5.14 The sensitivity of the thermal blankets (energy saving is compared to 3 W/(m^2•K) thermal blanket)

Among these important aspects of the solar greenhouse components, the front roof cover material and thermal transmittance of the thermal blanket played the most significant role in reducing the supplemental heating requirements. Thus, it is an energy-saving choice to cover the front roof with high thermal resistance materials and use thermal blanket with low thermal transmittance.

5.2.4 Energy cost analysis

With the annual simulation results, the annual energy consumption costs of the solar greenhouse were calculated for the weather conditions of Saskatoon. By comparing the energy costs of various energy sources and the natural gas bill of Grandora Gardens, the optimal energy source was chosen for the solar greenhouse.

The monthly energy consumption was organized according to the simulation results. Although some greenhouses use biomass, including woody fuels and animal wastes, as energy source for supplemental heating, this study selected electricity, natural gas, and coal as the heating fuels and the corresponding costs regarding solar greenhouse production in Saskatoon were compared.

1) According to the monthly electrical rate of Saskatoon's city service, the monthly service charge is $ 33.08 and 14.52 ¢/ kW•h for the first 14500 kWh and 7.67 ¢/ kW•h when the electrical rating is more than 14500 kW•h (Electrical Rates, City of Saskatoon, 2017). Thus, the total monthly cost Y_e for the supplemental heat is:

$$Y_e = 33.08 + 0.1452A \quad (A \leq 14500 \text{ kW} \bullet \text{h}) \tag{5.1}$$

$$Y_e = 33.08 + 0.1452 \bullet 14500 + 0.0767(A\text{-}14500) \quad (A > 14500 \text{ kW} \bullet \text{h}) \tag{5.2}$$

where A is the total monthly electrical rating, kW•h; and Y_e is the total monthly cost using electricity, $.

2) According to the national energy board (Natural Gas, National Energy Board, 2017), 1 m³ natural gas has 0.0373 GJ of energy content (based on 1000 Btu/cf). Based on the current commercial natural gas rates of SaskEnergy (0 to 100,000 m³/year), the monthly basic charge is $38.5, and the delivery charge is $0.0743/m³ (Commercial Rates of Natural Gas, SaskEnergy, 2017). Assume that the efficiency of the natural gas burner η is 92% (High-Efficiency Gas Furnaces, Payne, 2017). So, the monthly gas cost Y_n for supplemental heat is:

$$Y_n = 38.5 + \frac{0.0743B}{0.0373 \bullet 92\%} \tag{5.3}$$

where B is the total energy consumption, GJ, for the month; and Y_n is the total monthly cost using natural gas, $.

3) According to the All Canadian Coal-fired Heaters, 1 tonne of coal has 18 GJ of energy content and it is $42-$47 per tonne (Coal, All Canadian Coal-fired Heaters, 2017). Assume the price of coal is $45 per tonne and a high-efficiency furnace has a 90% AFUE (Furnaces and Boilers, ENERGY.GOV, 2017). Thus, the monthly coal cost Y_c for supplemental heat is equal to:

$$Y_c = \frac{45B}{18 \bullet 90\%} \tag{5.4}$$

where Y_c is the total monthly cost using coal, $.

However, compared to electricity and natural gas, the coal furnace introduces an ash problem and 3-7 kg/GJ of ash may be produced in the heating process. This study neglected the cost for residual disposal.

Based on above energy costs, the results were obtained. Table 5.1 provides a comparison of the energy costs of different energy sources.

Table 5.1 Annual energy cost of different energy sources

	Electricity	Natural gas	Coal
Total energy consumption (kW•h)	261,291.54	261,291.54	261,291.54
Total energy consumption (GJ)	940.58	940.58	940.58
Amount	261,291.54 kWh	27,409.2 m^3	58.0 tonne
Annual cost ($)	26,378.56	2,498.51	2,610
Ash quality (tonne)	0	0	2.8-6.6

Based on the results, electricity is the most expensive heating resource, but its advantages are its low capital cost, it is easy to use and it does not create local pollution. Natural gas and coal have a comparable annual cost in this case, which is only 1/10 of the electrical cost. However, natural gas has some unique advantages compared to coal. On the one hand, the capital cost for natural gas heating is lower and it is easily controlled for heating. On the other, the natural

gas combustion process does not produce solid by-product such as ash. This may reduce the cost caused by waste disposal. Thus, among these three energy sources, natural gas is the optimal choice for greenhouses.

The natural gas bill of Grandora Gardens from SASKENERGY is used to compare the annual energy cost of solar greenhouse production with that of traditional greenhouse production. According to the production schedule, Grandora Gardens closed greenhouses from the end of November to the beginning of February. Greenhouse growers only have to grow seedlings in a limited space in the greenhouse in December and January. While assuming that the monthly natural gas usage for housing and other facilities (one house, one trailer house and header house) on site was $500 based on experience, Table 5.2 summarizes the 2014 natural gas bill from Grandora Gardens. Thus, the annual energy consumption Y_G was the total balance minus the annual house use:

$$Y_G = \$47{,}225.82 - \$500 \cdot 12 = \$41{,}225.82 \tag{5.5}$$

Table 5.2 Natural gas bill of Grandora Garden

Date	Amount ($)	Balance ($)
09/01/2014	2,060.34	2,060.34
09/02/2014	2,547.74	4,608.08
09/03/2014	7,050.51	11,658.59
09/04/2014	4,494.33	16,152.92
09/05/2014	5,687.70	21,840.62
09/06/2014	3,961.71	25,802.33
09/07/2014	1,864.46	27,666.79
09/08/2014	2,045.33	29,712.12
09/09/2014	2,136.81	31,848.93
09/10/2014	3,152.69	35,001.62
09/11/2014	7,091.17	42,092.79
09/12/2014	6,096.82	48,189.61
31/12/2014	-963.79	47,225.82
Total	47,225.82	47,225.82

From the above simulated energy costs and natural gas bill of Grandora Gardens, a comparison was made in Table 5.3 considering the corresponding total growing area.

Table 5.3 Energy cost comparison between Grandora Gardens and simulation results of the study solar greenhouse

	Grandora Gardens	Study solar greenhouse
Total growing area (m²)	3252	1200
Natural gas cost ($)	41225.82	2498.51
Natural gas cost per unit area ($/m²)	12.68	2.08

As expected, the solar greenhouse had a much lower energy consumption due to its unique structure while traditional greenhouses in Grandora Gardens had to pay more even though seedlings were only applied in December and January. The energy saving rate η_e is 83.6%, which is calculated as:

$$\eta_e = \frac{12.68 - 2.08}{12.68} \cdot 100\% = 83.6\% \tag{5.6}$$

Chapter 6. CONCLUSIONS

In this study, several important modifications were made to an existing simulation model developed by Dr. Ma. Field data measured in a solar greenhouse in Elie, Manitoba, were used to validate the model, and then the energy consumption of a solar greenhouse was simulated under Saskatoon's weather conditions.

The Canadian Prairies have distinct weather conditions due to their geography. On one hand, the Prairies suffer from cold temperatures and high wind speed. On the other hand, they enjoy long durations of sunshine and a high solar irradiance. Thus, to meet the requirement of solar greenhouse production in the northern latitude, modifications were made to the original model RGWSRHJ including translation from Chinese to English, simulation feasibility, operation simplification, energy saving technologies as well as localized function. With new functions and modifications, the new simulation model SOGREEN could simulate the thermal environment of a solar greenhouse under Canadian weather conditions.

The model validation step evaluated the accuracy of the model. In this process, field data including structural parameters, indoor planting conditions, hourly outdoor weather conditions, and the hourly heating power of the electrical heater were collected in a commercial solar greenhouse in Elie, Manitoba. After predicting the thermal conditions of the solar greenhouse, comparisons were made between measured values and predicted values. According to the validation results, a 9.6%, 13.7%, 19.4%, and 10.4% discrepancy occurred in the temperature, RH, wall surface temperature, and soil surface temperature predictions respectively.

Simulation of a solar greenhouse in Saskatoon was also conducted. The typical meteorological year data of Saskatoon were invoked and tomatoes were planted in a fiber landscaping ground similar to the Grandora Gardens greenhouse. Since there were no solar greenhouses constructed in Saskatchewan yet, a study solar greenhouse (100 m x 12 m) was designed with similar construction materials to the Elie solar greenhouse. Based on the simulation results, to keep the tomato plants growing in the required temperature range, the energy consumption of the supplemental heating system would be maintained at a high level from November to March. However, energy consumption was eliminated between May and August which displayed the advantage of the solar greenhouse. In addition, the annual expense for the supplemental heat

of three different energy resources (electricity, natural gas and coal) was calculated, and the result showed that natural gas was the most affordable energy resource for the greenhouses.

Finally, a comparison between the simulation results and the natural gas bill of Grandora Gardens was done. This illustrated that $12.68/m^2 was spent in the traditional greenhouses at Grandora Gardens while only $2.08/m^2 was used in the study solar greenhouses. Both energy saving rate and heating cost saving rate are 83.6% according to the simulation results. Thus, solar greenhouses should be highly recommended for year-round production for Saskatchewan and Canadian greenhouse growers.

Chapter 7. RECOMMENDATIONS

The followings are some suggestions for the future study in thermal simulation of the solar greenhouse.

1) Due to most of the significant discrepancies in the indoor temperature and RH occurred during the ventilation period at noon, experiments could be conducted to quantify the ventilation rate from the air inlet. Thus, users can assume the ventilation rate more precisely. This helps users get better results.

2) According to the simulation results, the indoor RH was high at night, especially in the winter. Thus, dehumidifier or other dehumidification systems can be taken into consideration in the further study.

3) It is necessary to design a snow remover to prevent the snow from crushing the greenhouses and blocking the sunshine since it snows frequently and heavily in the Canadian Prairies.

REFERENCES

Ahamed, M.S., H. Guo, and K.K. Tanino. 2015. A pseudo dynamic model for simulation of greenhouse energy requirement. Paper presented at CSBE/SCGAB 2015 Annual Conference, Edmonton, AB, 5-8 July (pp. 1-12).

APEX Publishers. 2017. Greenhouse Hot Water Heating Systems. Accessed August 7, 2017. http://www.greenhouse-management.com/greenhouse_management/greenhouse_heating/greenhouse_hot_water_heating_systems.htm.

ASHRAE, SI Edition. 2013. ASHRAE Handbook of Fundamentals. Atlanta: ASHRAE Research.

Bai, Y., T. Li, W. Zhang. 2010. Experimental analysis and mathematical model on temperature field of the solar greenhouse's foundation. Northern Horticulture. 2010(13): 49-53.

Baird, Craig. 2011. Complete guide to build your own greenhouse: Everything you need to know explained simply. Atlanta: Atlantic Publishing Company.

Benavente, R.M., S. De la Plaza, L.M. Navas, J.L. Garcia, E. Hernandez, L. Luna. 1998. Establishment and validation of a model to estimate energy consumption of localized heating of greenhouse substrates. Acta Horticulturae. 456: 339–346.

Beshada, E., Q. Zhang, and R. Boris. 2006. Winter performance of a solar energy greenhouse in southern Manitoba. Canadian Biosystems Engineering. 48: 5.1-5.8.

China Academy of Building Research. 2017. Thermal design code of civil building. Beijing: China Planning Press.

Coal. All Canadian Coal-fired Heaters. 2015. Accessed June 14, 2017. http://www.allcanadianheaters.com/coal/.

Commercial Rates of Natural Gas. SaskEnergy. 2016. Accessed June 14, 2017. http://www.saskenergy.com/business/comrates_curr.asp.

Critten, D.L., and B.J. Bailey. 2002. A review of greenhouse engineering developments during the 1990s. Agricultural and Forest Meteorology. 112(2002): 1-22.

Electrical Rates. City of Saskatoon. 2017. Accessed June 14, 2017. https://www.saskatoon.ca/services-residents/power-water/saskatoon-light-power/electrical-rates.

Environment Canada. 2010. Accessed March 13, 2017. http://www.weatheroffice.gc.ca/canada_e.html.

Environment Canada. 2017. Accessed September 4, 2017. 1981-2010 Climate normal and averages. http://climate.weather.gc.ca/climate_normals/index_e.html

Furnaces and Boilers. ENERGY.GOV. 2017. Accessed June 14, 2017. https://energy.gov/energysaver/furnaces-and-boilers.

Gary, C., M. Tchamitchian, N. Bertun, L. Charasse, A. Pebillard, J.P. Cardi, T. Boulard, A. Baille. 1998. Simulserre: an educational software simulating the greenhouse crop system. Acta Horticulturae. 456: 451–458.

Garzoli, K.V., J. Blackwell. 1987. An analysis of the nocturnal heat loss from a double skin plastic greenhouse. Journal of Agricultural Engineering Research. 36(2): 75-86.

Gijzen, H., E. Heuvelink, H. Challa, L.F.M. Marcelis, E. Dayan, S. Cohen, M. Fuchs. 1998. HORTISM: a model for greenhouse crops and greenhouse climate. Acta Horticulturae. 456: 441–450.

Greenhouse Heating Efficiency Design Considerations. 1998. Accessed June 13, 2017. http://www.hort.vt.edu/ghvegetables/documents/Greenhouse%20Heating_Energy/HeatingEffnNGMA.pdf.

Guo, H., Z. Li, Z. Zhang, Y. Cui. 1994. Simulation of the temperature environment for solar greenhouse: Mathematic model and program verification. Journal of Shenyang Agricultural University. 25(4): 438-443.

High-Efficiency Gas Furnaces. Payne. 2017. Accessed September 10, 2017. http://ingramswaterandair.com/brochures/01-8110-994-25-060211.pdf.

Li, Y., C. Ma. 2000. Study on double-layer inflated film covering in greenhouse. Beijing: China Agricultural University.

Li, T. 2005. Current situation and prospects of greenhouse industry development in China. Journal of Shenyang Agricultural University. 36(2): 131-138

Li, W., R. Dong, C. Tang, S. Zhang. 1997. A theoretical model of thermal environment in solar plastic greenhouses with one-slope. Transactions of the CSAE. 13(2): 160-163.

Liloia, Z. 2012. The year of mud: Natural building workshops. Accessed January 29, 2018. http://www.theyearofmud.com/2012/04/02/build-your-own-attached-greenhouse/

Ling, J., C. Ma, C. Lin, Z. Huang, L. Shen. 2002. Preliminary experimental research on effect of aluminized thermal screens in greenhouse. Transactions of the CSAE. 18(1): 89-92.

Meng, L., Q. Yang, G.P.A. Bot, N. Wang. 2009. Visual simulation model for thermal environment in Chinese solar greenhouse. Transactions of the CSAE. 25(1): 164-170.

Ma, C. 2015. Original experimental data.

Ma, C., J. Han, R. Li. 2010. Research and development of software for thermal environmental simulation and prediction in solar greenhouse. Northern Horticulture. 2010(15): 69-75.

Natural Gas. National Energy Board. 2017. Accessed June 13, 2017. https://apps.neb-one.gc.ca/Conversion/conversion-tables.aspx?GoCTemplateCulture=en-CA#2-3.

Navas, L.M., S. de la Plaza, J.L. Garcia, J.M. Duran, N. Retamal, L. Luna, and R. Benavente. 1998. Formulation and sensitivity analysis of a dynamic model of the

greenhouse climate validation for a mild Mediterranean climate. Acta Horticulturae. 452: 305–312.

Ozturk, H.H., A.B. Ik. 2003. Effect of thermal screens on the microclimate and overall heat loss coefficient in plastic tunnel greenhouse. Turkish Journal of Agriculture and Forestry. 2003(27): 123-134.

Planet Natural. 2017. Heat Mat (1-Flat). Accessed June 7, 2017. https://www.planetnatural.com/product/seedling-heat-mat-1-flat/.

Qu, M., C. Ma, S. Li, T. Zhang. 2003. Analysis of thermal environment of greenhouse with floor heating system. Transactions of the CSAE. 19(1): 180-183.

Rorabaugh, P. A., M.H. Jensen, G. Giacomelli. 2002. Introduction to controlled environment agriculture and hydroponics. Controlled Environment Agriculture Center, Campus Agriculture Center, University of Arizona.

Samuel, P.S. 2016. Meteorology and energy security: Simulations, Projections, and Management. (1st ed.) Boca Raton: CRC Press.

Short, T.H., S.A. Shah. 1981. A portable polystyrene-pellet insulation system for greenhouses. Transactions of the ASAE. 16(81): 1291-1295.

Statistics Canada. 2016. Canola area surpassed spring wheat area in Saskatchewan. Accessed March 3, 2017. http://www.statcan.gc.ca/pub/95-640-x/2011001/p1/prov/prov-47-eng.htm.

Tong, G., B. Li, D.M. Christopher, T. Yamaguchi. 2007. Preliminary study on temperature pattern in Chinese solar greenhouse using computational fluid dynamics. Transactions of the CSAE. 23(7): 178-185.

University of Saskatchewan. 2017. Thesis Preparation. Student Services. Accessed December 8, 2017. https://students.usask.ca/graduate/thesis-preparation.php#Beforebeginning.

Vinje, E. 2013. Winter Growing: Heating Greenhouses. Accessed August 7, 2017. https://www.planetnatural.com/greenhouse-heating/.

Wei, X., C. Zhou, N. Cao, B. Sheng, S. Chen, S. Lu. 2012. Evolution of structure and performance of Chinese solar greenhouse. Jiangsu Journal of Agricultural Science. 28(4): 855-860.

Xu, F., S. Li, C. Ma, S. Zhao, J. Han, Y. Liu, B. Hu, S. Wang. 2013. Thermal environment of Chinese solar greenhouses: analysis and simulation. Transactions of the ASABE. 29(6): 991-997.

Xu, F., C. Ma. 2013. Daily change and math-expression method of outside temperature in winter for greenhouse environmental analysis. Transactions of the CSAE. 29(12):203-209.

Yan, S., T. Wang, Y. Zhang, S. Xu, G. Luo. 2013. The evolution and development of solar greenhouse technology. Agricultural Science and Technology and Equipment. 228(6): 97-98.

Zhou, C. 1999. Economic and technical assessment on double inflated plastic house. Transactions of the CSAE. 15(1): 159-163.